Universitat Politècnica de Catalunya

Stability and Folding of G-Protein Coupled Receptors Associated to Degenerative Diseases

A thesis submitted for the degree of

Doctor of Philosophy

By

Xiaoyun Dong

This work has been carried out at the Molecular and Industrial Biotechnology Group, Department of Chemical Engineering, under the direction of Professor Pere Garriga Solé and Dr. Eva Ramon Portés.

Prof. Pere Garriga Solé **Dr. Eva Ramon Portés**

Terrassa, 2016

UNIVERSITAT POLITÈCNICA DE CATALUNYA
BARCELONATECH
Escola de Doctorat

Curs acadèmic: 2015/2016

Acta de qualificació de tesi doctoral

Nom i cognoms
XIAOYUN DONG

Programa de doctorat
TECNOLOGIA AGROALIMENTÁRIA I BIOTECNOLOGIA

Unitat estructural responsable del programa
ENGINERIA AGROALIMENTÁRIA I BIOTECNOLOGIA

Resolució del Tribunal

Reunit el Tribunal designat a l'efecte, el doctorand / la doctoranda exposa el tema de la seva tesi doctoral titulada STABILITY AND FOLDING OF G-PROTEIN COUPLED RECEPTORS ASSOCIATED WITH DEGENERATIVE DISEASE

Acabada la lectura i després de donar resposta a les qüestions formulades pels membres titulars del tribunal, aquest atorga la qualificació:

☐ NO APTE ☐ APROVAT ☐ NOTABLE ☐ EXCEL·LENT

(Nom, cognoms i signatura)	(Nom, cognoms i signatura)	
President/a	Secretari/ària	
(Nom, cognoms i signatura)	(Nom, cognoms i signatura)	(Nom, cognoms i signatura)
Vocal	Vocal	Vocal

_____, _____ d'/de _____ de _____

El resultat de l'escrutini dels vots emesos pels membres titulars del tribunal, efectuat per l'Escola de Doctorat, a instància de la Comissió de Doctorat de la UPC, atorga la MENCIÓ CUM LAUDE:

☐ SÍ ☐ NO

(Nom, cognoms i signatura)	(Nom, cognoms i signatura)
President de la Comissió Permanent de l'Escola de Doctorat	Secretari de la Comissió Permanent de l'Escola de Doctorat

Barcelona, _____ d'/de _____ de _____

To

The friendship between

Spain and China

积土成山，风雨兴焉；积水成渊，蛟龙生焉；积善成德，而神明自得，圣心备焉。故不积跬步，无以至千里；不积小流，无以成江海。骐骥一跃，不能十步；驽马十驾，功在不舍。锲而舍之，朽木不折；锲而不舍，金石可镂。蚓无爪牙之利，筋骨之强，上食埃土，下饮黄泉，用心一也。蟹六跪而二螯，非蛇鳝之穴无可寄托者，用心躁也。 战国. 荀子

读万卷书，行万里路，胸中脱去尘浊，自然丘壑内营。 明. 董其昌

路漫漫其修远兮，吾将上下而求索。 战国. 屈原

ABSTRACT

G-protein coupled receptors (GPCRs) are the largest membrane protein superfamily encoded by the human genome and represent the largest class of drug targets for a wide range of pathological conditions. Two GPCRs members, the visual pigment rhodopsin associated with the retinal degenerative disease retinitis pigmentosa (RP), and the muscarinic acetylcholine (ACh) 3 receptor (M3R) associated with Alzheimer's disease (AD), are studied in this thesis.

Rhodopsin is the prototypical visual photoreceptor mediating scotopic vision and distributed throughout the retina. Upon illumination, the bound chromophore 11-*cis*-retinal isomerizes to all-*trans*-retinal and triggers the visual signaling cascade. Mutations found in rhodopsin, such as G90V and N55K, are responsible for the retinal degenerative disease RP. To counteract the low structural stability of these mutants, and to provide a deeper understanding of the molecular mechanisms leading to visual dysfunction, artificial membranes in the form of DMPC/DHPC bicelles and DDHA-PC liposomes were prepared. DMPC/DHPC bicelles and DDHA-PC liposomes provided a native-like bilayer environment, which preserved rhodopsin wild type and mutants structure and increased their thermal stability to varying degrees compared to the usual dodecyl maltoside (DM) detergent. Furthermore, chromophore regeneration of G90V and N55K mutants in DMPC/DHPC bicelles condition was enhanced compared to DM condition. Moreover, the kinetics for the active state metarhodopsin II (Meta II) decay indicated that retinal release rates of G90V and N55K mutants became faster in the presence of DMPC/DHPC bicelles and DDHA-PC liposomes compared to DM condition. The addition of hydroxylamine upon Meta II complete decay of WT and G90V in bicelles increased fluorescence intensity, suggesting that retinal can be retained inside the binding pocket. DMPC/DHPC bicelles and DDHA-PC liposomes provided stable conditions so that G90V opsin, obtained after Meta II completely decay, was able to regenerate upon the addition of exogenous retinal. On the other hand, N55K was not able to regenerate, indicating that the molecular mechanisms associated to this mutant has important differences which may be associated with their specific clinical phenotypes.

The interactions between rhodopsin and arrestin, and between M3R and tau protein are studied in their association with the degenerative diseases, RP and AD respectively. Active rhodopsin bound R175E mutant arrestin and slowed down the retinal release from the binding pocket.

Arrestin binding assays on mutants associated to RP would help uncover mechanisms related to visual cascade termination, not studied so far. M3R plays a role in muscarinic ACh signal transmission and on ion channels function especially in the central nervous system (CNS). In the M3R-tau interaction studies, M3R WT and mutants N132G and D518N did change the location of tau from the cytoplasm to the membrane when they were coexpressed in HEK293T cells. M3R mutants D518K and K523Q were affected when coexpressed with tau and trafficked from the membrane to the cytoplasm. These shifts in location likely result from the interaction between tau and M3R WT and mutants. This finding provides new clues about the specific tau binding/recognition sites on M3R and the possible involvement of such interaction in the pathophysiology of AD.

Overall, the artificial membranes DMPC/DHPC bicelles and DDHA-PC liposomes systems provide a better bilayer environment to stabilize rhodopsin WT and mutants than DM detergent environment thus reverting their intrinsic thermal sensitivity. The different behavior of G90V and N55K in artificial membranes could be associated with their specific clinical phenotypes. On the other side, the results obtained on the interaction between GPCRs and other proteins provide a foundation for further studies associated with GPCRs mutants and degenerative diseases.

RESUMEN

Los receptores acoplados a proteína G (GPCRs) representan la mayor superfamilia de proteínas de membrana codificada por el genoma humano y también la mayor clase de dianas terapéuticas para diversas enfermedades. En esta tesis se estudian dos miembros de los GPCRs; el pigmento visual rodopsina, asociado con la enfermedad degenerativa de la retina retinitis pigmentosa (RP) y el receptor de acetilcolina (ACh) muscarínico 3 (M3R) asociado con la enfermedad de Alzheimer (AD).

La rodopsina es el fotorreceptor visual prototípico responsable de la visión escotópica y se encuentra distribuido por toda la retina. Después de la iluminación, el cromóforo 11-*cis*-retinal se isomeriza a todo-*trans*-retinal y desencadena serie de reacciones intracelulares llegando al nervio óptico y permitiendo la unión. Mutaciones en rodopsina, tales como G90V y N55K son causantes de RP. Para entender más profundamente los mecanismos moleculares causantes de esta disfunción visual debido a estas mutaciones, se han preparado membranas artificiales tales como bicelas de DMPC/DHPC y liposomas de DDHA-PC. Estos sistemas lipídicos ofrecen un entorno bicapa más nativo, comparado con el que proporciona el detergente dodecil maltosido (DM), usado más tradicionalmente, lo que preserva la estructura de la rodopsina nativa y de los mutantes y aumenta su estabilidad térmica. La regeneración cromóforo para de G90V y N55K en bicelas de DMPC/DHPC es más elevada en comparación con el valor obtenido en DM. La cinética de decaimiento de la conformación activa metarodopsina II (Meta II) indica que la velocidad de liberación del retinal de los mutantes G90V y N55K es más alta en presencia de las bicelas de DMPC/DHPC, y de los liposomas de DDHA-PC, en comparación con las velocidades obtenidas en DM. La adición del reactivo hidroxilamina después del decaimiento completo de Meta II de WT y del mutante G90V en las bicelas provoca un incremento de la intensidad de fluorescencia, indicando que parte de Meta II aún mantiene el retinal en su sitio de unión. Las bicelas de DMPC/DHPC y los liposomas de DDHA-PC también estabilizan la opsina del mutante G90V, obtenida después del decaimiento de Meta II, pudiendo ser regenerada a rodopsina después de añadir retinal exógeno. Por lo contrario, el mutante N55K no regenera, lo que indica que los mutantes actúan con diferentes mecanismos, pudiéndose correlacionar este diferente comportamiento con los fenotipos clínicos específicos de cada mutante.

Las interacciones entre la rodopsina y arrestina, y entre M3R y tau, han estudiado para entender el mecanismo funcional de las enfermedades degenerativas de RP y AD respectivamente. La unión de rodopsina activa con el mutante de arrestina R175E, ralentiza la liberación de retinal desde el sitio de unión. Estudios futuros de esta interacción con mutantes asociados a RP ayudarán a explorar los mecanismos de terminación de señal visual, y su conexión con las degeneraciones retinanas aspecto no muy estudiado hasta el momento. M3R desempeña funciones sobre la transmisión de la señal del muscarínico ACh y los canales ionicos, especialmente en el sistema nervioso central (SNC). Por otro lado, la interacción de M3R WT y los mutantes N132G y D518N, produce un cambio en la localización de tau desde el citoplasma a la membrana cuando se coexpresan en células HEK293T. Además, los mutantes M3R D518K y K523Q también son afectados cuando se coexpresan pasando de la membrana al citoplasma. Estos cambios en las localizaciones celulares tanto de tau como del receptor sugieren interacciones específicas entre ellos. Estos resultados proporcionan claves importantes sobre los sitios de unión de tau y M3R, así como la posible implicación de este complejo en la AD.

En general, las membranas artificiales de DMPC/DHPC y DDHA-PC, proporcionan un mejor entorno para estabilizar la rodopsina WT y los mutantes asociados a RP. Las diferentes propiedades obtenidas de los mutantes G90V y N55K en estas membranas artificiales pueden estar asociadas a sus distintos fenotipos clínicos específicos. Por otra parte, los resultados obtenidos en el estudio de las interacciones entre los GPCR y otras proteínas proporcionan una base adicional a los estudios asociados a enfermedades degenerativas.

Abbreviations, acronyms and symbols

ABCR	ATP binding cassette transporter
Abs	Absorbance
ACh	Acetylcholine
AD	Alzheimer's disease
A_{max}	Absorption maximum
AP2	β2-adaptin
APS	Ammonium persulfate
ATP	Adenosine-5'-triphosphate
BN PAGE	Blue native PAGE
BSA	Bovine serum albumin
BTP	Bis-tris-propane
CHAPS	3-(3-Cholamidopropyl dimethylammonio)-1-propanesulfonate hydrate
CMC	Critical micelle concentration
CNS	Central nervous system
DAG	Diacylglycerol
DAPI	4',6-diamidino-2-phenylindole
DDHA-PC	1,2-didocosa-hexaenoyl-*sn*-glycero-3-phosphocholine
DHA	Docosahexaenoic acid
DHPC	1,2-dihexanoyl-*sn*-glycero-3-phosphocholine
DM	*n*-dodecyl-β-D-maltoside
DMEM	Dulbecco's modified eagle's medium
DMPA	1,2-dimyristoyl-*sn*-glycero-3-phosphate
DMPC	1,2-dimyristoyl-*sn*-glycero-3-phosphocholine
DMPG	1,2-dimyristoyl-*sn*-glycero-3-phospho-1'-rac-glycerol
DMPS	1,2-dimyristoyl-*sn*-glycero-3-phospho-L-serine
DOPC	1,2-dioleoyl-*sn*-glycero-3-phosphocholine
DOPE	1,2-dioleoyl-*sn*-glycero-3-phosphoethanolamine
DNA	Deoxyribonucleic acid

Dyn	Dynamin
EB	Ethidium bromide
EC	Extracellular
FBS	Fetal bovine serum
FITC	Fluorescein isothiocyanate
FRET	Fluorescence resonance energy transfer
Gα	G protein alpha subunit
Gβ	G protein beta subunit
GDP	Guanidine-5'-diphosphate
Gγ	G protein gamma subunit
GPCRs	G-protein coupled receptors
Gt	G protein transducin
GTP	Guanidine 5'-triphosphate
GTPγS^{35}	Guanidine 5'-O-(3-thio)-triphosphate
GnTI	N-acetylglucosaminyltransferase
H1-H7	α-helix 1 to helix 7
HDL	High density lipoprotein
HRP	Horseradish peroxidase
IC	Intracellular
IP$_3$	Inositol 1,4,5-trisphosphate
IPTG	Isopropyl-β-D-1-thiogalactopyranoside
λ_{max}	Wavelength maximum
LRAT	Lecithin-retinol acyltransferase
mAChRs	Muscarinic acetylcholine receptors
MAP	Microtubule associated protein
MAPT	Microtubule associated protein tau
M1R	Muscarinic acetylcholine 1 receptor
M3R	Muscarinic acetylcholine 3 receptor
Meta II	Metarhodopsin II
nAChRs	Nicotinic acetylcholine receptors

NADPH	Nicotinamide adenine dinucleotide phosphate
NMR	Nuclear magnetic resonance
PAGE	Polyacrylamide gel electroporesis
PBS	Phosphate buffered saline
PC	Phosphatidylcholine
PE	Phosphatidylethanolamine
PEI	Polyethyleneimine
PI	Phosphatidylinositol
PIP_2	Phosphatidylinositol 4,5-bisphosphate
PKC	Protein kinase C
PLC	Phospholipase C
PMSF	Phenylmethanesulfonyl fluoride
PS	Phosphatidylserine
PNS	Peripheral nervous systems
RDH5	11-*cis* retinol dehydrogenase 5
RDH8/12	All-*trans* retinol dehydrogenase 8/12
Rho	Rhodopsin purified from ROS
ROS	Rod outer segment
RP	Retinitis pigmentosa
RPE	Retinal pigment epithelium
RPE65	Retinal pigment epithelium-specific 65 kDa protein
RT	Room temperature
Sector RP	Sector retinitis pigmentosa
SB	Schiff base
SDS-PAGE	Sodium dodecyl sulfate polyacrylamide gel electrophoresis
$T_{1/2}$	Half-life time
TAE	Tris acetate-EDTA
TBS	Tris buffered saline
TTBS	Tween tris buffered saline
TEMED	N,N,N',N'-tetramethylethane-1,2-diamine

TM-EC	Transmembrane extracellular
TM-IC	Transmembrane intracellular
TRITC	Tetramethylrhodamine
UV-Vis	Ultraviolet-visible
WB	Western Blot
WT	Wild type

Amino Acids

A	Ala	alanine
C	Cys	cysteine
D	Asp	aspartic acid
E	Glu	glutamic acid
F	Phe	phenylalanine
G	Gly	glycine
H	His	histidine
I	Ile	isoleucine
K	Lys	lysine
L	Leu	leucine
M	Met	methionine
N	Asn	asparagine
P	Pro	proline
Q	Gln	glutamine
R	Arg	arginine
S	Ser	serine
T	Thr	threonine
V	Val	valine
W	Trp	tryptophan
Y	Tyr	tyrosine

Contents

FIGURES LIST

TABLES LIST

1. INTRODUCTION

1.1 The G-protein coupled receptors (GPCRs) superfamily

1.1.1 GPCRs

GPCRs represent the largest membrane protein superfamily encoded by the human genome. GPCRs can sense external stimuli and elicit specific responses within the cell by activating numerous signaling pathways that regulate virtually all physiological processes and a wide range of pathological conditions [1–3]. GPCRs can be differentiated from other protein families according to their structural characters, and particularly to their landmark structural signature consisting of seven transmembrane helical sequence stretches of about 25 to 35 consecutive hydrophobic amino acid residues. The crystal structure has proven that the seven α-helices span the plasma membrane in a counter-clockwise manner, forming a receptor, or a recognition and connection unit, enabling an extracellular (EC) ligand to exert a specific effect into the cell. The other requirement (from which they get their name) is the ability of interacting with heterotrimeric G-proteins that have GTPase activity as a main functional feature [4].

Analysis of gene sequences revealed that there are over 800 GPCRs in the human genome [5] responsible for communication at the cellular level, upon activation by a variety of EC signals including light, odorants [6], pheromones, hormones, neurotransmitters, and larger entities ranging from peptides to large proteins [4,7,8]. Therefore, GPCRs are involved in numerous physiological processes such as sensory perception, immune defense, cell communication, chemotaxis, and neurotransmission. Indeed, GPCRs are the largest class (~30%) of pharmacological targets of approved drugs for diverse diseases [9–13].

Based upon sequence homology and the functional similarity, human GPCRs have been grouped into five families/classes (A-F) which share little sequence homology and some functional similarity among each other. The five families of GPCRs are as follows [1,4,14]:

- **Class A (rhodopsin-like family)**: The rhodopsin-like family is the largest family of GPCRs and contains ~670 full length human receptor proteins including receptors for odorants and small ligands. The family can be further divided into four groups - α, β, γ, δ - in which the largest cluster of members, the olfactory receptors, is found in the δ-group. The rhodopsin-like family of GPCRs is highly heterogeneous when both primary structure and ligand preference are considered. Nuclear magnetic resonance (NMR) and X-ray

crystallography revealed a common fold formed by an N-terminal α-helix and two β-sheets stabilized by a conserved disulphide bridge in the EC space. Ligands interact with these EC domains to induce receptor activation. Within the seven transmembrane regions, most class A receptors do share specific sequence motifs [2,4,14].

- **Class B (secretin-like family)**: The secretin-like family recruits about 60 members and is characterized not only by the lack of the structural signature present in class A but also by the presence of a large N-terminal ectodomain. The ligands include high molecular weight hormones such as glucagon, secretin, calcitonin, growth hormone-releasing hormone, corticotropin-releasing factor, VIP-PACAP and the black widow spider toxin, α-latrotoxin. The secretin receptors share between 21 and 67% sequence identity and most of the variation is in the N-terminal regions. Most of the secretin family receptors contain conserved cysteine residues in the first and second EC loops. Also, almost all of these receptors contain conserved cysteine residues that form a network of three cysteine bridges in the N-terminal region [2,4,14,15].

- **Class C (glutamate family)**: The glutamate family consists of two dozen GPCRs such as the metabotropic glutamate receptors and the Ca^{2+}-sensing receptors. This family also includes GABA-B receptors, sweet and umami taste receptors, olfactory receptors and a group of putative pheromone receptors coupled to the G protein Go (termed VRs and Go-VN). These receptors possess large ectodomains responsible for ligand binding and most glutamate members bind their respective ligand within the N-terminal region [2,4,14].

- **Class D (the adhesion family)**: The adhesion family, formed by 33 members, presents a proteolytic domain which gets activated on ligand binding. This family is also referred to as the LNB7TM family, where LN stands for long N terminal and the rest contributes to the sequence similarity between transmembrane regions of class B receptors. The diverse N terminal of class D may contain several domains that also exist in other proteins, such as cadherin, lectin, laminin, olfactomedin, immunoglobulin and thrombospondin domains. These domains have an important role in the specificity of receptor ligand binding interactions [2,14].

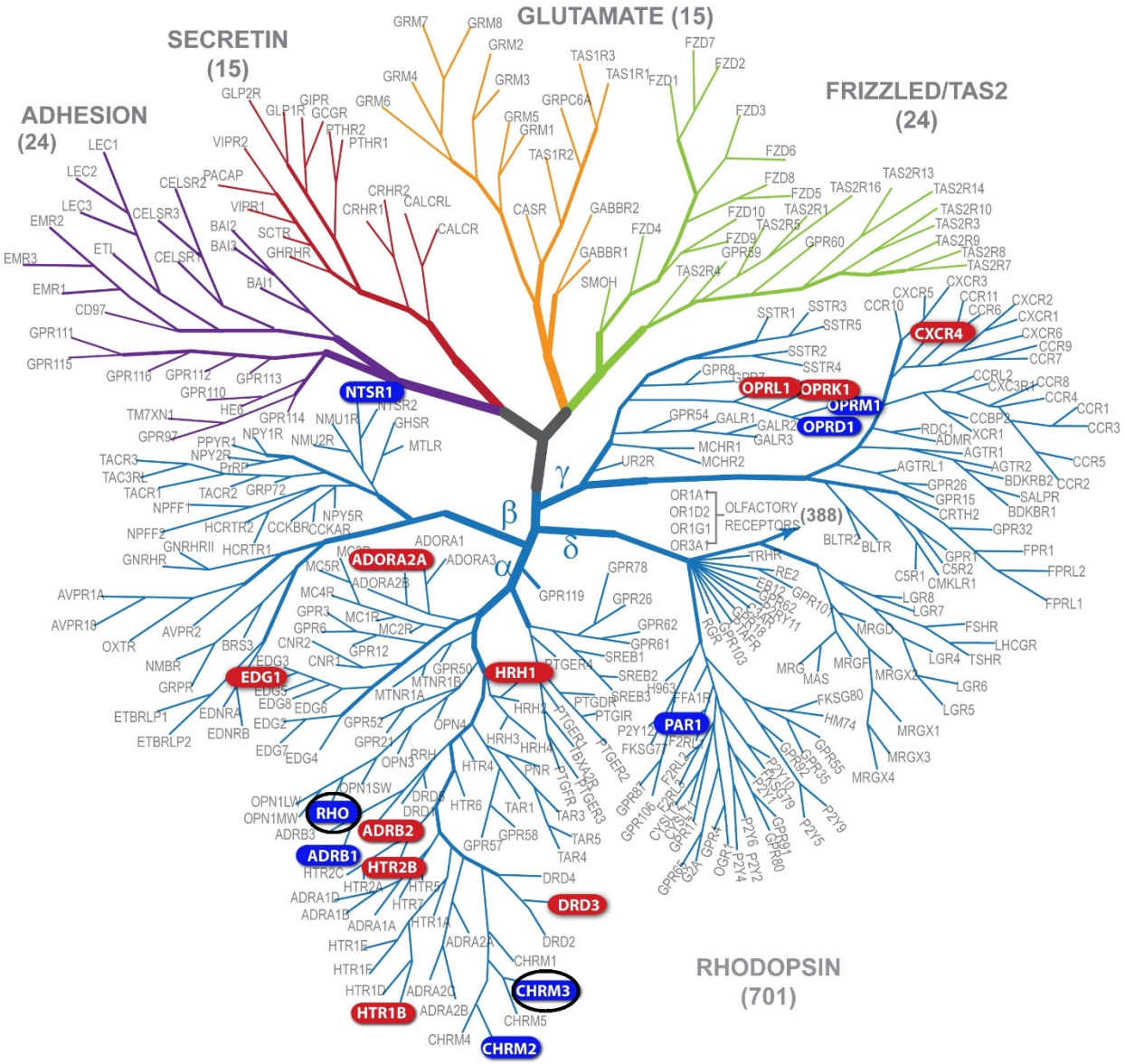

Figure 1.1 Phylogenetic tree representation of the human GPCR superfamily.

There are more than 800 human GPCRs, which can be classified into five major families: Rhodopsin (class A); Secretin (class B); Glutamate (class C); Adhesion (class D) and Frizzled/taste receptor 2 (class F). These families can be further divided into subfamilies on the basis of sequence similarity. GPCRs are named here according to their gene name as used by the UniProt database. Family members with reported structures are highlighted within the tree. CHRM3, M3R (PDB code: 4DAJ) and rhodopsin (PDB code: 1F88 and 1JFP) (labeled with a black circle) [1] have been studied in this thesis.

- **Class F (frizzled/taste2 family)**: The group consists of frizzled receptors and the smoothened receptor. The relationship to the GPCRs was further strengthened when sequence comparisons with secretin revealed resemblance in the EC regions and the presence of the well conserved cysteines in the first and second EC loops [2,4,14].

Each family covers several subfamilies of GPCRs. The rhodopsin-like family (class A) has the

largest number of receptors composing nearly 90% of all GPCRs [4,5,10,11,16] and the proteins studied in this thesis, rhodopsin and muscarinic acetylcholine (ACh) receptor M3 (M3R), belong to class A.

Nearly 800 human GPCRs were used to construct the GPCRs phylogenetic tree by sequence similarity within the seven-transmembrane region. Figure 1.1 shows the main human GPCR subfamilies and the proteins highlighted in blue and red have had their crystal structures reported [1,17].

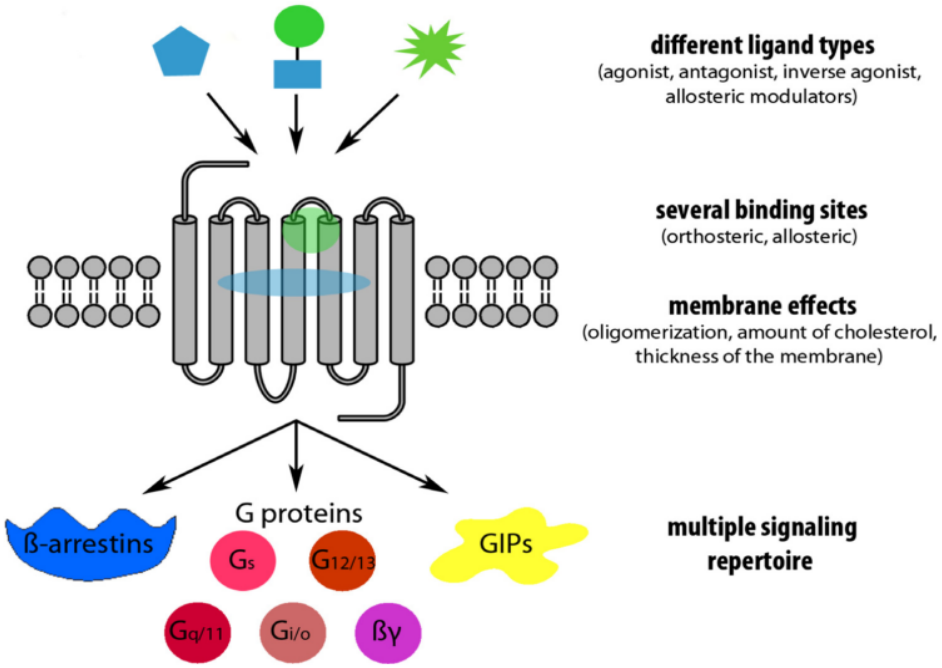

Figure 1.2 GPCRs are highly dynamic signaling machines.

Numerous distinct receptor conformations can be stabilized differently by a diverse of ligand types that bind to several binding sites: orthosteric (light green circle) or allosteric (blue ellipsoid), which results in highly complex signaling networks [18].

The GPCRs rearranges the conformation by binding the ligand and activates G-protein independent signaling pathways [19,20]. G protein is composed of α-, β-, and γ-subunits. The activated GPCRs with ligand-bound catalyzes the exchange of guanidine-5'-diphosphate (GDP) for guanidine 5'-triphosphate (GTP) on the α-subunit (Gα) of the G protein thereby dissociating Gα from the dimeric β- and γ-subunits (Gβγ) and stimulating a distinct signaling pathway. Furthermore, GPCRs also triggers mechanisms for signal switch-off such as binding to arrestin protein or other GPCR-interacting proteins and hence they can be described as integrative and highly dynamic signaling units (Figure 1.2) [13,18,19,21].

The X-ray structure of bovine rhodopsin was solved in 2000 [22], being the first crystal structure of a GPCR reported. The rhodopsin structure was used as a template for the GPCRs superfamily for years [4,11,23–25]. It took seven more years for other GPCRs crystal structure to be published. β2 and β1 adrenergic receptors were obtained by employing new receptor stabilization and crystallization techniques, which accelerated solving the three-dimensional structures of other receptors [26]. Until 2014, structures of 20 different class A, two class B, one class C and one frizzled GPCR, spanning large sections of the phylogenetic tree (Figure 1.1), have been published [1,26].

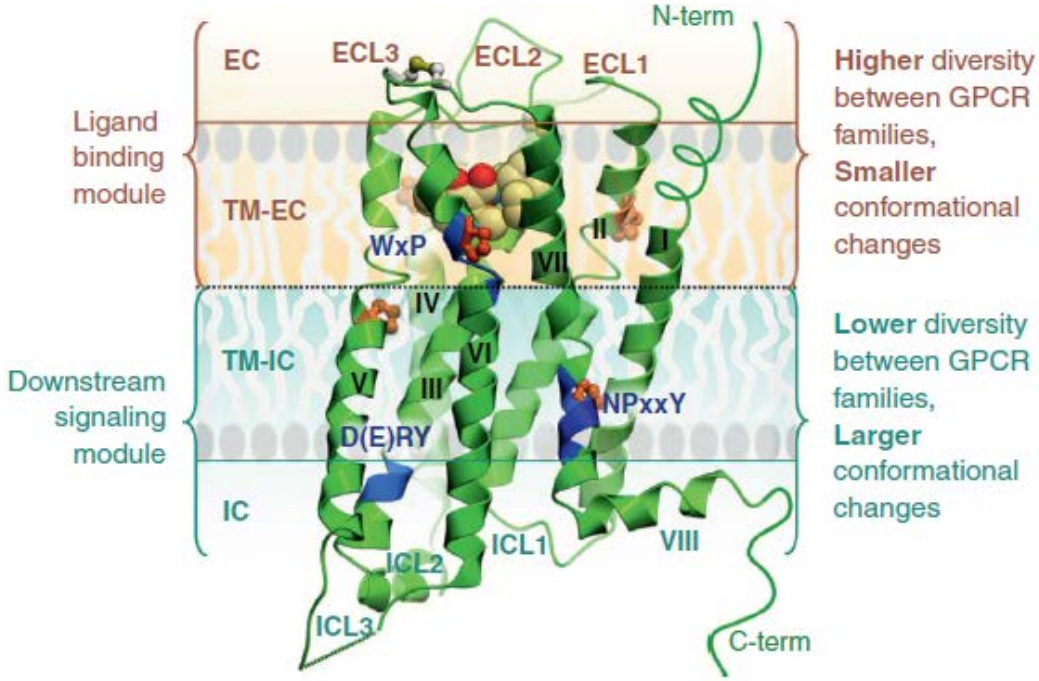

Figure 1.3 General architecture and modularity of GPCRs.

Major domains and structural features of GPCRs are shown on the dopamine D3 receptor crystal structure (PDB ID 3PBL) as an example. The EC region includes three EC loops and the N-terminus. The EC module (EC and TM-EC regions) is responsible for binding different ligands and it has much higher structural diversity. By contrast, the IC module (IC and IC-TM regions), involved in binding downstream effectors including G proteins and arrestins, is more conserved between GPCRs, but undergoes larger conformation changes upon receptor activation. The C terminus in most GPCRs is formed by a short helix 8 which parallels to the lipid bilayer, and some receptors have palmitoylation sites anchoring helix 8 to the membrane [17].

GPCRs comprise a bundle of seven transmembrane α-helices (H1-H7) which are connected by three intracellular (IC) and three EC polypeptide loops. The EC part, responsible for ligand binding, also includes the N-terminus, which can range from relatively short and often unstructured sequences in rhodopsin-like and bitter taste receptors to large globular EC domains in other GPCR classes [2]. The IC part, including the C-terminus, interacts with G proteins,

arrestins and other accessory proteins and downstream effectors. Transmembrane helices H1-H7 are characterized as the highly conserved and hydrophobic components harboring several functionally important motifs. Upon comparison of all the crystal structures of GPCRs, EC and transmembrane-EC (TM-EC) domains are considered as the basic module of ligand binding. These domains show higher diversity between GPCR families and conformational changes upon activation. Contrarily, IC and transmembrane-IC (TM-IC), as the downstream signaling module, depict lower diversity between GPCR families and larger conformational changes (Figure 1.3) [17,27–29].

Class A GPCRs exhibit the largest functional diversity among all GPCR classes because of the diversity ligands binding. The Class A are also characterized by conserved sequence motifs implying that share activation mechanisms. In this thesis, rhodopsin and M3R from class A GPCRs have been studied.

1.1.2 The photoreceptor rhodopsin

The visual photoreceptor rhodopsin is a prototypical member of class A GPCRs responsible for scotopic (or dim-light) vision. As a model of GPCRs, rhodopsin has been extensively studied since the first report of its crystal structure by X-ray crystallography [4,11,23–25]. The proteins involved in visual phototransduction are located mainly in the photoreceptor outer segments of the rod and cone photoreceptor cells. Rhodopsin is located in the rod outer segment (ROS) membranes of the rod cells of the retina, embedded in the lipid bilayer of disk membrane surrounded by ~65-70 phospholipids per protein molecule. Each mammalian ROS consists of a stack of 1000-2000 distinct disks surrounded by a plasma membrane. The disk is formed from evaginations of the plasma membrane and moves up the length of the rod cell as the disks age. Rhodopsin represents more than 90% of proteins in the disk, occupying approximately one third of its area [30]. Figure 1.4A shows the main morphological and structural organization of the retinal rod photoreceptor [31–33]. Rhodopsin monomer was considered as the functional unit, while more experiments indicated that rhodopsin and opsin can form dimers and higher oligomers organized in the disk membranes by atomic force microscopy [34] and fluorescence resonance energy transfer (FRET) [35]. As all of GPCRs, rhodopsin includes: a. N-terminal domain is located at the EC side at the intradiscal side of the disk membrane, b. seven transmembrane helices are

located in the membrane and H8 is lying adjacent and parallel to the membrane, c. a cytoplasmic C-terminal domain. Cys110 and Cys187 form the highly conserved disulfide bond which limit the conformational flexibility of the molecule (Figure 1.4B) [22,36,37].

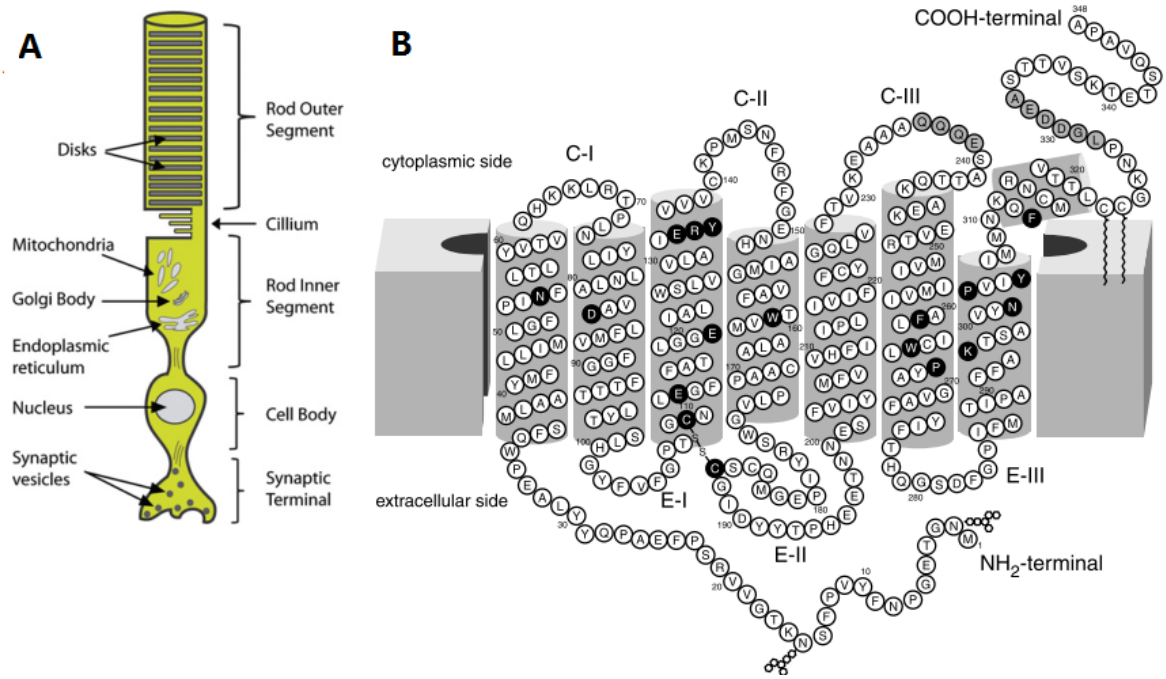

Figure 1.4 Schematic organization of the retinal rod photoreceptor cell and secondary structure of rhodopsin.

A. Rod photoreceptor cell showing major cellular elements and their distributed along the cell [33]. B. Secondary structure diagram of rhodopsin. The seven transmembrane helices are embedded in the membrane and the H8 is lying adjacent and parallel to the membrane. N-terminus is toward the EC side, and cytoplasmic domain is toward the cytosolic side. N2 and N15 are sites of glycosylation. Cys110 and Cys187 form the essential and conserved disulfide bond [22,36,37]. Black circles correspond to highly conserved amino acid residues in rhodopsin.

Rhodopsin consists of the opsin apoprotein and the 11-*cis*-retinal ligand which is covalently bound through a protonated Schiff base (SB) linkage to K296 at the seventh transmembrane helix of the photoreceptor [38–40]. Upon photon absorption, the 11-*cis*-retinal chromophore isomerizes to all-*trans*-retinal and triggers the formation of the active photointermediate metarhodopsin II (Meta II) [39,41] in which the retinal SB is still intact but deprotonated. During the activation process, the wavelength maximum (λ_{max}) of the visible band in the absorbance (Abs) spectrum of rhodopsin shifts from 500 nm to 380 nm. Figure 1.5 shows the structures of inactive state rhodopsin and the Meta II activated state [42–44]. The activated Meta II conformation can recruit and bind IC G proteins to continue the visual signaling cascade.

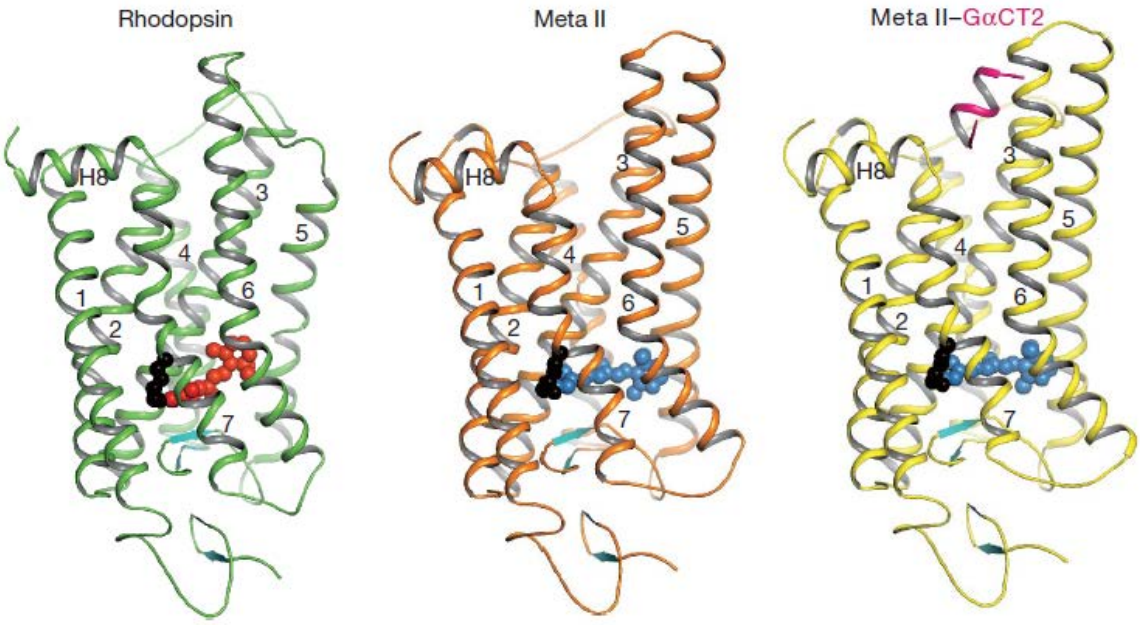

Figure 1.5 Structures of inactive rhodopsin, active Meta II and Meta II in complex with a Gt fragment.

The cartoon models of rhodopsin (PDB code 1U19), Meta II (PDB code 1LN6) and Meta II together with a C-terminal peptide derived from transducin Gα subunit (PDB code 3PQR). The inactive rhodopsin (left) consists of the apoprotein opsin in its resting conformation with the inverse agonist 11-*cis*-retinal (red spheres) covalently bound to K296 (black spheres) via a protonated SB. In Meta II (middle), the agonist all-*trans*-retinal (blue spheres) is covalently linked to K296. Meta II with Gα fragment (right) is identified and the Gα fragment is shown in purple [43].

Dissociation of the proton from the SB breaks a major constraint in the protein and enables further activating steps, including an outward tilt of TM6 and stimulating a signaling cascade beginning with binding and activating hundreds of molecules of the trimeric G protein transducin (Gt). This eventually leads to rod photoreceptor cell hyperpolarisation, and synaptic signaling to adjacent rod bipolar cells [37,43,45].

The visual cycle is a transcellular process by which retinal pigment epithelium (RPE) cells maintain the supply of chromophores for the regeneration of visual opsin pigments in photoreceptors. After the activation phase, Meta II decays and the signal is terminated by phosphorylation kinase and subsequent arrestin binding to the phosphorylated receptor. The SB between opsin and all-*trans*-retinal is hydrolysed to release free all-*trans*-retinal chromophore from the protein. The adenosine-5'-triphosphate (ATP) binding cassette transporter (ABCR) carries all-*trans*-retinal from the intradiscal to the cytosolic area of the disc membrane. The all-*trans*-retinol dehydrogenase 8/12 (RDH8/12) catalyzes the reduction of all-*trans*-retinal to all-*trans*-retinol by reduced nicotinamide adenine dinucleotide phosphate (NADPH).

All-*trans*-retinol leaves the photoreceptor cell, traverses the interphotoreceptor matrix and enters the RPE where it is esterified by lecithin-retinol acyltransferase (LRAT). The all-*trans*-retinyl ester is converted to 11-*cis*-retinol and free fatty acid by an isomerohydrolase of retinal pigment epithelium-specific protein 65 kDa (RPE65). 11-*cis*-retinol can be esterified by LRAT and stored or oxidized to 11-*cis*-retinal by 11-*cis*-retinol dehydrogenase 5 (RDH5). Other sources of 11-*cis*-retinol are the blood and the photoreceptor outer segments phagocytosed by the RPE. 11-*cis*-retinal diffuses into the photoreceptor cell where it associates with opsin to regenerate the visual pigment (Figure 1.6) [46–49].

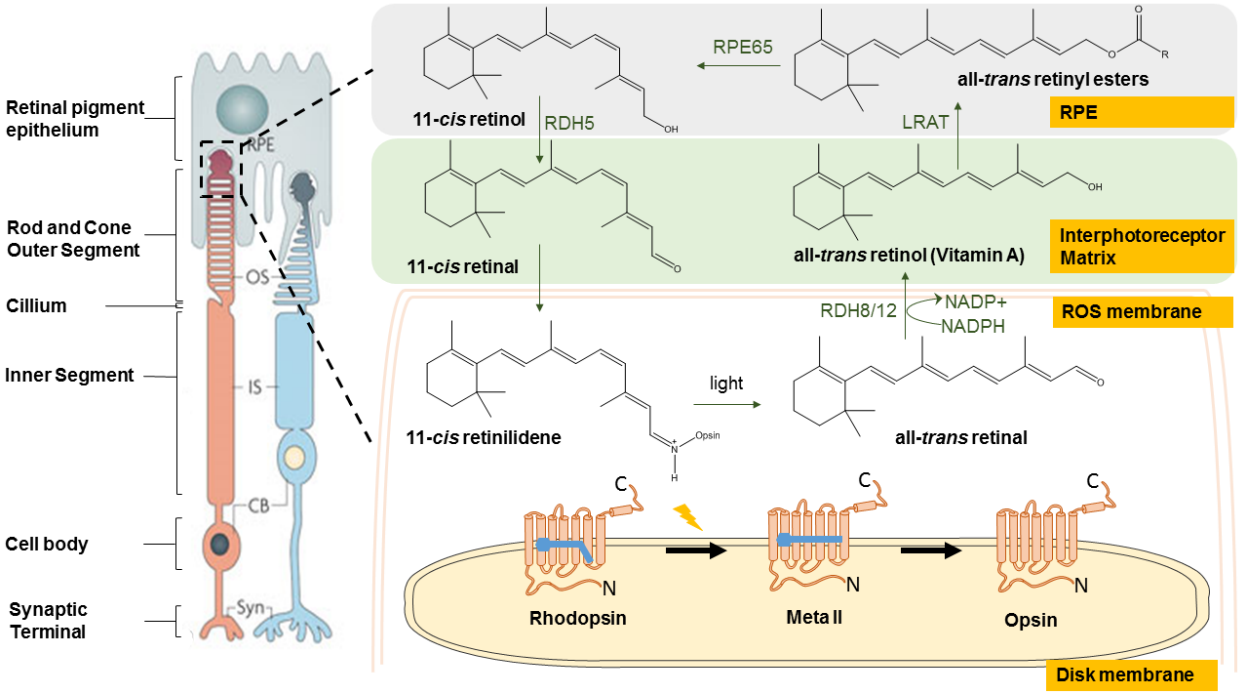

Figure 1.6 The visual cycle in the vertebrate retina.

In the ROS disks, light converts the 11-*cis*-retinal chromophore of rhodopsin to all-*trans*-retinal. All-*trans*-retinal is released from rhodopsin and undergoes an elaborate multistep enzymatic process (called the visual cycle) to regenerate 11-*cis*-retinal for subsequent opsin regeneration in a next cycle. All-*trans*-retinal is first reduced to all-*trans*-retinol by RDH8/12. In the RPE, all-*trans*-retinol is esterified by LRAT to all-*trans*-retinyl esters. RPE65 mediates the conversion of all-*trans* retinyl esters to 11-*cis*-retinol, which is oxidized to 11-*cis*-retinal by RDH5. 11-*cis*-retinal returns to the ROS where it binds to opsin to regenerate the rhodopsin photopigment.

1.1.3 M3R receptor

ACh is a known neurotransmitter in both the peripheral (PNS) and central (CNS) nervous systems, and neurons containing ACh as a neurotransmitter are called cholinergic neurons. ACh transduces signals through muscarinic and nicotinic ACh receptors, both of which influence synaptic plasticity and cognition. Muscarinic ACh receptors (mAChRs) and nicotinic

acetylcholine receptors (nAChRs) belong to class A GPCRs [50]. mAChRs are found in plasma membranes of certain neurons, among other cell types, and are classified in five different subtypes (from M1R to M5R) [51,52]. Based on the IC α subunit type of the G protein they bind to, mAChRs are divided into two main types. The first group includes M1R, M3R and M5R interacting with Gq type proteins [53], and the second group consists of M2R and M4R which interact with Gi/o proteins [54]. mAChRs activation affects the function of many ion channels, through a variety of IC signaling cascades, resulting in changed conductances of mainly potassium and calcium channels [50].

The binding of ACh to the M3R induces a conformational change, which triggers association with and activation of the heterotrimeric Gq proteins by exchanging GTP for GDP on the Gα subunit. Then, the released Gα subunit activates phospholipase C (PLC) which hydrolyzes phosphatidylinositol 4,5-bisphosphate (PIP_2) into inositol 1,4,5-trisphosphate (IP_3) and diacylglycerol (DAG), IP_3 binds to IP_3 receptors on the endoplasmic reticulum, releasing Ca^{2+} from IC stores whereas DAG activates protein kinase C (PKC) (Figure 1.7) [55–57].

M3R is broadly expressed in the brain, smooth muscles of the blood vessels and lungs [58]. M3R is involved in modulation of neurotransmitter release, temperature homeostasis, and food intake in the CNS, as well as in the induction of smooth muscle contraction, gland secretion and indirect relaxation of vascular smooth muscle in the PNS [38]. In 2012, the X-ray structure of the M3R was reported [59].

M3R consists of seven transmembrane helices architecture as other GPCRs, with N-terminus on the EC side of plasma membrane and C-terminal tail located on the cytoplasmic side. All the helices are connected by either IC or EC loops. Cys141 and Cys221 are responsible for the disulfide bond between the second EC loop and the TM3 helix (Figure 1.8) [60,61].

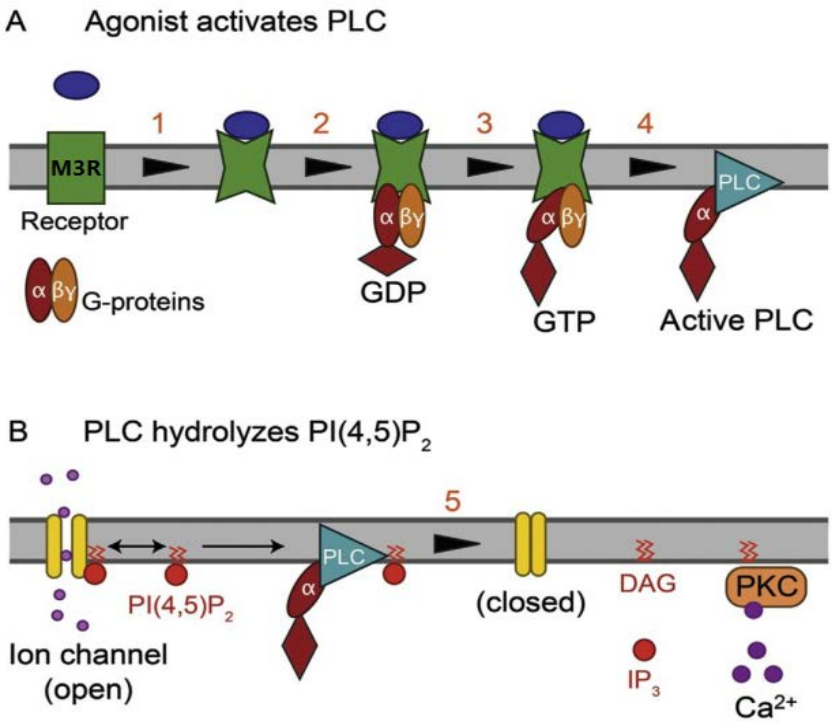

Figure 1.7 Schematic cartoon of early steps in the signaling pathway of channel modulation.

A. Agonist ligands bind to the Gq coupled muscarinic receptor and activate the G protein. The G protein turns on the enzyme PLC. B. Active PLC cleaves membrane PIP_2, the ion channel is inhibited as it loses PIP_2, and several second messengers are generated [56].

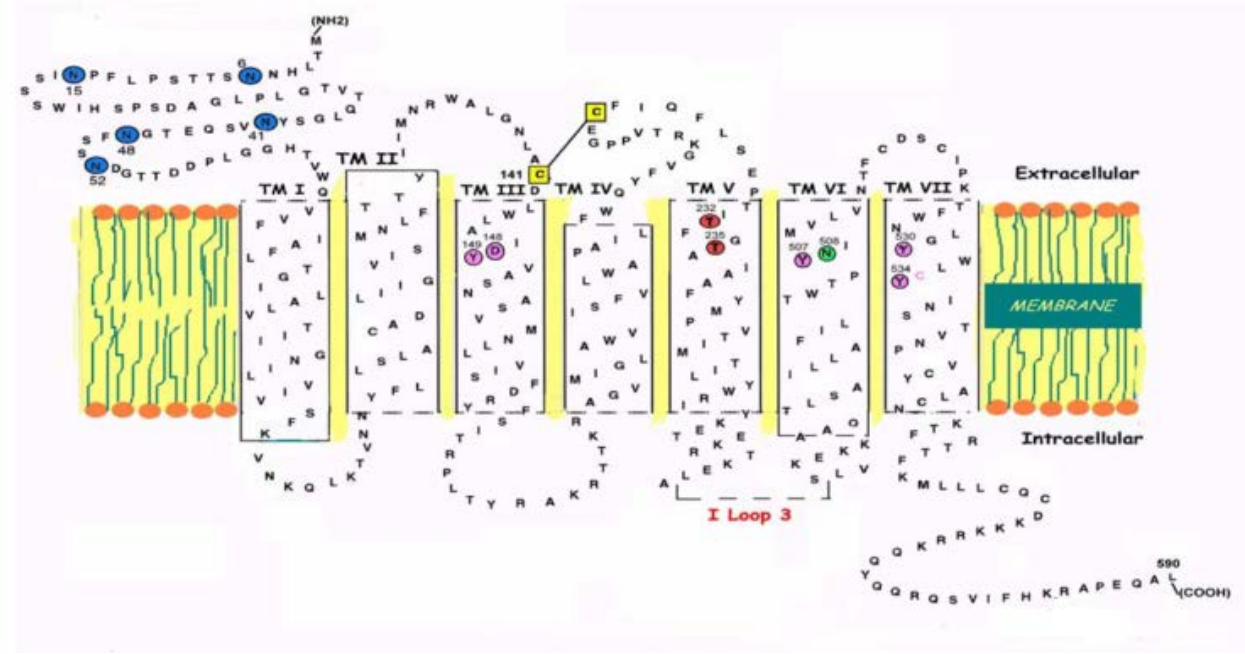

Figure 1.8 Secondary structure of M3R.

Seven transmembrane helices are located in the membrane, N-terminus is located on the EC side of the membrane and the C-terminus is located on the cytoplasmic side. In blue the N-methylglycosilation of the N-terminus, in yellow the cysteine bridge between C141-C221, in red, purple and green the residues of the binding pocket. IC loop

3 in red represents the third IC region that has been removed [60,61].

1.2 Degenerative diseases associated with GPCRs

Considered the largest and the most diverse group, GPCRs are responsible for the proper conduction of many physiological processes, such as vision, IC communication, neuronal transmission, hormonal signaling and also involved in many pathological processes [2,5]. GPCRs are involved in a wide spectrum of hereditary and somatic disorders and diseases such as CNS disorders, inflammatory diseases, cancer, metabolic imbalance, cardiac disease, monogenic diseases and more [62]. The mutations or variations in the genes coding for GPCRs may lead to misfolding, altered expression and activity. When mutations change the process of ligand binding and signal transduction, they frequently lead to disease [5,63].

In the thesis, two GPCRs associated degenerative diseases are studied. One is the retinitis pigmentosa (RP) which is associated to rhodopsin and mutations. Another is the Alzheimer's disease (AD) associated with the M3R and tau protein.

1.2.1 RP

Inherited retinal degenerations and malfunctions are clinically and genetically heterogeneous. Many diseases in this group cause visual loss because of the premature death of the rod and cone photoreceptor cells [64]. Mutations in rhodopsin are one of the main reasons of RP, which is a genetically heterogeneous disorder involving rod photoreceptor cell progressive death and eventually leading to blindness [5,38,65,66]. Epidemiological studies have revealed that RP is heterogeneous both genetically and clinically [67]. More than 150 different mutations in rhodopsin are associated to RP. Approximately 30% of autosomal dominant RP is caused by mutations in rhodopsin [65,68]. Rhodopsin mutants associated with RP could contribute to protein misfolding, increased protease sensitivity, retinal binding impairment and thermal instability [66,69–72], finally alter the cellular fate and induce cell death [66,73]. The worldwide prevalence of RP is about one in 4000 [38,72].

In most of RP cases, the retina degenerates with the rod and cone cell death. Thus, the typical RP can lead to a rod-cone dystrophy, in which loss of rod function exceeds the reduction in cone sensitivity [74]. In the progression of RP symptoms, night blindness generally precedes tunnel vision by years or even decades. At early stage, night blindness is the main symptom and mild

night blindness is often ignored by the patients. There may be peripheral visual field defects in dim light which could not exist or be minimal in day light. In the mid stage, night blindness is obvious, with difficulties to drive and walk during the night. Fundus examination reveals the presence of bone spicule shapes composed of pigment deposits in the mid periphery, along with atrophy of the retina. In the third stage, peripheral vision loss restricts the movements of the patients. The disease progression remains slow and eventually leads to completely blindness [74]. However, in many cases of RP, the dominant gain of misfolded rhodopsin induces degeneration, and some mutants of one allele only lead to visual impairment.

RP can be divided into two groups: non-syndromic RP and syndromic RP [74,75]. Non-syndromic RP is restricted to the eyes, without other systemic manifestations, while syndromic RP is associated with non-ocular disease, the latter representing 20-30% of total cases. On the basis of its inheritance pattern and prevalence, RP can be divided into three main groups: autosomal dominant (30–40%), autosomal recessive (50–60%) and X linked (5–15%). Patients with no other affected relatives are typically autosomal recessive, although a few might represent new dominant mutations, instances of uniparental isodisomy or, for males, X-linked mutations, or even non-Mendelian inheritance patterns [75].

Sector retinitis pigmentosa (sector RP) is an atypical variant of RP. In sector RP, only isolated areas of the fundus show pigmentary changes. It is characterized by regionalized areas of bone spicule pigmentation usually found in the inferior quadrants of the retina, abnormal electro-retinograms, visual-field defects, and slow to no progressive retinal degeneration [76].

Despite of the fact that diverse technical approaches are being investigated for the treatment of RP, there is no standardized and efficient treatment for the disease. Currently, gene therapy represents the most promising therapeutic option for many inherited and acquired retinal diseases [77]. Gene-silencing therapy was used to silence the mutant allele of rhodopsin mutants, but maintaining the expression of the wild type (WT) allele [77]. More advanced lines of research in RP therapy include: the use of neurotrophic factors, gene therapy, cell-based therapy, optogenetics approaches, retinal transplants and electronic prosthesis.

Mutations associated with RP are spread all over the opsin gene throughout the three domains of the receptor: intradiscal, TM and cytoplasmic. The analysis of such mutations associated with RP

provides information about the molecular mechanism of this pathological process. The structural and functional studies on rhodopsin mutants give insights into common structural motifs of GPCRs and common activation mechanisms [78]. TM1 and TM2 play an important role in the stability and function of rhodopsin. RP mutations on rhodopsin show different structure and function characters. Some rhodopsin mutants, like G90V and N55K, present thermal sensitivity. This low stability could affect the rhodopsin cycle of intermediates, altering the normal rhodopsin turnover and prompting receptor malfunction and aggregation [70,79].

1.2.2 AD

AD is diagnosed by the progressive loss of cognitive function and behavioral deficits and is characterized by the presence of senile plaques, neurofibrillary tangles, cholinergic neuron loss and the decrease of ACh neurotransmitter level in the brain (Figure 1.9) [80,81].

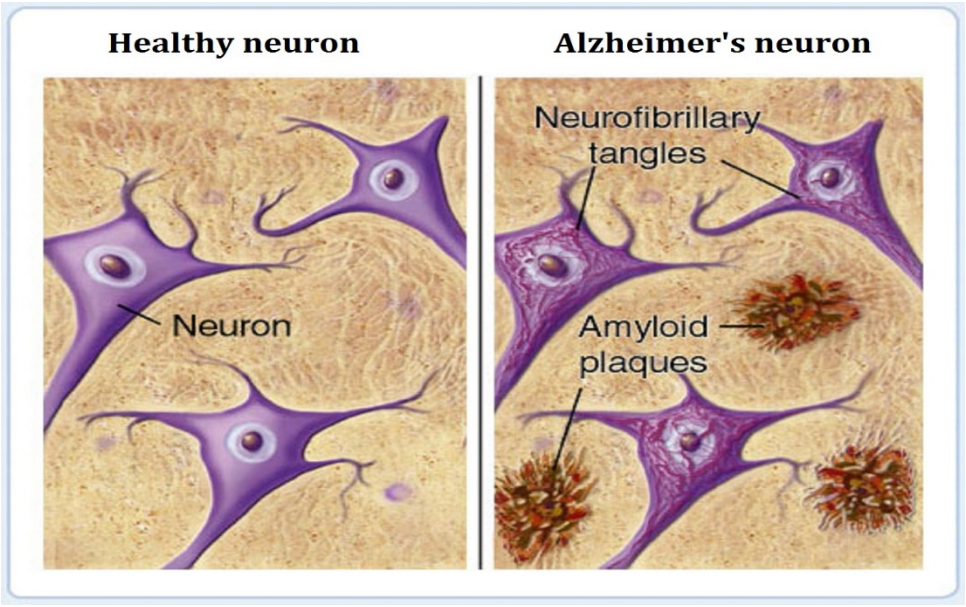

Figure 1.9 Healthy and AD neurons.

Healthy Neuron (left), neurofibrillary tangles, amyloid plaques in AD (right) (Referred from http://www.ahaf.org/alzheimers).

Senile plaques consist of small β-amyloid peptides which are deposited in the brain and cause the primary stage of AD [82,83]. Neurofibrillary tangles affecting neuron degeneration are formed by the accumulation of microtubules and hyperphosphorylated tau protein which is a microtubule binding protein that stabilizes the microtubule and facilitates fast axonal transport. The tangles also affect neuron degeneration in AD [82,83]. Another AD character is the neurotransmitter cholinergic ACh hypofunction linked with β-amyloid and tau pathologies [84–87].

Muscarinic acetylcholine receptors (mAChRs), as the major receptor group for ACh in the neurotransmission, have also been implicated in the pathophysiology of AD. Some studies indicate that the interaction between mAChRs and tau protein could be part of an underlying molecular mechanism causing AD.

By the different characterizations, there are mainly three hypotheses in AD: cholinergic hypothesis of memory dysfunction, the muscarinic receptor regulation of amyloid metabolism and the tau hypothesis. This thesis tries to find some clues between mAChRs associated with amyloid metabolism and tau protein. In AD, abnormal phosphorylation/hyperphosphorylation decreases tau affinity for microtubules resulting in the trafficking of tau proteins from the microtubules to the IC neuronal space. This makes the microtubules unstable and initiates their collapse. The hyperphosphorylated free tau proteins move down the axon from where they dissociate from the microtubules and self-aggregate in the neuron cell body forming neurofibrillary tangles [88]; these tangles usually impair axonal transport causing the dysfunction of the synapse and leading to neuronal death (Figure 1.10).

Recently, AD has been associated with the interaction between EC tau and M1R/M3R that could play a role in the loss of cholinergic neurons [89]. During neuron death, IC tau released to the EC area could interact with surface receptors such as M3R of the neuronal cells and cause calcium increase due to calcium permeable channels. M3R has been involved in the interaction with EC tau that are responsible for raising IC calcium [90]. In this thesis, tau will be overexpressed in cell culture and its interaction with specific M3R mutants will be studied.

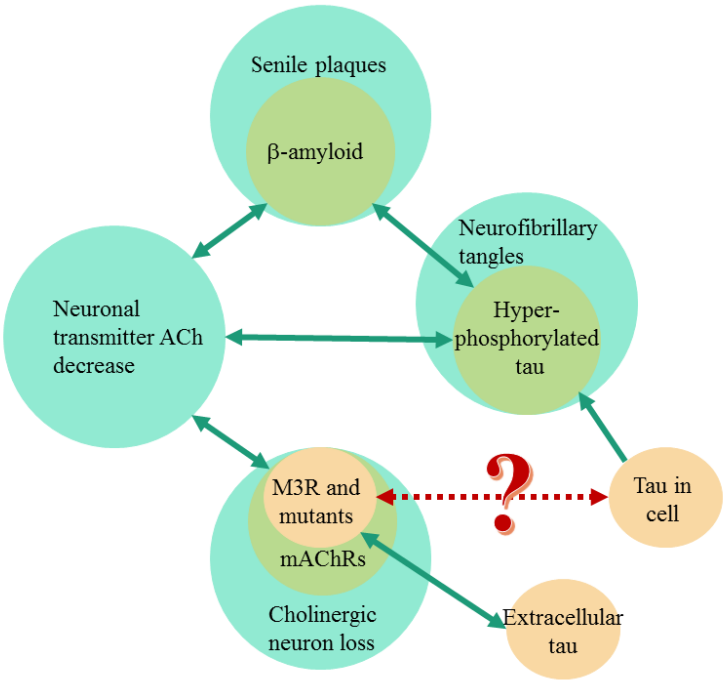

Figure 1.10 Proteins associated with AD.

There are four main players (cyan circles) in AD. Proteins such as β-amyloid, hyperphosphorylated tau and mAChRs are the responsible for AD phenotype. Tau in the cell becomes hyperphosphorylated and is one of the proposed causes of AD. In this thesis the interaction between overexpressed tau and M3R WT or M3R mutants will be investigated.

1.3 Rhodopsin conformational stability

As the largest and most diverse group of membrane proteins in mammals, GPCRs respond to a variety of endogenous and exogenous ligands to regulate physiological processes. GPCRs also interact with membranes lipids which modulate the G protein binding process. GPCRs conformational stability and functional efficiency depend on many factors, such as structural features, salts [91–93], detergents [70,94,95], lipids [96–103] and ligands [104]. In a membrane environment GPCRs naturally function mainly constitute of proteins, lipids and cholesterol. To study the structure and function relationships of GPCRs, the protein has been dissociated and extracted from the membrane and dissolved into detergent, or alternatively studied in native membrane [91,105,106].

1.3.1 Detergents

Detergents are compounds with amphipathic properties with the occurrence of a polar head group and hydrophobic tail in the same molecule [107]. They are the most commonly used strategy for extracting, purifying and dissolving membrane proteins. In order to achieve optimum

solubilization of membrane proteins, nonionic and zwitterionic detergents are particularly popular to solubilize membrane proteins keeping their function. 3-(3-Cholamidopropyl dimethylammonio)-1-propanesulfonate hydrate (CHAPS) and *n*-dodecyl-β-D-maltoside (DM) are the main members of this class of detergents (Figure 1.11).

CHAPS is a mild, non-denatured, and zwitterionic detergent (Figure 1.11A). CHAPS has low absorbance at 280 nm and lacks of circular dichroic signature in the far-UV region, thereby making it an ideal detergent for studies of membrane proteins using optical spectroscopy. For this reason, CHAPS is widely used in solubilizing membrane proteins including GPCRs [106,108]. DM is also widespread used in solubilization and purification of diverse functionally active membrane proteins. As a mild, non-ionic detergent with a low critical micelle concentration (CMC), DM forms by an intermediate length of the hydrophobic moiety and a bulky hydrophilic sugar headgroup that has been found to be effective in solubilizing GPCRs (Figure 1.11B). The CMC of DM in water is 0.17 mM (0.009%, w/v). Above the CMC, DM micelles form ablate ellipsoids where the polar axis is shorter than the equatorial axes that are essential to form crystal contacts [106,109]. For several GPCRs, DM micelles offer the advantage of preventing membrane protein aggregation. However, this limits the structural studies since DM masks the proteins to a large extent in protein detergent complexes.

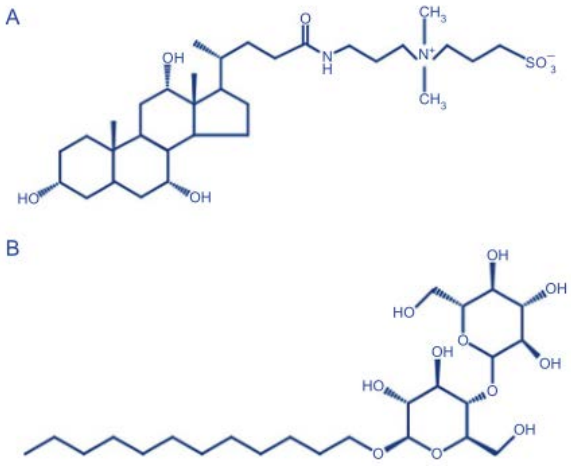

Figure 1.11 Chemical structures of detergents commonly used for solubilization of GPCRs.

A. CHAPS and B. DM.

1.3.2 ROS disk membrane lipid composition

Cell plasma membranes are composed of lipids and proteins. Lipids make the membrane nearly

impermeable to most water-soluble solutes, and proteins serve as transporters and signaling devices. The membrane lipids are arranged with polar or charged head groups oriented towards the aqueous environment and acyl chains interacting within the hydrophobic membrane core [98]. The membrane proteins activity is influenced at the lipid-protein interface surrounded by a lipid matrix. Cholesterol, cardiolipin, and phospholipids such as phosphatidylcholine (PC), phosphatidylethanolamine (PE), phosphatidylserine (PS) and phosphatidylinositol (PI) affect the protein function by changing the properties of the lipid-protein interface, membrane fusion, and the freedom of movement of phospholipid acyl chains and proteins [98].

In the ROS, the phospholipids composition of the stacked disks is shown in Table 1.1. Phospholipids are formed by different fatty acids, mainly 16:0, 18:0, and 22:6 with different head groups (PC, PE and PS). The average of disk membrane phospholipid composition is approximately of 44% PC, 41% PE, 13% PS, and 2% PI [98,110].

Cholesterol is a representative lipid in higher eukaryotic cellular membranes and is crucial in membrane organization, dynamics, function, and sorting [111]. By far cholesterol is the major sterol in the retina. In plasma membrane and in the newly synthesized disk, cholesterol presents the highest level with almost 40%. Cholesterol is rapidly lost when disks are apically displaced retaining only 5% in the membrane [98,111,112].

Docosahexaenoic acid (DHA, 22:6n-3) is the major and conserved fatty acid in the retina, accounting for over 50% of the phospholipid hydrocarbon chains in the disk membranes and 43% of ROS which is much higher than in plasma membrane [98]. DHA promotes the formation of Meta II from Meta I. The 16:0 fatty acyl chain in PC dramatically decreases whereas the 22:6 (DHA) fatty acyl chain increases with disk age. The increase in unsaturated lipids in the disk is apically displaced further causing the depletion of cholesterol during spatial displacement.

Table 1.1 Phospholipid composition of ROS.

The fatty acid composition in the different polar heads forming PC, PE, and PS. Fatty acids making up less than 0.3% in any fraction are omitted. Values are averages with standard deviation from five preparations [98].

		Outer segments	Phosphatidyl choline (PC)	Phosphatidyl ethanolamine (PE)	Phosphatidyl serine (PS)
Phospholipid composition			30.6 ± 1.5	44.1 ± 1.6	15.2 ± 0.9
Fatty Acids	**16:0**	19.9 ± 0.3	30.6 ± 2.2	12.6 ± 0.3	4.1 ± 0.4
	18:0	22.1 ± 0.6	19.4 ± 1.0	25.0 ± 0.4	21.0 ± 1.1
	18:1 ω9	3.3 ± 0.1	4.5 ± 0.5	4.2 ± 0.1	1.5 ± 0.4
	18:2 ω6	< 0.1	0.9 ± 0.1	0.9 ± 0.1	< 0.1
	20:4 ω6	4.8 ± 0.1	2.7 ± 0.1	2.4 ± 0.1	4.3 ± 0.5
	22:4 ω6	1.6 ± 0.1	0.4 ± 0.1	0.8 ± 0.1	3.0 ± 0.2
	22:5 ω6	2.3 ± 0.1	0.9 ± 0.1	1.5 ± 0.1	1.6 ± 0.3
	22:5 ω3	1.9 ± 0.2	1.4 ± 0.1	1.4 ± 0.1	3.3 ± 0.2
	22:6 ω3	43.0 ± 0.4	35.9 ± 2.2	50.2 ± 0.8	48.1 ± 0.8
	24:4	1.2 ± 0.1	< 0.1	< 0.1	3.9 ± 0.4
	24:5	1.2 ± 0.1	< 0.1	< 0.1	9.3 ± 0.7

1.3.3 Artificial membranes

Even though detergents can form micelles to solubilize GPCRs, they often show poor conformational stability, low activity and even denatured character [97,98,113]. In the native membranes, the lipids such as cholesterol and DHA interact with membrane proteins and help maintaining protein structure and function. Lipid bilayer environment is essential and affects the physical and chemical properties of GPCRs. Understanding the molecular mechanism of GPCRs in a native-like environment will have a large impact on both basic knowledge of cell signaling and pharmacological research [100,102,110,114–116]. Different lipids and membrane-mimic phases are used for GPCRs, especially for rhodopsin reconstitution. Currently, the classes of mimetic

membrane systems mainly include micelles, bicelles, liposomes, nanodiscs (or nanocarriers) [117], planar lipid membranes and lipid cubic phases [118].

1.3.3.1 Micelles

Detergent monomers in aqueous solutions self-associate to form a basic phase called micelles. At a broad threshold of monomer concentration called the CMC, self-association occurs and micelles form (Figure 1.12A). A variety of detergents is available for studies of GPCRs, and obviously the choice must fall on a detergent that is gentle enough to avoid immediate denaturation of the protein such as DM. Mixed micelles are also formed by a mixture of detergents or a mixture of detergent and lipid to stabilize the protein. Compared with the native membrane, many detergents irreversibly denature membrane proteins and provide interferences and background problems with the protein in spectroscopic measurements [119]. Once added into the native membrane-protein complex, the detergents start to perturb the membrane and separate the proteins from the membrane. With increasing concentration of detergent, the protein can be embedded in the detergent micelles [106].

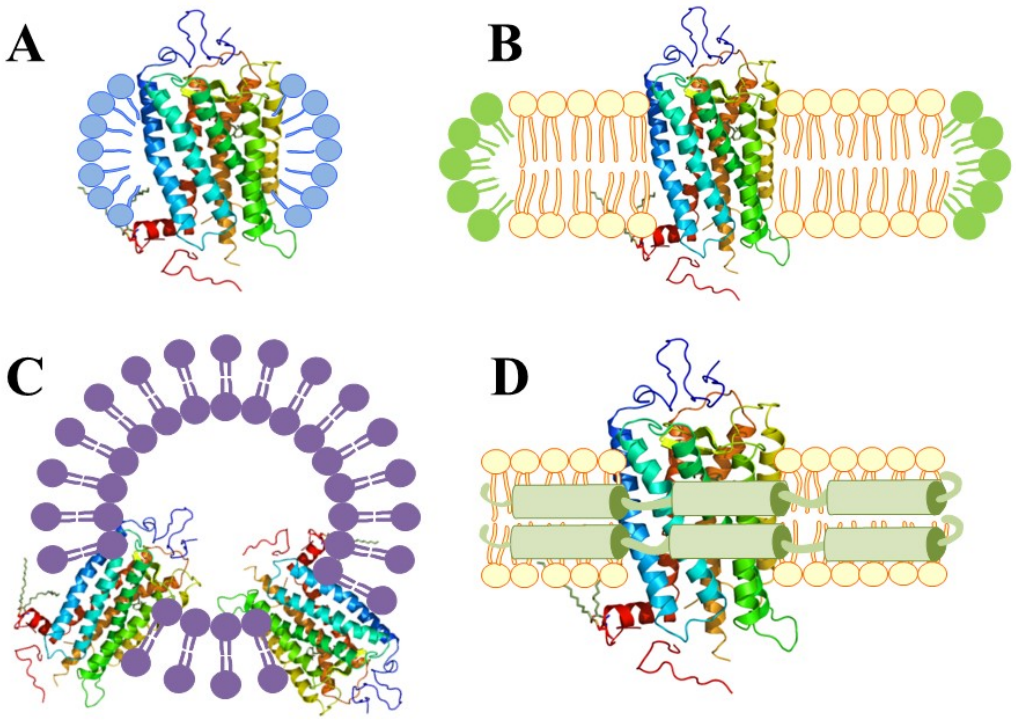

Figure 1.12 Schematic models for rhodopsin in micelles, bicelles, liposomes and nanodiscs.

A. Schematic model for DM micelles containing rhodopsin. B. Rhodopsin in bicelles. C. Rhodopsin in liposomes. D. Rhodopsin in nanodiscs.

Figure 1.13 shows the standard process of GPCRs solubilization by detergents. The presence of the detergents and lipids may interfere with normal ligand and/or G protein binding. Furthermore, the detergents increase the risk of destabilizing or denaturing GPCRs. Considering all the drawbacks of detergents, the artificial membrane, in principle, is a more desirable model system for characterization studies [118,119].

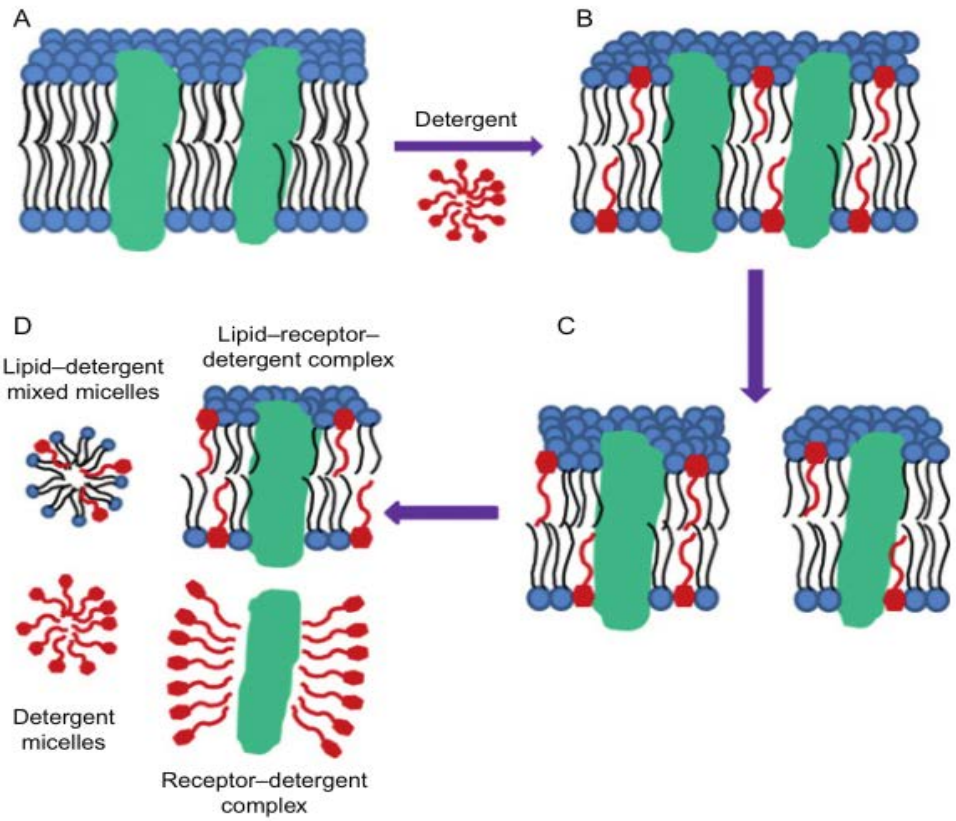

Figure 1.13 Schematic representation of different stages for the solubilization of biological membranes by detergents.

A. GPCRs are embedded in biological membranes. B. Detergent at low concentrations is added to interact with the membrane and cause membrane perturbation. C. The membrane bilayer is further perturbed because of the increasing detergent concentration. D. Addition of detergent concentrations above CMC, the complexes of detergent, lipid, and receptors are formed. Finally the four possible complexes are lipid-detergent mixed micelles, lipid-receptor-detergent complex, receptor-detergent complex and detergent micelles [106].

1.3.3.2 Bicelles

Bicelles morphology is hallmarked by a disk-like bilayer composed of long chain phospholipids that are capped by either short chain phospholipids or detergents [120,121]. Bicelles offer distinct advantage over other artificial membrane models since they can be easily prepared obtaining high yields. Additionally, bicelles do not interfere with the majority of biophysical measurements and increase the stability of purified GPCRs compared to solubilization in detergents. The structure of bicelles is highly dependent on lipid composition, temperature, pH and hydration, and the biochemical properties can be influenced by phospholipid specific differences in chain lengths, saturation, and head groups. Figure 1.12B shows the models for rhodopsin in bicelles [121].

1.3.3.3 Liposomes

A liposome is a spherical vesicle having at least one lipid bilayer. The liposomes have been widely used for many applications, from membrane models to drug delivery systems [122]. Liposomes normally are composed of phospholipid, especially PC to form the lipid bilayer structure. Normally the liposomes provide a better physiologically relevant milieu to stabilize the protein [97,118]. 1,2-didocosa-hexaenoyl-*sn*-glycero-3-phosphocholine (DDHA-PC) is an unsaturated phospholipid and constitutes membrane-like bilayers to carry rhodopsin. Liposomes provide a stable bilayer that strengthens protein-protein interactions [97,102,118] (Figure 1.12C). The study of rhodopsin mutants in DDHA-PC liposomes may help to understand the structural and functional mechanisms of RP and retinal degeneration.

1.3.3.4 Nanodiscs

Nanodiscs are small patches of membrane bilayer whose edge is stabilized by high density lipoprotein (HDL) or nanoscale apolipoprotein bound bilayers. These have been shown to incorporate 1 to 2 rhodopsin molecules and have excellent stability properties (Figure 1.12D) [117,118]. Nanodiscs structure is compact and decrease the number of freely diffusing lipids or detergent molecules. All these features permit high protein concentration per volume, enabling bulk spectroscopic measurements. One drawback of nanodiscs is the strict limit on the diameter of the particles [113,117,118].

1.3.3.5 Planar lipid membranes

Planar lipid membranes can be subdivided into two broad classes. The first, a lipid bilayer covering a small aperture between two aqueous phases, is referred to as a black membrane; the second class consists of solid support planar lipid membranes. The planar lipid membrane represents a trade-off between stability and versatility. The interaction with EC loops or domains of GPCRs with the solid support may interfere with the mobility or even the activity [118].

1.3.3.6 Lipid cubic phases

Lipid cubic phases are sponge-like, multilamellar, continuous lipidic phases perforated by aqueous channels supplying an ordered hydrophobic matrix that permits free diffusion of protein and encourages GPCR crystallization in three dimensions. The lipid cubic phases have been

limited to preparing crystals in GPCRs research. The system represents an intriguing possibility both as a possible vehicle for reconstituted GPCRs and as a replacement for detergents in the difficult process of GPCR purification [118].

1.4 Two artificial membrane systems

1.4.1 DMPC/DHPC bicelles

Phospholipids constituting ROS are the best options to form the artificial membranes. To stabilize rhodopsin and its mutants, the head groups, such as PC, PE, PS and PI and the fatty acid chains with different lengths and saturations have an impact on the biochemical properties of the artificial membrane. 16:0, 18:0, and 22:6 (DHA) are the main fatty acid chains in the rod disk. Other phospholipids 1,2-dimyristoyl-*sn*-glycero-3-phosphate (DMPA), 1,2-dimyristoyl -*sn*-glycero-3-phosphocholine (DMPC), 1,2-dimyristoyl-*sn*-glycero-3-phospho-1'-rac-glycerol (DMPG), 1,2-dimyristoyl-*sn*-glycero-3-phospho-L-serine (DMPS), 1,2-dioleoyl-*sn*-glycero-3-phosphocholine (DOPC) and 1,2-dioleoyl-*sn*-glycero-3-phosphoethanolamine (DOPE) [35,121,123–126] are also used for artificial membranes. The use of phospholipids with single or mixture of lipids at different ratios increases the diversity of the membranes.

For bicelles composition, short-chained phospholipids such as 1,2-dihexanoyl-*sn*-glycero-3-phosphocholine (DHPC(6:0)) or detergents like CHAPS are used to cap the long chain phospholipids. Phospholipid bicelles have been shown to improve the stability of rhodopsin [35,120,121]. In order to improve the stability of G90V and N55K rhodopsin we have introduced these mutants in bicelles. To do that, saturated 1% (w/v) long chain DMPC (14:0) and 1% (w/v) DHPC detergent are mixed, and upon temperature exchange process bicelles are formed.

1.4.2 DDHA-PC liposomes

DDHA-PC consists of two DHA chains and one PC head group which accounts for 44% in disk membrane. DHA appears to optimize the retinal integrity and visual function [97,127–129]. DDHA-PC is used to form liposomes which constitute a membrane-like bilayer suitable for the study of rhodopsin and its mutants [97,102,118]. The comparison of the structural and functional features of rhodopsin mutants, inserted into DDHA-PC liposomes and in DM detergent, would be attractive to understand the molecular mechanisms of RP disease. NMR studies have proved

that DHA can interconvert between conformations more rapidly, and prefers to be in the hydrophobic core of bilayers near the lipids/water interface. DHA is also capable of engaging in partially specific interactions with rhodopsin. Bilayers rich in DHA may alter protein function both by a change of general membrane properties and by specific interactions with particular regions of the protein. Rhodopsin adjusts its structure far more nimbly to the lipid environment than generally assumed. It is not just the lipid matrix that deforms in response to the needs of the protein, but the protein may adjust structurally to the lipid matrix as well [130,131]. Figure 1.14 shows the crystal structure of rhodopsin (1U19) where the packing score for each residue in rhodopsin against DHA, stearic acid, and cholesterol in bilayers were computed. The result showed the overlapping groups between H6 and H7 are largely nonspecific for DHA, stearic acid, and cholesterol. Except this, DHA (blue) interaction with 51 residues is significantly higher than that for stearic acid (red) with 16 residues and cholesterol (purple) with 5 residues.

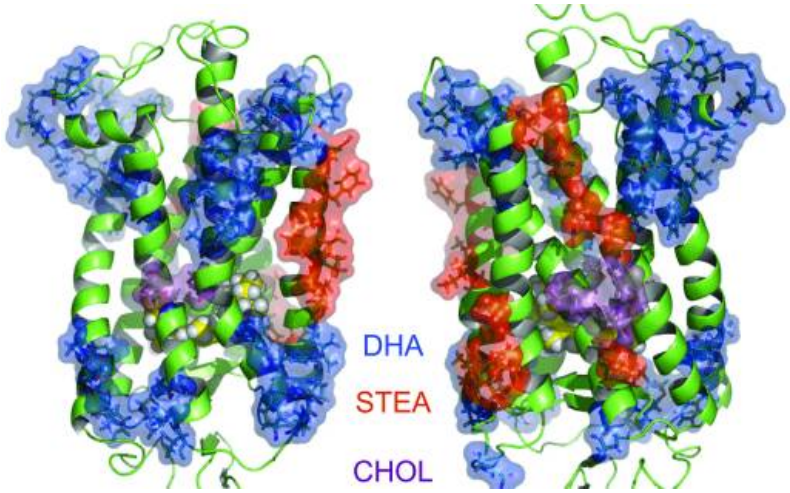

Figure 1.14 Binding sites of stearic acid, DHA and cholesterol in rhodopsin.

Rhodopsin interacts preferentially with DHA (22:6) (blue), stearic acid (18:0) (red) or cholesterol (purple). The preferential interaction sites were identified by means of molecular dynamics simulations [130,131].

1.5 GPCR Interaction with other proteins and ligands

1.5.1 Signaling through GPCRs

Heterotrimeric G proteins constitute important components of cell signaling cascades. GPCRs senses many EC signals and transduce them to the G protein for the downstream signals to play important roles in various signaling pathways. Upon activation by the ligand, the GPCRs undergo a conformational change and activate the G protein by promoting a GDP/GTP exchange in the Gα subunit. Gβγ dimer dissociates from the Gα subunit and both units interact with

different specific effectors and initiate unique signaling responses. Once the GTP in the binding pocket of Gα-GTP is hydrolyzed to GDP, Gα returns to its inactive Gα-GDP state which will re-associate with Gβγ to form the inactive heterotrimeric complex (Figure 1.15) [5,14,132].

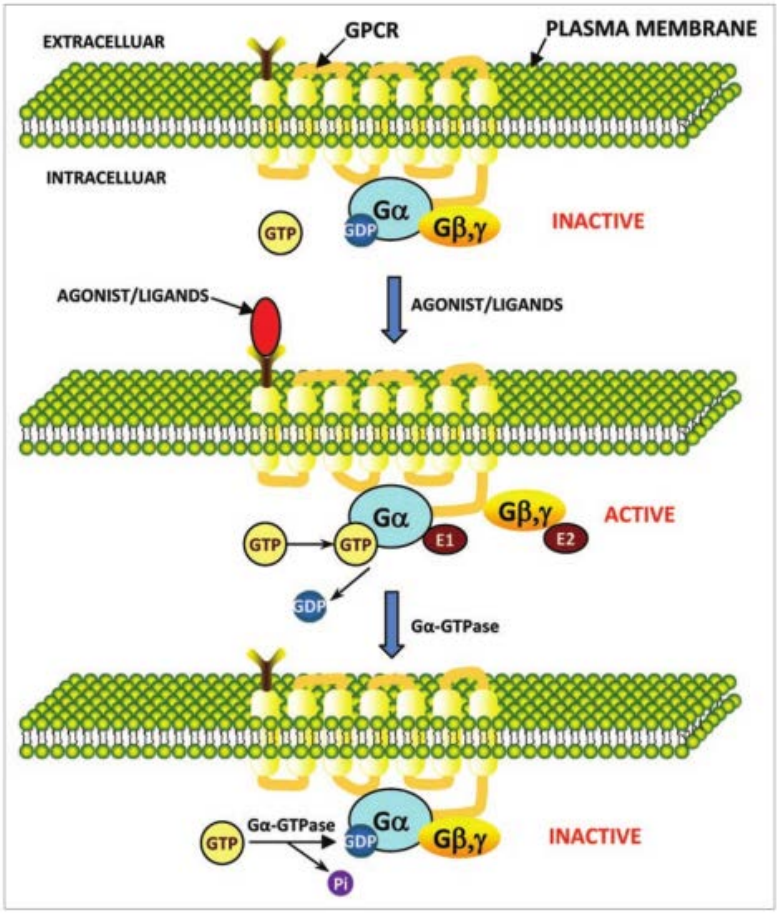

Figure 1.15 Model for signal transduction by activation/inactivation of the heterotrimeric G protein through GPCR activation.

The subunits of heterotrimeric G protein (Gα and Gβγ) in their inactivated states are associated with each other. In the inactivated state, GDP is bound to Gα (Gα-GDP). During signal transduction, first the GPCR is activated, changing its conformation due to the binding of agonist/ligand to the EC region. This activated GPCR further activates the G protein by dissociating the Gα from Gβγ. In the active state, GTP is bound to Gα (Gα-GTP). Now free Gα and Gβγ have their own effectors (E1 and E2, respectively) to further transmit the signals and initiate unique IC signaling responses. Signal transduction is terminated when Gα-GTPase activity hydrolyzes the bound GTP to GDP and Pi and the G protein complex is reformed by Gα binding to Gβγ [14].

1.5.2 A model GPCR system: rhodopsin-arrestin interaction

As a model of GPCRs, understanding rhodopsin signaling and its dynamic protein-protein interactions is very important. Upon photon absorption, the photoactivated conformation of rhodopsin, Meta II, binds to and activates the Gt, which exchanges the GDP/GTP nucleotide and

then interacts with other downstream effectors. Meta II decays to free opsin by releasing the retinal chromophore from the binding pocket. Signaling is terminated by a process that begins with phosphorylation of Meta II by rhodopsin kinase and binding of arrestin, which stops signaling by physically occluding the G protein binding site [133]. Visual arrestin belongs to the arrestin superfamily, which includes rod and cone arrestins. This visual arrestin, a ~48 kDa soluble protein, is an important model system to understand not only the visual response but also the broad reaching mechanism for controlling cellular signal transduction cascades mediated by GPCRs [134]. The loop V-VI of arrestin is an important element that moves while arrestin binds to activated receptor. This movement is essential for high affinity binding [134,135]. Figure 1.16 shows the crystal structure of human rhodopsin in complex with visual arrestin [136].

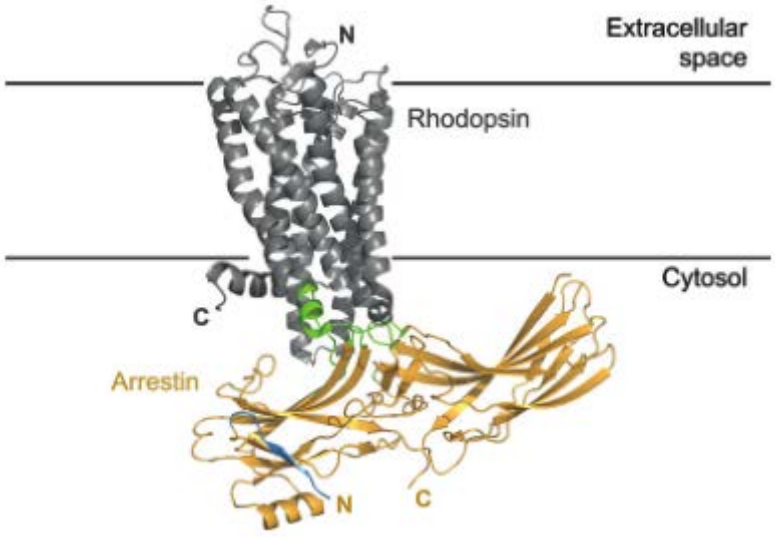

Figure 1.16 Crystal structure of human rhodopsin in complex with visual arrestin.

The interaction regions on rhodopsin and arrestin (PDB 4ZWJ) are highlighted in green.

Figure 1.17 shows the signal pathway of rhodopsin with arrestin. The rhodopsin is activated by the light to form Meta I/II state and desensitized by the arrestin. This arrestin binds components of the clathrin endocytic machinery including clathrin, β2-adaptin (AP2) and dynamin (Dyn) to form the endosomal vesicle carrying the Meta II-arrestin complex dissociates from arrestin upon internalization and receptors recycle to the plasma membrane [137].

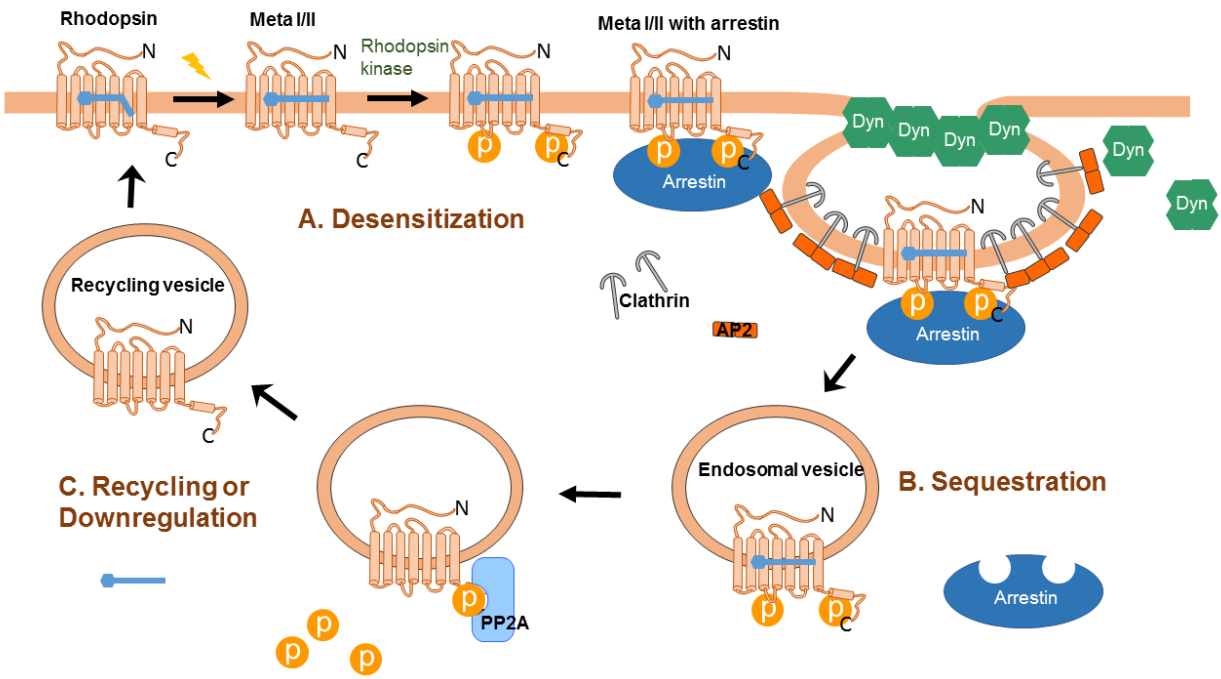

Figure 1.17 Role of arrestin in the desensitization, sequestration and IC trafficking of rhodopsin.

A. Rhodopsin is activated and desensitized by arrestin. Meta I/II-arrestin complex play an important role as adapter proteins, binding to components of the clathrin endocytic machinery such as clathrin and AP2. B. Receptor sequestration reflects the Dyn dependent endocytosis of rhodopsin via clathrin coated pits. C. Rhodopsin dissociates from arrestin for final degradation or slow recycling to the membrane [137,138].

In the visual pathway, arrestin not only attenuates rhodopsin signaling, but also protects the cell from excessive retinal levels under bright light conditions. Besides, arrestin is known to bind to phosphorylated Meta II, in which the photolyzed chromophore all-*trans*-retinal is still attached by a deprotonated SB. In contrast, arrestin does not bind to phosphorylated opsin, only all-*trans*-retinal added exogenously can stimulate arrestin to bind this phosphorylated opsin [139].

1.5.3 Tau protein interaction with M3R

Tau is a structural microtubule associated protein (MAP) which is located in the axons of neurons of the CNS. MAP tau (MAPT) contains three major domains: an amino terminal projection domain, a C-terminal domain of microtubule binding repeats and a short tail sequence [140]. In the human CNS, six tau isoforms are found by alternative mRNA splicing [140] from the tau gene encoded on chromosome 17q21. These Tau isoforms differ in their domain composition and overall length ranging from residue 352 to 441 amino acids [141]. Tau is a highly soluble, natively unfolded, and intrinsically disordered protein, with only a low content of transient secondary structure. Tau, as other MAPs, stabilizes microtubule polymers, suppresses microtubule

dynamics and probably because of these effects is able to promote cytoplasmic extensions or neuritogenesis (Figure 1.18) [142–144].

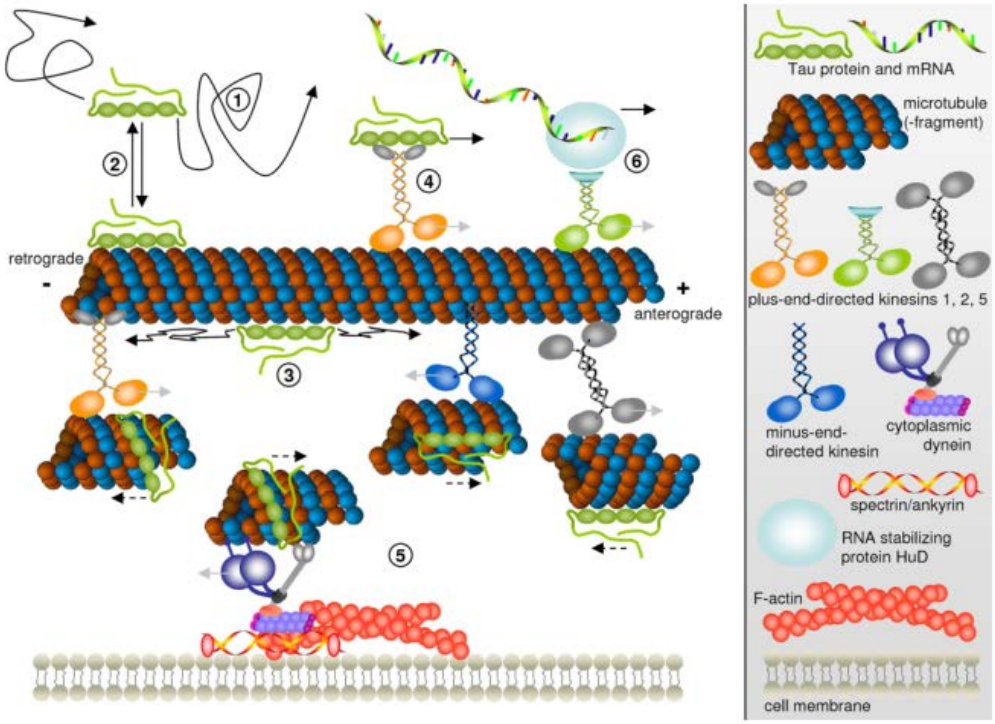

Figure 1.18 Proposed mechanisms of tau dispersion in cells.

Free diffusing tau molecules in the cytosol (1) in rapid equilibrium with tau bound to microtubules; (2) tau is free to diffuse along the microtubule lattice; (3) motor-dependent tau transport by kinesin molecules; (4) or piggybacking on short microtubule fragments translocated by kinesin family members or cytoplasmic dynein; (5) transport of tau mRNA by kinesin-2 followed by local translation in the axon; (6) light gray arrows indicate the directions of motor protein movement while solid black arrows denote the directions of tau protein or mRNA motion by diffusion or as cargo of kinesin motor proteins [143].

As explained in section 1.2, tau protein and M3R are both involved in AD [145,146]. Currently, the tau hypothesis of AD presumably involves abnormal hyperphosphorylation of tau as a result of an imbalance in the kinase and phosphatase activities. In AD brains, the total tau level is about eight-fold higher than in controls and the increased tau protein is in an abnormally hyperphosphorylated form [86]. The reason of this is not well understood. As a MAP protein, tau molecules contribute to maintaining the cell shape and serve as tracks for axonal transport. In neural cells of AD patients, the phosphorylation of tau takes place in some sites causing a decrease of the protein electrophoretic mobility [147]. Tau can undergo two types of modifications, phosphorylation and aggregation, which can regulate its interaction with cytoplasmic, nuclear, or membrane components resulting in cell toxicity [148]. The phosphorylation of the N-terminal

region could affect its interaction with the plasma membrane. The phosphorylation in the microtubule binding domain, and its adjacent regions, will impair the interaction of tau with microtubules, as well as prevent tau-tau self-assembly. Phosphorylation at the C-terminal region affects the interaction of tau with other proteins, like muscarinic receptors [144,148].

Tau hyperphosphorylation can induce tau aggregation which is toxic for the cell (Figure 1.19) [89]. IC tau could be toxic due to its hyperphosphorylation level or due to its aggregation. The tau protein released as a result of neuronal death is toxic to neighboring cells, an effect that is thought to be mediated through the activation of muscarinic M1R or M3R receptors that increases IC calcium in neuronal cells upon tau binding [89].

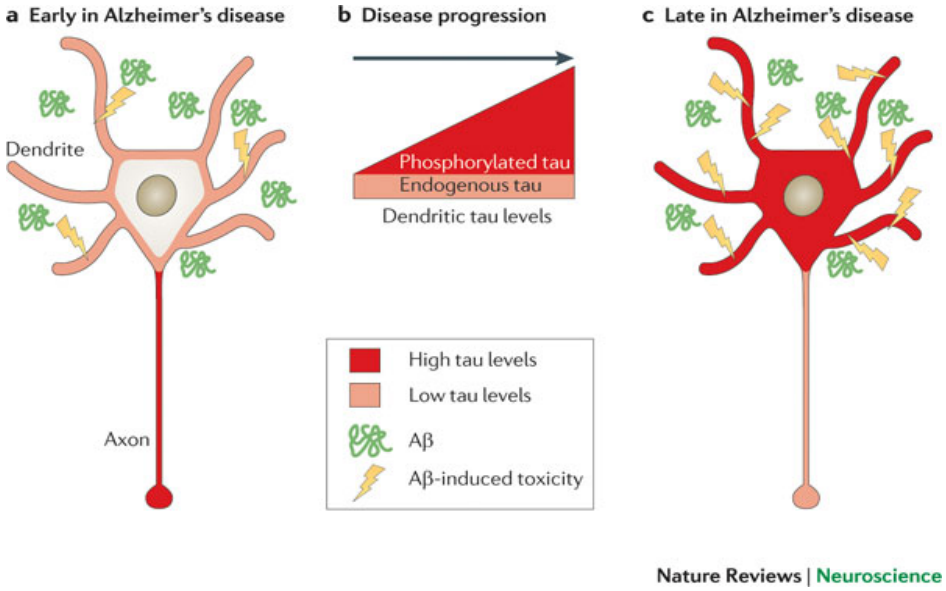

Figure 1.19 Proposed tau axis hypothesis of AD: progressively increasing levels of dendritic tau make neurons vulnerable to β-amyloid.

A. The onset of AD is characterized by the initiation of β-amyloid formation in the brain. But low levels of dendritic tau are associated with a limited vulnerability of neurons to synaptic β-amyloid toxicity. B. With disease progression, tau becomes increasingly phosphorylated and tau accumulates in the somatodendritic compartment of neurons, progressively increasing dendritic tau levels. C. In fully manifested AD, high levels of tau are in the dendritic compartment and increased β-amyloid toxicity exacerbates tau phosphorylation and its somatodendritic accumulation [140].

Indeed, exogenously applied non-phosphorylated tau can also interact with muscarinic receptors on the surface of cultured neuronal cells, promoting an increase in IC calcium that can alter cell signaling pathways [90]. In this thesis, four M3R mutants at the EC domain of the receptor, N132G, D518N, D518K and K523Q, were coexpressed with tau in cultured cells to analyze their potential interactions.

M3R residues N132, D518 and K523 are all located at the EC loops of the receptor and they are predicted to play a role in the binding and regulation of allosteric modulators. The mutants N132G and D518K were chosen because the substituted residues were those corresponding to the M1R subtype. As the amino acids D518 and K523 are charged, the uncharged mutants D518N and K523Q, were also contacted in order to analyze any possible charge effect [149].

2. OBJECTIVES

The main aim of the thesis is to investigate the intramolecular and intermolecular aspects of two GPCRs, the visual receptor rhodopsin and the muscarinic receptor. Intramolecular aspects include protein folding and stability, while intermolecular aspects are related to the interaction of these receptors with associated proteins. For this purpose, the stability and folding properties of WT rhodopsin and N55K and G90V mutants and the interaction between rhodopsin and arrestin, as well as M3R interaction with tau protein are studied.

Rhodopsin and two RP associated mutants will be spectroscopically and functionally characterized and their behavior in detergent micelles and in mimic membranes compared. DM micelles, DMPC/DHPC bicelles and DDHA-PC liposomes will be used to stabilize purified bovine rhodopsin and recombinant rhodopsin WT and the G90V and N55K mutants. The thermal stability and retinal binding behavior of rhodopsin and its mutants, and their Gt activation capacity will be analyzed.

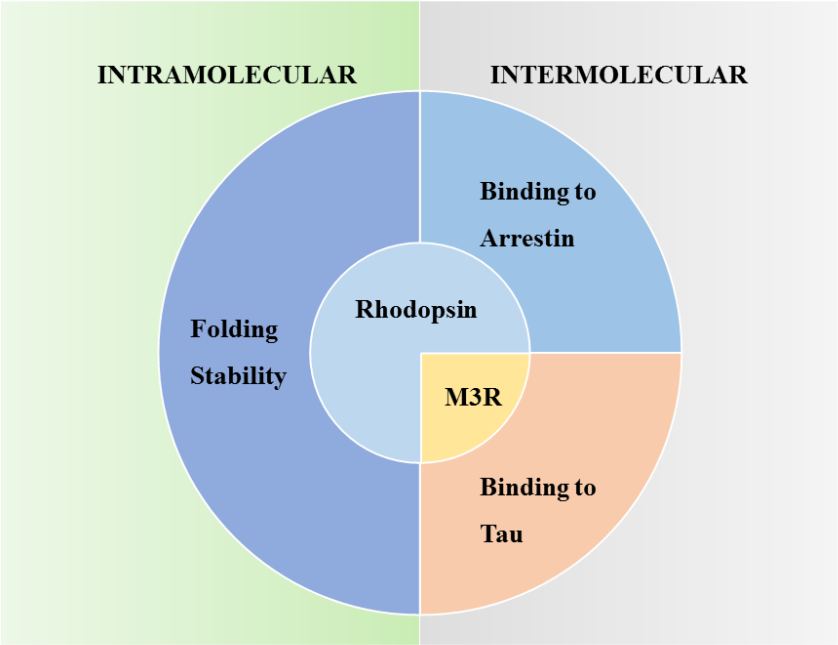

Figure 2.1 Study proposed in this thesis.

The visual protein rhodopsin and mutants and the M3R and mutants (in the central circle) are the GPCR studied in this thesis. The outermost circle represent the intramolecular and/or intermolecular studies on rhodopsin and muscarinic receptors performed during this thesis.

We also aim at investigating the mechanisms of GPCRs interaction with other proteins associated to their signaling pathways. The work will focus on two such interactions, rhodopsin binding to arrestin in the signal termination of the phototransduction cycle, and M3R interaction

with tau protein and its potential role in AD. Figure 2.1 schematically summarizes the proposed topics of study of this thesis.

In line with the main goals outlined, the specific objectives of this thesis are:

1. To establish the optimal DMPC/DHPC bicelles and DDHA-PC liposomes system conditions for WT and mutant rhodopsins stabilization.
2. To compare the biochemical and biophysical properties of WT rhodopsin and N55K, G90V mutants in DM micelles, DMPC/DHPC bicelles and DDHA-PC liposomes systems.
3. To purify R175E arrestin mutant and to characterize its binding to photoactived rhodopsin by means of fluorescence spectroscopy and electrophoresis.
4. To express M3R and its mutants, and to coexpress them with tau protein to determine the features of the interaction between M3R mutants and tau protein by means of electrophoretic and immunocytochemical techniques.

3. MATERIALS AND METHODOLOGY

This section describes the materials and the procedure used in this thesis. The molecular biology and biophysical techniques are described in detail to understand the specific features of GPCRs, especially rhodopsin and M3R.

3.1 Materials Reagents

3.1.1 Reagents

Bovine retinas was obtained from J.A. Lawson (Lincoln, NE). The chromophores 11-*cis*-retinal, and 9-*cis*-retinal, were provided by Dr. R. Crouch (National Eye Institute, National Institutes of Health (USA)) and Sigma-Aldrich, respectively. Lipids for liposomes and bicelles formation, DMPC (14:0), DHPC (6:0) and DDHA-PC (22:6n-3) were purchased from Avanti Polar Lipids Inc (Alabaster, AL, USA). DM was from Anatrace (Maumee, OH, USA). Chloroforrn was purchased from Sigma-Aldrich (Sant Louis, MO), methanol was from Panreac (Barcelona, Spain) and the polystyrene beads (Bio-beads SM-2) were provided by Bio-Rad Laboratories, Inc. (Hercules, CA).

Purified monoclonal antibody for rhodopsin, rho-1D4, was obtained from Cell Essentials (Boston, MA, USA). The 1D4 9-mer peptide corresponding to the last 9 amino acids of Rho (TETSQVAPA) was synthesized by Serveis Cientificotècnics (Universitat de Barcelona, Barcelona, Spain). CNBr-activated Sepharose 4B, hydroxylamine, protease inhibitor cocktail and phenylmethanesulfonyl fluoride (PMSF), bis-tris-propane (BTP), isopropyl β-D-thiogalactopyranoside (IPTG) were from Sigma-Aldrich (St. Louis, MO, USA). Polyethyleneimine 25 kDa (PEI) was purchased from Polysciences (Warrington, PA, USA). Other reagents were purchased from Sigma, Fisher or Panreac.

3.1.2 Cloning vectors and cell lines

WT, G90V and N55K opsin mutations were cloned into the pMT4 vector. M3R and mutants M3R-N132G, M3R-D518N, M3R-D518K and M3R-K523Q cloned in pEF5/FRT/V5-DEST vectors were obtained as previously described (Laura Iarriccio’s thesis reference). Arrestin R175E in pG58 vector was provided by Dr. Eva Ramon. Human MAPT/tau transcript variant 4 natural ORF cloned in pCMV3 (HG10058-UT) (Tau-pCMV3) was bought from Sino Biological Inc. Tau gene was also subcloned into pET-17b plasmid. These five vectors containing the

corresponding genes of study are depicted in the following schemes (Figure 3.1).

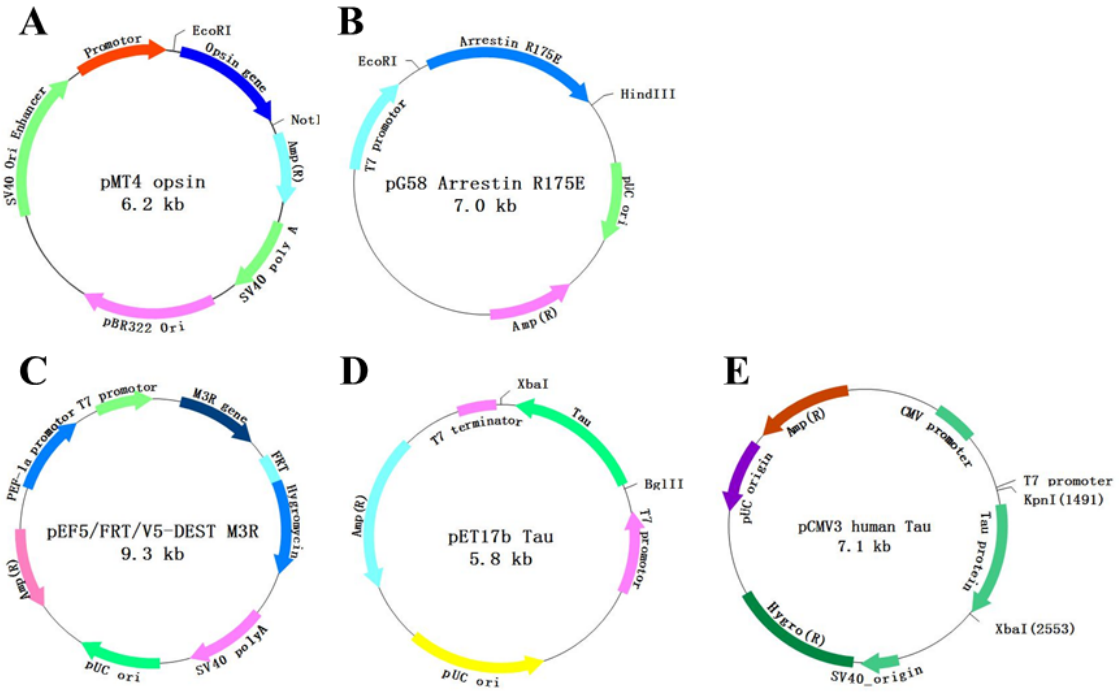

Figure 3.1 The five plasmid vectors used in this thesis.

A. pMT4 plasmid with opsin and the mutants G90V, N55K which can be expressed in eukaryote cells; B. pG58 plasmid with R175E arrestin for expression in *E.coli* and IPTG induction; C. pEF5/FRT/V5-DEST plasmid with M3R and the mutants M3R-N132G, M3R-D518N, M3R-D518K and M3R-K523Q which were expressed in eukaryote cells; D. pET-17b with the inserted tau gene for expression in BL21 cells by IPTG induction; E. pCMV3 plasmid with inserted tau gene for eukaryotic cell expression.

3.2 Equipment

Cell culture equipment: type II class cell culture cabinet (NuAire), CO_2 incubators for cell culture (NuAire), and liquid nitrogen containers (Air Liquide), 4ºC centrifuge biofuge (Heraeus (Primo R)), low temperature fridge (Mo-Bio, AE390), optical inverted microscope (Olympus (CK 30)).

Deoxyribonucleic acid (DNA) and protein expression purification devices: ultracentrifuge Beckman Coulter (Optima LE-80K), centrifuge (Alresa), refrigerated centrifuge (Kubota (6500)), DNA agarose gel electrophoresis, sodium dodecyl sulfate polyacrylamide gel electrophoresis

(SDS-PAGE), Western Blot (WB) system (BioRad), UV Transilluminator 2000 and Molecular Imager ChemiDoc documentation system (BioRad) and transparency viewer (IEWLight 5000), bacterial incubator (Sanyo MIR-262 model).

Radioactive facilities: hood for chemical material (CaptairChem), liquid scintillation counter (TRI CARB Packard).

Spectrophotometry: Ultraviolet-visible (UV-Vis) spectophotometer (Cary (100Bio)), spectro--fluorimeter (PTI, QM-1), and high intensity illuminator (Fiber-Lite MI-150).

Microscopy: fluorescence microscope (Nikon/Eclipse Ti-S), long-life mercury light source (Nikon intensilight).

General lab devices: microprocessor pH meter 213 (Hanna), cold room (Isark by Coldkit), sonicator 2070 (Bandelin), analytical balance (Mettler Toledo / NewClassic MS), autoclave (Darlab), ice machine (Bar-line), ICW-3000 water purification system (Merck Millipore), vortex (Heidolph), polymerase chain reaction (PCR) apparatus (BioRad (MJ Mini)), microtube centrifuge (Biocen), microtube centrifuge (Eppendorf 5424), microtubes incubator (Biosan/S-100), shaking incubator (Infors AG), refrigerated incubator (Sanyo MIR-254), -20ºC freezer (Zanussy, tropic system), -80ºC freeze (REVCO, ULT13863V35).

3.3 DNA purification and protein expression methodologies

3.3.1 Competent cells preparation and transformation

Transformation is the process by which a foreign plasmid is introduced into a bacterial cell. Competent cells were prepared with specific treatments to modify the membrane permeability allowing DNA entrance into the cells. Here, DH5α and BL21 strains were used to prepare the competent cells or ultra-competent cells. Compared the competent cells, the ultra-competent cells showed more efficient activity that especially were used for ligated DNA, or low yield PCR products transformations. After transformation, the DNA plasmid could be replicated as the bacteria grew in large cell culture volumes. DH5α strain normally is used for the plasmid amplification and the BL21 strain is used for the protein expression. The competent and ultra-competent cells preparation and the transformation processes are described in this section.

3.3.1.1 Competent cells preparation

One colony was incubated in 50 ml of LB at 37ºC and shook at 200 rpm overnight. Then, 1 ml of the overnight culture was transferred to 100 ml fresh LB medium and incubated at 37ºC, and 200 rpm, until $A_{600\,nm}$ reached 0.6 which typically took between 3 h and 4 h. After the culture growth was stopped by incubating on ice for 25 min, the cells were spun down for 20 min at 4000 rpm and 4ºC. The pellet was re-suspended with 40 ml $CaCl_2$ and incubated 30 min on ice. The cells were centrifuged 20 min at 4000 rpm and 4ºC, the pellet was re-suspended with 2 ml $CaCl_2$ containing 20% glycerol, and aliquoted in 50 µl samples and stored at -80ºC. Finally 100 ng DNA was used to check the transformation efficiency of the cells.

Buffers:

- 100 mM $CaCl_2$ solution, autoclaved and kept at 4ºC until use.
- 100 mM $CaCl_2$ containing 20% of glycerol solution, autoclaved and kept at 4ºC until use.

3.3.1.2 Ultra-competent cells preparation

DH5α cells were cultured on LB agar plates at 37ºC overnight and 12 large colonies were picked up and cultured in 250 ml SOB in a 1 L flask at 19ºC with vigorous shaking to reach $A_{600\,nm}$ = 0.5 which normally took from 2 to 3 days. Then the flask was placed on ice for 10 min to stop culture growth and cells were spun down at 4000 rpm for 20 min at 4ºC, and 80 ml ice-cold TB was used to resuspend the pellets. After incubation on ice for 10 min cells were centrifuged at 4000 rpm for 20 min at 4ºC. Then the pellet was gently re-suspend in 5 ml ice-cold TB containing 350 µl DMSO and stored at -20ºC overnight before use. Finally, the sample was divided into 100 µl aliquots and used directly for transformation or stored at -80ºC.

Buffers:

- SOB solution: 0.5% yeast extract, 2% tryptone, 10 mM NaCl, 2.5 mM KCl, 10 mM $MgCl_2$, 10 mM $MgSO_4$ dissolved in milliQ water. It was autoclaved to sterilize and kept at 4ºC.
- TB solution: 10 mM PIPES, 15 mM $CaCl_2$ and 250 mM KCl. Then dissolved in milliQ water and adjust pH to 6.7 with KOH or HCl and then add 55 mM $MnCl_2$, dissolved in milliQ water. It was sterilized by filtration with 0.45 µm filter and kept at 4ºC.

3.3.1.3 DNA transformation

DH5α competent cells were chosen for large amounts of plasmid purification, while BL21 competent cells were chosen for the prokaryotic expression of proteins, for example tau-pET17b expression. When the competent cells were prepared, all the processes were performed near the flame to avoid any contamination and on ice to keep the cell function. The transformation process was as follows:

The competent cells were taken out from -80ºC and thawed on ice for 10 min. 1µl of plasmid DNA (50-100 ng) was added into the competent cells tube and mixed by gently rolling the tube for several times on ice. The mixture was incubated on ice for 30 min. Then, heat shock was carried out by heating the competent cells at 42ºC for 60 s and then the cells were kept on ice for 3 min to cool down. 1 ml 2YT medium was added to incubate cells at 37ºC, 250 rpm for 45 min to help cell recovery. Finally, 100 µl of cells was plated on LB solid medium dish with appropriate antibiotics (ampicillin or kanamycin) and incubated at 37ºC overnight to allow colonies growth.

The chemically-obtained competent *E.coli* (DH5α and BL21) cells were suitably used for transformation and protein expression.

Media:

- 2YT medium: 1.6 g Tryptone, 1.0 g Yeast Extract, 0.5 g NaCl, adjust pH to 7.2 in 100 ml ddH_2O and autoclaved.
- LB medium: 1.0 g Tryptone, 0.5 g Yeast Extract, 0.05 g NaCl, pH 7.2 in 100 ml ddH_2O and autoclaved.

3.3.2 DNA maxi preparation and quantitation

After transformation of the derived plasmid, the cells were grown in larger volumes to increase DNA amount. DNA was extracted by using the maxi-preparation Kit and quantitated by UV-Vis spectroscopy. DNA agarose gel electrophoresis was also used to determine DNA purity.

3.3.2.1 DNA maxi preparation

To satisfy the large scale requirement for transfection, DNA Maxiprep purification was

performed by the Hi-pure plasmid maxiprep kit (Invitrogen). In this kit, a modified alkaline lysis method was used.

One colony was cultured in 500 ml of LB medium with the corresponding antibiotics (ampicillin or kanamycin) for overnight incubation at 250 rpm and 37ºC. The cells were harvested by spinning down the sample at 4000 rpm for 20 min, and the medium was removed. 20 ml resuspension buffer (R3) with RNase A (20 mg/ml) suspended the pellet. Then, 20 ml of lysis buffer (L7) was added to break the cells, and mixed by inverting the capped tube five times and incubated at room temperature (RT) for 5 min. 20 ml of precipitation buffer (N3) was mixed with the sample immediately by inverting the tube until the formation of white clumps. A funnel with gauze was used to separate the flocculate from the liquid. Meanwhile, the Hi pure filter maxi column was equilibrated with 30 ml of equilibration buffer (EQ1), and the liquid flowed through from the gauze was loaded onto the column and drained by gravity flow. 60 ml of wash buffer (W8) was used to wash the column and drained by gravity flow. Now, the DNA bound on the column was eluted with 15 ml of elution buffer (E4). 10.5 ml of isopropanol was added into the eluted DNA and subject to centrifugation for 45 min at 18000 g and 4ºC. DNA was precipitated and re-suspended with 10 ml of 70% ethanol and centrifuged at 18000 g for 10 min again. The supernatant was carefully removed and the pellet was air-dried for 10 min. 1 ml ddH_2O was added to dissolve the DNA.

The DNA concentration and purity was determined by UV-Vis spectroscopy by measuring the absorbance at 260 nm. The Lambert-Beer law was used to calculate the concentration of the purified DNA. The equation is:

$$\mathbf{A = \varepsilon \cdot c \cdot l}$$

where A is the absorbance of 260 nm; ε is the molar extinction coefficient with units in ml $\cdot \mu g^{-1} \cdot cm^{-1}$ ($\varepsilon_{DNA} = 0.02$); l is the path length of the cuvette (1 cm) and c is the concentration of the chromophoric compound in solution, expressed in $\mu g \cdot ml^{-1}$.

Buffers:

- Resuspension buffer (R3): 50 mM Tris-HCl, 10 mM EDTA, pH 8.0.
- Lysis buffer (L7): 0.2 M NaOH, and 1% (w/v) SDS.

- Precipitation buffer (N3): 3.1 M potassium acetate, pH 5.5.
- Equilibration buffer (EQ1): 0.1 M sodium acetate pH 5.0, 0.6 M NaCl, and 0.15% (v/v) TritonX-100.
- Wash buffer (W8): 0.1 M sodium acetate pH 5.0 and 825 mM NaCl.
- Elution buffer (E4): 100 mM Tris-HCl, pH 8.5 and 1.25 M NaCl.

3.3.2.2 DNA agarose gel electrophoresis

Gel electrophoresis is the standard laboratory procedure for separating DNA by size to determine purification efficiency. Electrophoresis uses an electrical field to move the negatively charged DNA towards a positive electrode through an agarose gel matrix. 1% (w/v) agarose gel with Tris acetate-EDTA (TAE) buffer was prepared. 1g agarose powder was dissolved in 100 ml TAE buffer and microwaved until agarose was completely melted. The agarose solution was cooled down nearly to 55ºC - 65ºC which normally took 10 min. The agarose solution was poured down into a gel tray with a comb to form the wells and after complete gel solidification, the DNA samples were loaded together with 6x DNA loading buffer, and run in TAE buffer at 70 V for 80 min by an electrophoresis system (Bio-Rad). The gel was stained by the Ethidium bromide (EB) buffer for 30 min and an image system (Bio-Rad) was used to visualize the DNA fragments.

Buffers:

- TAE buffer (10x): 48.4 g Tris Base, 7.44 g EDTA dissolved in 800 ml ddH_2O, 11.42 ml CH_3COOH was added and homogenized. Add more ddH_2O to 1 L.
- EB buffer: 2 µl EB dissolved in 100 ml 1x TAE buffer.

3.3.3 Eukaryotic cell culture techniques

HEK293T cells and COS-1 cells, as mammalian cell lines, were used to express WT rhodopsin and its mutants, M3R and its mutants, and tau-pCMV3 protein. HEK293S-GNTI$^-$ cells were also used to express the protein but mainly for WB analysis.

3.3.3.1 Mammalian cells thawing

Before cell thawing, the culture medium should be warmed at 37ºC. The cell vial was quickly

taken out from liquid nitrogen and completely defrosted at 37ºC. The cells were rapidly transferred to a 15 ml tube containing 7 ml of warmed medium and spun down at 900 rpm for 5 min. The cell pellet was seeded onto a 10 ml cell culture dish containing 15 ml of medium and cultured at 37ºC in an incubator with 5% CO_2 for the subsequent experiments. Depending on the different types of cells, different medium were chosen (see section 3.3.3.2).

3.3.3.2 Cell culture

HEK293T cells were routinely cultured in complete Dulbecco's Modified Eagle's Medium (DMEM) supplemented with 10% fetal bovine serum (FBS), 2 mM L-glutamine and 100 units/ml penicillin/streptomycin at 37ºC in an atmosphere of 5% CO_2. After cells reached 70% - 80% of confluence, the cells could be used for generation, transfection, cryopreservation or immunofluorescence. When the cells were used for maintenance, the medium was removed from the 15 cm cell culture dishes and were gently washed with 7 ml phosphate buffered saline (PBS). Then, 9 ml of fresh medium was added and the cells were detached by repeated pipetting. 3 ml of medium containing cells was transferred to a new 10 ml cell culture dish containing 15 ml of warmed medium, and then the cells were incubated at 37ºC in a 5% CO_2 humidified incubator.

COS-1 cells were cultured in DMEM medium supplemented with 10% FBS, 2 mM L-glutamine and 100 units/ml penicillin/streptomycin at 37ºC and in an atmosphere of 5% CO_2. After 70% - 80% confluence, cells were carefully washed with 7 ml PBS after removing the old medium and 5 ml 1% trypsin EDTA solution was added to detach the cells for 1 min at 37ºC. Trypsin was decanted and 9 ml of complete medium was added to inactivate trypsin. The cells were separated by repeated pipetting and 3 ml of medium with cells was transferred into a new 10 ml cell culture dish with 15 ml of warmed medium and incubated at 37ºC in a 5% CO_2 humidified incubator.

HEK293S-GNTI$^-$ cells were cultured in DMEM+Ham F12 (1:1) mixture medium supplemented with 10% FBS, 2 mM L-glutamine and 100 units/ml penicillin/streptomycin at 37ºC and in an atmosphere of 5% CO_2. There is not N-acetylglucosaminyltransferase (GnTI) activity in HEK293S-GnTI$^-$ cells and the protein expression lacks complex N-glycans which is appropriate for recombinant protein detection especially by electrophoresis. The maintenance protocol is the same as HEK293T cells.

3.3.3.3 Mammalian cells storage

The mammalian cells were incubated to nearly 60% - 70% confluence, which means that the cells were on the logarithmic phase. Once thawed they still can keep their active condition. The cells were harvested by either trypsin or pipetting in 5 ml corresponding medium and spun down at 900 rpm at 25ºC for 5 min, the cell pellet was re-suspended with the freezing medium. The freezing medium was composed of 20% FBS, 10% DMSO and 70% corresponding to the cell medium. The freezing medium should be filtered before use. Then, all the cells in freezing medium were aliquot into sterile cryovials and kept at 4ºC for 2 h. The vials were transferred to a -20ºC freezer until frozen (4 - 6 h), and then at -80ºC to help sequential freezing while maintaining cell viability. Finally the frozen cells were stored in liquid nitrogen.

3.3.3.4 DNA transfection and cotransfection

Mammalian cells were cultured at 37ºC in a 5% CO_2 incubator to reach 70% - 90% confluence in 15 cm cell culture dish. DNA and PEI mixture were prepared separately. DNA mixture contains 30 μg DNA and 2.5 ml Opti-MEM and the PEI mixture, 100 μl PEI (for stock 1mg/ml, pH 6.0) and 2.5 ml Opti-MEM. After 5 min incubation, DNA and PEI solutions were mixed and incubated for 20 min at RT. The cells were incubated with 15 ml cultured medium and 5 ml DNA-PEI mixture. When co-transfection was carried out such as M3R and tau vectors, 30 μg DNA was composed of 15 μg M3R vector and 15 μg tau vector. Cells were incubated for 48 h (Figure 3.2). The transfected proteins were overexpressed in the cell lines and subsequently purified in section 3.4 for further characterization.

When the mammalian cells were cultured in a 6-well plate containing sterile coverslips to carry out the immunofluorescence experiments, different DNA and PEI volumes were used. 100 μl cells were cultured in each well and incubated for 24 h at 37°C with 5% CO_2 to reach 60% - 70% confluence. After changing the medium, 3 μg DNA mixed with 400 μl Opti-MEM and 15 μl PEI (1 mg/ml, pH 6.0) mixed with 400 μl Opti-MEM were prepared separately. After 5 min incubation, DNA and PEI buffer were mixed and incubated for 20 min and added to each well. The transfected cells, in the 6-well plate, were cultured for 24 h and used for immunofluorescence analysis.

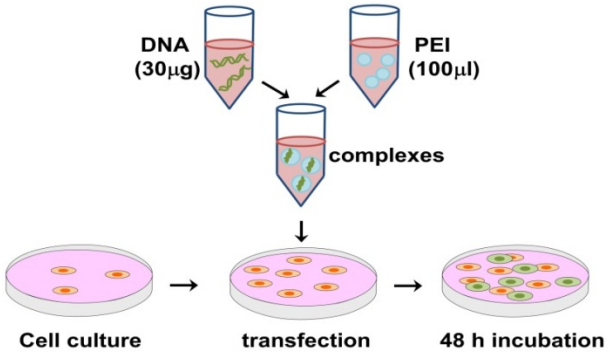

Figure 3.2 Cell transfection process.

The desired DNA (30 μg) and PEI (100 μl) were dissolved in Opti-MEM medium separately for 5 min incubation. Then DNA and PEI were mixed for 20 min to transfect the cells. After 48 h incubation, the protein will be expressed in cells.

3.4 Protein Purification Methodology

3.4.1 Coupling of 1D4 antibody to sepharose beads

Modified sepharose (Cyanogen bromide-activated-Sepharose 4B) beads coupled with rho-1D4 antibody were needed for rhodopsin purification from mammalian cells and ROS.

1.51 g sepharose powder was dissolved into a final volume of 6 ml of 1 mM HCl (pH 2~3) for 15 min till all the white clumps were completely dissolved. Then the beads were washed using a filter funnel with G3 porosity (Duran) for 30 min by using 300 ml 1 mM HCl (pH 2~3) in several aliquots to remove any additives. Beads were washed with 3 volumes (18 ml) of coupling buffer (pH 8.3) in aliquots to increase the pH of beads and to allow antibody coupling. 7.5 ml of 5.3 mg/ml 1D4 antibody was mixed with sepharose beads by using a spatula and incubated overnight at 4°C. According sepharose manufacture instructions, 5~10 mg of antibody per 1 ml medium is recommended. Here, 7.5 mg protein per 1 ml medium was used.

The unbound rho-1D4 antibody was washed away by using 2 volumes (12 ml) of coupling buffer. Then, washed rho-1D4 beads were transferred into a 50 ml tube containing 6 ml of 1 mM Tris-HCl pH 8.0 and agitated for 2 h on RT to block any remaining active group. Filter funnel porosity G3 was used to remove the 6 ml Tris-HCl (pH 8.0) and the beads were washed sequentially with alternative cycles of 5 volumes (30 ml each) of 0.1 M NaAc pH 4.0 with 0.5 M NaCl, and 0.1 M Tris-HCl pH 8.0 with 0.5 M NaCl, for 4 times. Finally the beads were

transferred to a falcon tube containing 6 ml of beads storage buffer at 4°C. These beads were used for rhodopsin purification from either ROS or mammalian cells expression.

Buffers:

- 1 mM HCl (pH 2~3): 41.6 µl of 12 M/37% HCl dissolved in 500 ml ddH_2O, adjust pH 2~3.
- Coupling buffer: 0.1 M $NaHCO_3$ pH 8.3 containing 0.5 M NaCl.
- Beads storage buffer: 2 mM Na_2PO_4 (pH 6.0) with 0.004% (w/v) NaN_3.

3.4.2 Purification of WT rhodopsin, and G90V and N55K mutants from mammalian cells

WT rhodopsin, and the G90V and N55K mutant genes constructed in the pMT4 plasmid vector [150] were transiently transfected in 10 plates of COS-1 cells, or HEK293S-GNTI$^-$ cells, by chemical transfection with PEI reagent. After 48 h, cells were harvested and regenerated with 10 µM 11-*cis*-retinal in solvent buffer for overnight incubation. 1% (w/v) DM with PMSF and protease inhibitors was added for 1 h and gently nutated to solubilize the cells, followed by ultracentrifugation for 35 min at 35000 rpm (using rotor 50 Ti). The supernatant was used for the immunoaffinity chromatography purification by sepharose coupled to the rho-1D4 antibody. After 3 h incubation, the sepharose-bound WT and mutants were spun down and washed with washing buffer containing 0.05% (w/v) DM for 5 times at 4000 rpm, 5 min at 4°C. Then WT and mutant rhodopsin were eluted with elution buffer containing peptide (Figure 3.3) [94]. The protein was either immediately characterized or stored at -80°C for a few days.

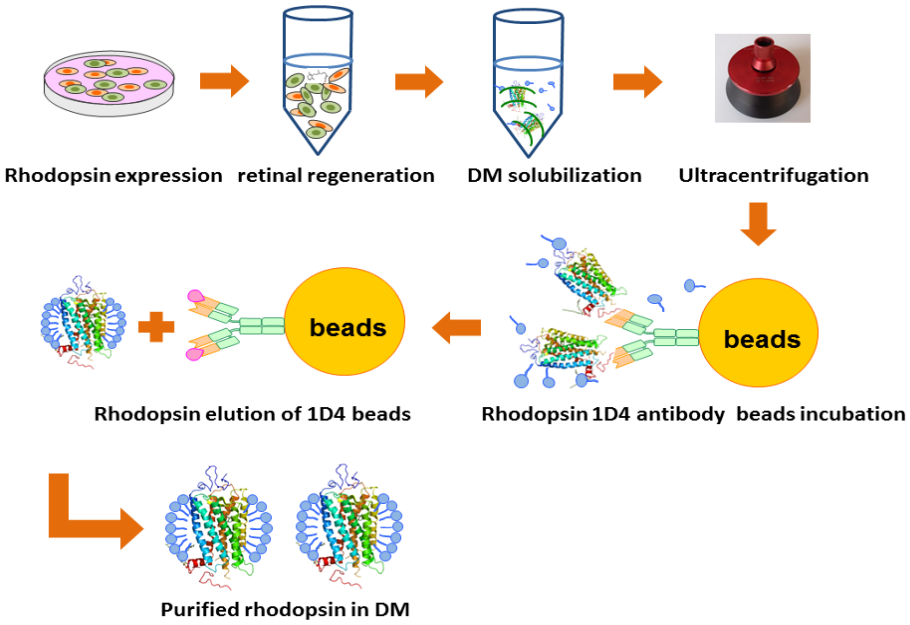

Figure 3.3 Rhodopsin purification process.

Rhodopsin apoprotein or the mutants were overexpressed in eukaryotic cells and regenerated with 11-*cis*-retinal to obtain rhodopsin WT and mutants. DM detergent was added to solubilize the protein which was eluted with the rho-1D4 9-mer peptide and analyzed by means of UV-Vis spectroscopy.

Buffers:

- Solvent buffer (DDHA-PC liposomes study (3.5.2)): 137 mM NaCl, 2.7 mM KCl, 1.5 mM KH_2PO_4, and 8 mM Na_2HPO_4, pH 7.4.
- Solvent buffer (DMPC/DHPC bicelles study (3.5.2)): solvent buffer was also named as Bicelles buffer A: 10 mM BTP, 140 mM NaCl, 2 mM $MgCl_2$, 2 mM $CaCl_2$, pH 6.0.
- Washing buffer: solvent buffer with 0.05% (w/v) DM.
- Elution buffer: washing buffer with 100 μM 1D4 9-mer peptide.

3.4.3 Rhodopsin purification from retinal ROS

ROS membranes were purified from bovine retinas, under dim red light, using a sucrose gradient method [151,152]. The membranes were suspended in 70 mM potassium phosphate, 1mM $MgCl_2$, 0.1mM EDTA, pH 6.9, then centrifuged and the pellets were re-suspended in 5 mM Tris-HCl (pH 7.5) containing 0.5 mM $MgCl_2$. Two alternating washes with these buffers were carried out to remove any further contaminating proteins. Finally, ROS membranes were split into several aliquots and stored in the dark at -80°C for the further use. The ROS membranes were used for

rhodopsin purification. ROS membranes were solubilized in solvent buffer with 1% (w/v) DM in the dark for 1 h at 4°C. The pigments were purified by immunoaffinity chromatography on 1D4-Sepharose 4B in the same buffer. The protein sample was incubated with the 1D4-Sepharose beads for 3 h and the purified protein was eluted in the corresponding solvent buffer containing 100 μM 1D4 9-mer peptide. All the procedures were performed in the dark at 4°C.

3.4.4 Isolation of the Gt from bovine retinas

Gt is naturally expressed in vertebrate retinal rods and cones, with different α, β and γ subunits in rod and cone photoreceptors. Light causes conformational changes in rhodopsin, leading to the binding and activation of Gt. So, Gt was purified to study the different ability of WT rhodopsin and its mutants to bind and activate Gt.

Fifty bovine retinas were thawed and exposed to light at 4°C for overnight to allow Gt binding to photoactivated rhodopsin. Retinas, re-suspended in 150 ml of 47% (w/w) sucrose in Tris buffer A, were homogenized with a 50 ml syringe. Then the solution was centrifuged at 42000 g for 20 min. The supernatant containing the orange ROS membranes were collected, diluted with 200 ml of Tris buffer A and homogenized again with a 50 ml syringe. Finally, the homogenate was centrifuged at 30000 g, at 4ºC for 20 min. The pellet was re-suspended in 50 ml Tris buffer A with the help of a 21 gauge needle for three times. Sucrose density gradient was used to separate the ROS membranes from cell debris and remaining retinal tissues. To do that, 9 ml of 30% and 25% sucrose were used as two gradients from bottom to top respectively in the centrifuge tubes. Finally, the membrane suspension was added on the top of the sucrose gradient. The gradient sample was centrifuged at 42000 g for 30 min at 4°C. The orange band located between 30% and 25% sucrose was collected using a 21-gauge needle and diluted with 160 ml of Tris buffer A, followed by centrifugation at 42000 g for 20 min to remove the sucrose. The pellet was resuspended in 100 ml of Tris buffer C and centrifuged at 42000 g for 20 min. The pellet was resuspended again in 100 ml of Tris buffer D and spun down at 42000 g for 20 min. This step was repeated twice. The pellet was resuspended with 50 ml Tris buffer D containing 0.04 mM GTP and incubated for 30 min at 4°C. The sample was centrifuged at 45000 rpm (using the Ti50 rotor) for 45 min at 4°C and the supernatant was filtered (0.45 μm) and concentrated with an

Ultra-15 centrifugal filter (Amicon) with a 10 kDa cut off to a final volume of nearly 10 ml. The concentrated sample was transferred into a dialysis tube and dialyzed against 900 ml of Tris buffer E which should be changed twice. The protein was collected and purity was determined by means of SDS-PAGE with Coomassie blue staining

Buffers:

- Tris buffer A: 20 mM Tris, pH 7.4, 1 mM $CaCl_2$, 2 mM DTT.
- Tris buffer C: 10 mM Tris, pH 7.4, 100 mM NaCl, 5 mM $MgCl_2$, 2 mM DTT.
- Tris buffer D: 10 mM Tris, pH 7.4, 0.1 mM EDTA, 2 mM DTT.
- Tris buffer E: 20 mM Tris, pH 7.5, 100 mM NaCl, 50% glycerol, 5 mM DTT and 5 mM $MgCl_2$.
- 47% sucrose: 117.5 g sucrose in 250 ml Tris buffer A.
- 30% sucrose: 75 g sucrose in 250 ml Tris buffer A.
- 25% sucrose: 62.5 g sucrose in 250 ml Tris buffer A.

0.1 mM PMSF was added in all the buffers before use.

3.4.5 Expression and preparation of M3R WT and mutants

M3R as WT and mutants M3R-N132G, M3R-D518N, M3R-D518K, and M3R-K523Q genes constructed in pEF5/FRT/V5-DEST vectors were transfected into HEK293S-GNTI$^-$ cells by means of the PEI reagent. After 48 h, cells were harvested using solvent buffer and centrifuged at 4000 rpm for 20 min. The cell pellet was resuspended with 100 μl PBS pH 7.4 containing 1% DM and shook for 1 h. After 40 min centrifugation at 6000 rpm, the protein in the supernatant was detected by measuring the absorbance at 280 nm. The total protein samples adjusted to $A_{280\ nm}$ = 0.8 were subject to SDS-PAGE. The cells cotransfected with tau-pCMV3 and M3R mutants were prepared following the same protocol.

3.5 Lipid bilayer preparation

To understand the detailed structure of the rhodopsin and its mutants associated with RP, rhodopsin WT and mutants were inserted into mimic membrane models: DMPC/DHPC bicelles

and DDHA-PC liposomes. Here, the mild neutral detergent (DM) was used to purify rhodopsin and three lipids, DMPC, DHPC and DDHA-PC, were prepared in different bilayer for protein insertion. Figure 3.4 shows the molecular structures of the lipids used.

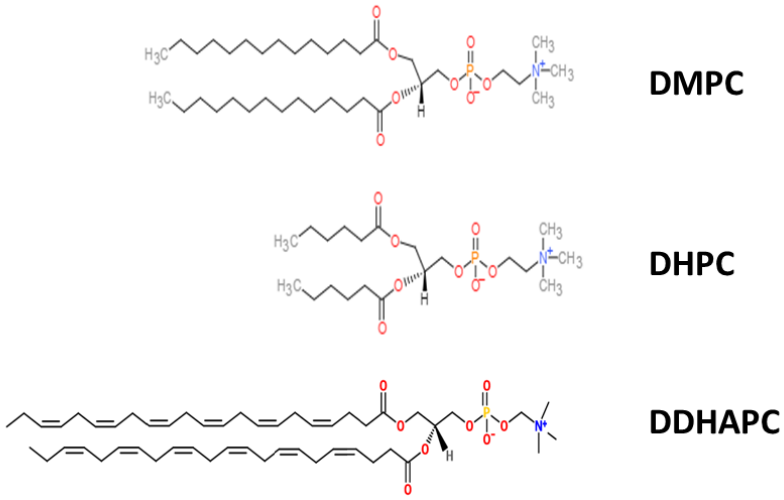

Figure 3.4 Molecular structures of the lipids.

Three kinds of lipids (DMPC, DHPC, DDHA-PC) were used in this thesis. DMPC/DHPC was used for the bicelles and DDHAPC was used for liposomes preparation.

3.5.1 DMPC/DHPC bicelles preparations

A 10% (w/v) DMPC sample was prepared by dissolving the powder in bicelles buffer A and gently vortexing, followed by incubating the solution at 42°C for 5 min and then cooling to RT. 10% (w/v) DHPC was also prepared in bicelles buffer A. Final 2% (w/v) DMPC/DHPC (1:1) mixtures were mixed briefly, heated to 42°C for 10 min, and then stirred at RT for 1 h until the mixtures were clear. The bicelles were mixed with rhodopsin dissolved in DM and agitated for 1 h. Rhodopsin was transferred from DM to the bicelles. The residual DM in the sample was neglected because of its presumed very low concentration. All bicelles were used within 36 h from preparation [35].

Buffers:

- Bicelles buffer A: 10 mM BTP, 140 mM NaCl, 2 mM $MgCl_2$, 2 mM $CaCl_2$, pH 6.0.

- Buffer A containing 0.05% (w/v) DM was used as a DM-buffer A control buffer.
- Buffer A containing 2% (w/v) DMPC/DHPC bicelles was prepared as the description above.

The bicelles buffer A was used in all the experiments associated with DMPC/DHPC bicelles.

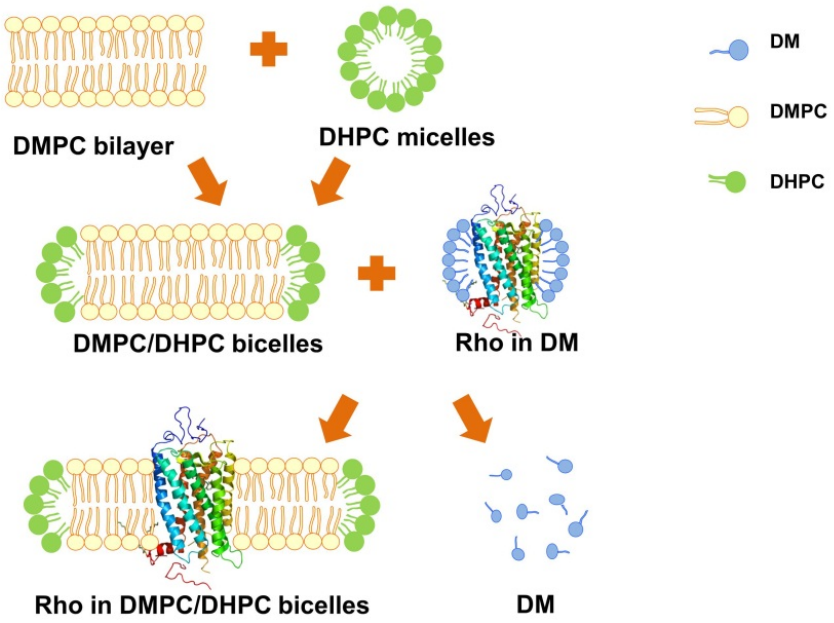

Figure 3.5 Protein insertion into DMPC/DHPC bicelles.

DMPC and DHPC were used to prepare the DMPC/DHPC bicelles by using different temperature changes. Once DMPC/DHPC bicelles were formed, concentrated rhodopsin dissolved in DM was added. After the incubation, rhodopsin was transferred to the DMPC/DHPC bicelles.

3.5.2 DDHA-PC liposomes preparation and protein insertion

DDHA-PC powder was dissolved in chloroform: methanol (2:1, v/v) and the solution was evaporated to dryness under a stream of nitrogen. The lipid film was hydrated with PBS pH 7.4 to form the liposomes. The liposomes were mixed with 0.5% DM and the solubilized protein subject to gentle agitation for 3 h at 4°C. Bio-beads SM-2 were added in order to extract the extra DM [153,154]. Finally, the proteoliposomes system included 0.375 mM DDHA-PC liposomes and 0.5 µM WT rhodopsin or mutants (representing a 750:1 ratio) (Figure 3.6).

Buffers:

- During the DDHA-PC liposomes preparation process, the solvent buffer (see section 3.4.2) was used and all the experiments involving DDHA-PC liposomes.
- DM detergent buffer: solvent buffer containing 0.05% (w/v) DM.
- DDHA-PC liposomes buffer: solvent buffer containing 0.375 mM DDHA-PC liposomes with 0.5 µM WT rhodopsin or mutants, which would be 750:1, as per the above description.

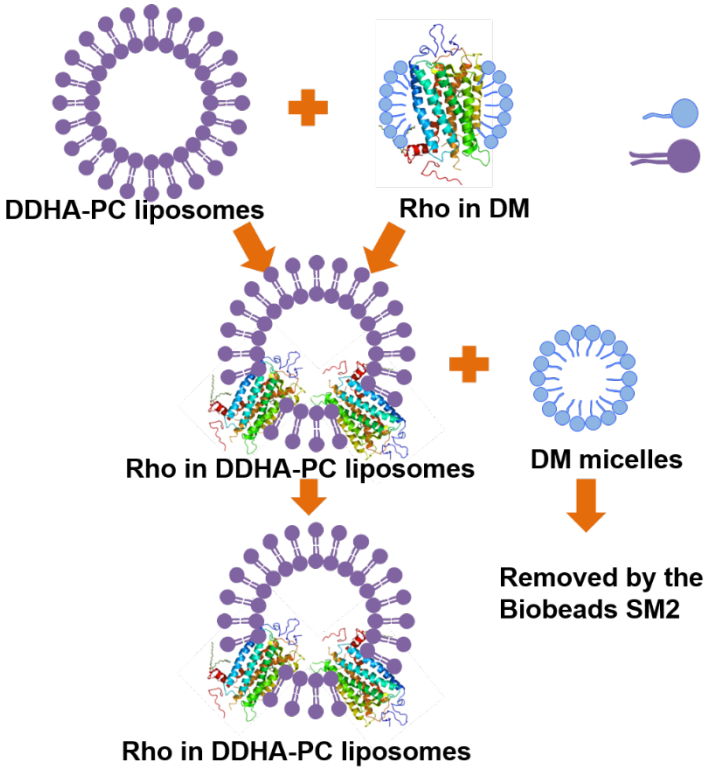

Figure 3.6 Protein insertion into DDHA-PC liposomes.

DDHA-PC powder was dissolved in PBS pH 7.4 to form the DDHA-PC liposomes and mixed with rhodopsin in DM detergent. Biobeads were added to the system for three times to remove the DM detergent, embedding the final protein in the DDHA-PC liposomes.

3.6 Protein detection

3.6.1 Protein characterization by UV-Vis spectroscopy

UV-Vis spectra measurements were carried out with a Cary 100 Bio spectrophotometer (Varian, Australia), equipped with water-jacketed cuvette holders connected to a circulating water bath. Temperature was controlled by a Peltier accessory connected to the spectrophotometer. All spectra were recorded in the 250 nm - 650 nm range with a bandwidth of 2 nm, a response time of 0.1 s, and a scan speed of 300 nm/min. The spectral ratio is defined as absorbance at 280 nm

divided by absorbance at the visible λ_{max} value to measure the pigment yield and stability. The protein concentration was determined by measuring the absorbance at λ_{max}. Lambert-Beer law was used to calculate the concentration of the purified protein. The formula is:

$$\mathbf{A = \varepsilon \cdot c \cdot l}$$

A is absorbance of λ_{max}; ε is the molar absorptivity with units of $M^{-1}cm^{-1}$; l is the path length of the cuvette (1 cm); c is the concentration of the chromophore in solution, expressed in M.

For mutants, each ε value was calculated with the equation: $\varepsilon = (A/A_{Rho}) \cdot (A_{440Rho}/A_{440})\ \varepsilon_{Rho}$, where A is the absorbance at the λ_{max} value, A_{440} is the absorbance at 440 nm after acid denaturation, and the ε_{Rho} is the molar extinction coefficient of Rho ($\varepsilon_{Rho}= 42.7\times10^3\ M^{-1}cm^{-1}$) [70].

In this thesis, WT rhodopsin and mutants were characterized by their UV-Vis spectra. UV-Vis spectroscopy was also used for the photobleaching, thermal bleaching and chromophore regeneration experiments.

3.6.1.1 Photobleaching and acidification of purified WT, and G90V and N55K mutants

WT rhodopsin and mutant samples, purified from COS-1 cells and dissolved in the appropriate buffers, were monitored in the dark state and then photobleached with a 150-watt power source equipped with an optic fiber guide with a 495 nm cut-off filter for 30 s to ensure complete photoconversion to 380 nm absorbing species. For some mutants in specific conditions, a second illumination was also performed to facilitate complete photoconversion. Acidification was carried out immediately after photobleaching, by adding 2 N H_2SO_4 to a final pH of 1.9, and an absorption spectrum was recorded 1 min after acidification.

3.6.1.2 Thermal stability of WT, and G90V and N55K mutants

The thermal stability of rhodopsin and its mutants was followed by means of UV-Vis spectrophotometry. Pigment thermal bleaching rates were obtained, in the dark, by monitoring the decrease of absorbance at λ_{max} of the visible spectral band as a function of time at either 55°C, 48°C or 37°C. Spectra were recorded every min. Data points were obtained by using the equation: $\Delta A = (A\text{-}A_f) / (A_0\text{-}A_f)$, where A is the absorbance recorded at λ_{max}, A_f is the absorbance at the final time, and A_0 is the absorbance at time 0. The half-life time ($t_{1/2}$) for the process was determined by fitting the experimental data to a single exponential decay curves using Sigma

Plot version 11.0 (Systat Software, Chicago, IL, USA).

3.6.1.3 Chromophore regeneration of WT, and G90V and N55K mutants

Two main buffers were used for chromophore regeneration depending on the different lipids used. For the chromophore regeneration in bicelles, we used the bicelles buffer A containing DM or DMPC/DHPC bicelles, pH adjusted to 6.0; for the chromophore regeneration in DDHA-PC liposomes, the solvent buffer containing DM or DDHA-PC liposomes (pH adjusted to 6.0) was used.

2.5 fold molar excess of 9-*cis*-retinal or 11-*cis*-retinal was added to the purified samples, in the dark, followed by illumination with a 150-watt power source equipped with an optic fiber guide using a > 495 nm cut-off filter to avoid photobleaching of the free retinal. The samples were illuminated for 30 s at 20°C and spectra were recorded every min until no further increase in $A_{\lambda max}$ was detected.

3.6.2 Pigment characterization by fluorescence spectroscopy

All fluorescence assays were performed by using a Photon Technologies QM-1 steady-state fluorescence spectrophotometer. Sample temperature was controlled with a cuvette holder Peltier accessory TLC 50 (Quantum Northwest, Liberty Lake, WA, USA) connected to a hybrid liquid coolant system Reserator XT (Zalman, Garden Grove, CA, USA). The changes on Trp fluorescence were monitored over time. All fluorescence scans were carried out by exciting the samples for 2 s at 295 nm and a bandwidth slit of 0.5 nm and blocking the excitation beam for 28 s with a beam shutter to avoid photobleaching of the sample. Trp emission was monitored at 330 nm with a bandwidth slit of 10 nm.

3.6.2.1 Meta II decay stability of WT and mutants

The Meta II active conformation decay process was followed in real time by fluorescence spectroscopy [155]. 0.5 µM rhodopsin, or mutants, was stabilized for 10 min at 20°C in the fluorimeter, followed by illumination for 30 s with a > 495 nm cut-off filter. The increase in Trp fluorescence, due to retinal release from the Meta II conformation, was monitored and after the fluorescence reaching a plateau, 50 mM of hydroxylamine hydrochloride (adjusted to pH 7) was added to confirm complete retinal release. The $t_{1/2}$ values for the retinal release curves were

determined by fitting the experimental data to a single-exponential curve using Sigma Plot version 11.0 (Systat Software, Inc., Chicago, IL, USA).

3.6.2.2 Chromophore uptake of opsin upon retinal release

The retinal entry process was monitored, in real time, by means of fluorescence spectroscopy. After Meta II complete decay, 2.5 fold 9-*cis*-retinal, or 11-*cis*-retinal, over pigment concentration was added into the cuvette, and changes in fluorescence intensity were recorded. The volume of the concentrated retinal stock added to the protein sample was less than 1% of the total sample volume to avoid any ethanol effect on the sample spectral behavior.

Fluorescence spectroscopy was also used for the Gt activation assay (3.5.4), and rhodopsin-arrestin interaction experiments (3.5.8).

3.6.3 Gt activation assays for WT rhodopsin and mutants in DM and liposomes

In the thesis, two methods to monitor the Gt activation were performed; the radio-nucleotide filter binding assay and a fluorescence spectroscopic method.

3.6.3.1 Radionucleotide filter binding assay for Gt activation

The ability of WT rhodopsin, and mutants, to activate Gt was determined by means of a radionucleotide filter binding assay by measuring the uptake of guanidine 5'-O-(3-thio)-triphosphate ($GTP\gamma S^{35}$) by Gt purified from bovine retinas. The assays were performed by mixing 10 nM rhodopsin purified from ROS (Rho) with 500 nM Gt in 25 mM Tris, pH 7.5, 100 mM NaCl, 5 mM MgAc, 5% glycerol, 2.5 mM DTT, and 3 µM $GTP\gamma S^{35}$ (0.156 Ci/mmol) at RT. To determine the Gt activity, a final concentration of 0.012% DM or 2.5 µM DDHA-PC liposomes was needed. The reactions were initiated by the addition of rhodopsin in the dark and all the samples were filtered after different incubation times, either in the dark or after illumination, to determine the amount of bound $GTP\gamma S^{35}$. The bound $GTP\gamma S^{35}$ was measured by means of a Tri Carb 2100TR liquid scintillation counter (Perkin-Elmer, The Netherlands).

The activity measured as cpm which is coverted to pmol using the formula:

$$\text{Concentration} = \frac{dpm}{2.22 \cdot 10^{12} \cdot radioactivity\ of\ ligand}$$

Here,

dpm = $\frac{cpm}{counter\ efficiency}$; counter efficiency = 55%; 1 Ci = 2.22· 1012 dpm; radioactivity of the ligand = 1250 Ci/mMol.

3.6.3.2 Gt activation by fluorescence spectroscopy

Fluorescence spectroscopy was also used to detect Gt activation of WT and G90V, N55K mutants. The rate of GTPγS uptake by Gα was followed by monitoring the increase in intrinsic fluorescence of a Trp which is conserved in all G proteins [156]. Excitation (λ = 285 nm) and emission (λ = 338 nm) wavelength were determined by scanning a protein sample. Spectra excitation and emission band were set at 1 nm with a signal integration of 5 s. For the assay, 25 nM Rho was mixed with 1 mM of Gt in 25 mM Tris pH 7.5, 100 mM NaCl, 5 mM MgAc, 2.5 mM DTT and 0.012% DM in a 200 µl cuvette and was maintained in the instrument for a few minutes to achieve a stable baseline. Then, 5 µM GTPγS was added for 5 min to measure the interaction of rhodopsin and Gt in the dark. The sample was illuminated for 1 min at 25°C. The increase in fluorescence was recorded until it reached a plateau.

3.6.4 SDS-PAGE and Blue-Native PAGE (BN PAGE)

3.6.4.1 SDS-PAGE and Coomassie blue staining

SDS-PAGE is used to separate proteins from a mixture according to their size. SDS-PAGE system was composed of a separating gel (bottom) and a stacking gel (upper) which were prepared using the reagents listed in Table 3.1. Separating gel was added to the glass slot and of isopropanol was used to flat and seal up the surface. Once the separating gel was solidified, isopropanol was removed and the stacking gel was prepared. A comb was inserted to form the lanes. Proteins were prepared and mixed with 4x protein loading buffer and loaded onto the gel. The gel was run in the 1x TGS buffer for 2.5 h at 100V. After electrophoresis, the gel was stained with Coomassie brilliant blue buffer for 3 h and destained with Coomassie destain buffer until the protein bands were visible.

Buffers:

- 4x protein loading buffer: 0.0625 M Tris, 2% SDS, 10% Glycerol, 0.4 M DTT, 0.1% Blue Bromophenol dissolved in ddH_2O.
- 1x TGS buffer: 3 g Tris, 14.4 g Glycine, 1 g SDS pH 8.3, up to 1 L with ddH_2O.
- Coomassie brilliant blue buffer: 10% (v/v) MetOH, 10% (v/v) AcOH and 0.025% (w/v) Coomassie-G
- Coomassie destain buffer: 400 ml Methanol, 100 ml Glacial Acetic Acid dissolved in 1 L ddH_2O.

Table 3.1 SDS-PAGE preparation.

SDS-PAGE was composed of separating gel and stacking gel. APS: ammonium persulfate; TEMED: N,N,N',N'-tetramethy--lethane-1,2-diamine; TEMED is used with APS to catalyze acrylamide polymerization.

	Separating gel		**Stacking gel**	
Components (stock)	Final concentration	10 ml	Final concentration	5 ml
Acr/Bis (37.5%)	12%	3.2 ml	5%	0.67 ml
Tris-HCl (1.5 M pH 8.8)	0.75 M	5 ml	----	----
Tris-HCl (0.5 M pH 6.8)	----	----	0.125 M	1.25 ml
SDS (10%)	0.1%	0.1 ml	0.1%	0.05 ml
APS	0.1%	0.1 ml	0.1%	0.05 ml
TEMED	0.5%	0.05 ml	0.5%	0.025 ml
ddH_2O		1.55 ml		2.955 ml

3.6.4.2 Blue Native PAGE (BN-PAGE)

For the BN-PAGE, the gel was composed of separating gel and stacking gel as described in Table 3.2. The protein was expressed in HEK293S-GNTI$^-$ cells which lack N-linked glycans to avoid smeary bands of proteins on the gel. Samples were loaded into the gel and run 4 h at 4°C and 100V. The BN loading buffer used glycerol prevents protein denaturation and the BN running buffer containing Coomassie blue G stains the protein directly [69]. The gel was destained to reveal the protein bands after electrophoresis.

Buffers:

- Loading buffer: 5% glycerol and 0.01% Ponceau Red.
- Running buffer: the gel running buffer is 50 mM Tricine, 15 mM Bis-Tris and 0.02% Coomassie blue G with pH 7.0.

Table 3.2 BN gel preparation of separating gel and stacking gel.

BN gel was composed of stacking gel (upper) and separating gel (bottom). The gels were usually polymerized between two glass plates in a gel caster with a comb inserted in the stacking gel to create the sample wells. After the gel is polymerized, the comb can be removed and the gel is ready for electrophoresis.

	Separating gel (13%)	**Stacking gel (4.2%)**
30% Acrylamide/Bis Solution (37.5:1)	3.5 ml (13%)	0.7 ml (4.2%)
1 M Bis-Tris (pH 7.0)	0.4 ml (50 mM)	0.25 ml (15 mM)
ddH_2O	4.0 ml	4.0 ml
APS (10%)	0.1 ml (1.2%)	0.05 ml (1%)
TEMED	0.05 ml (0.6%)	0.05 ml (0.6%)

3.6.5 WB

The WB is a widely used analytical technique to detect specific proteins in a sample of tissue homogenate or extract. Protein samples (nearly 100 ng) were prepared with loading buffer and subject to SDS-PAGE. Gel electrophoresis was carried out at 100V for 2.5 h to separate the denatured protein by polypeptide size. Then, the protein samples were transferred onto a nitrocellulose membrane (Bio-Rad). The membrane was blocked by 5% (w/v) milk dissolved in tris buffered saline (TBS) for 1 h to avoid any nonspecific binding of antibodies on the surface of the membrane. Then, the membrane was incubated for 1 h with a primary antibody which could specifically bind to the proteins and subsequently with a secondary antibody which binds the primary antibody (Table 3.3). The membrane was washed with tween tris buffered saline (TTBS) buffer for 3 times before each antibody incubation and every wash lasted for 10 min to remove the unbound antibody. Considering the protein samples, we used different primary antibodies, shown in detail in Table 3.3. All antibodies were dissolved in TBS buffer, stored at 4°C and used for several times.

Horseradish peroxidase (HRP) conjugated to the secondary antibody is an enzyme frequently used as an indicator in WB. A substrate named Super-Signal West Pico Chemiluminescent Substrate (Thermo Fisher Scientific) reacts with HRP and produces a signal which is detected on the Medical X-ray film (AGFA) in an electrophoresis systems autoradiography cassette.

Buffers:

- TBS buffer: 8.7 g NaCl, 1.21 g Tris, 0.4 ml HCl in 1L ddH_2O, pH 8.0.
- TTBS buffer: 1 ml Tween 20 dissolved in 1L TBS solution.

Table 3.3 WB samples and antibody classification.

There are mainly three different protein samples that have been used. These include rhodopsin and mutants, M3R and mutants and Tau protein. All the protein samples were incubated with their antibodies correspondingly and finally detected using the Super-Signal West Pico Chemiluminescent Substrate (Thermo Fisher Scientific).

Samples	rhodopsin and mutants	M3R and mutants	Tau protein
Source and expression	COS-1, HEK293S-GNTI$^-$ cells	COS-1, HEK293S-GNTI$^-$ cells	BL21, COS-1, HEK293S-GNTI$^-$ cells
Primary antibody	Rho-1D4 mouse IgG	mAChR M3R rabbit polyclonal IgG	Tau-5 mouse monoclonal IgG
Primary antibody dilution	1:10000	1:1000	1:5000
Secondary antibody	Goat anti-mouse IgG-HRP	Goat anti-rabbit IgG-HRP	Goat anti-mouse IgG-HRP
Secondary antibody dilution	1:5000	1:5000	1:5000

3.6.6 Arrestin R175E purification by means of Bio-Scale mini profinity cartridges

Arrestin R175E pG58 vector was transformed into *E.coli* BL21-RP competent cells (as described in section 3.3.1.3) to obtain a colony to start a mini-culture of 10 ml LB medium containing ampicillin (100 µg/ml) for an overnight culture until $A_{600\,nm}$ = 4.0. This medium was diluted in 1L LB medium with ampicillin and incubated at 37°C and 230 rpm until $A_{600\,nm}$ reached nearly 0.8, which took 3 - 5 h. 1 ml culture was kept as a control sample and 100 µM of IPTG was added into the remaining culture to induce protein expression. The culture was incubated overnight (between 16 and 20 h) at 37°C and 230 rpm.

The cells were harvested by centrifugation and re-suspended with 40 ml arrestin buffer and lysed by sonication (HD 2070, sonopulse) for 3 min/time, 7 cycles on ice. Then, the solution was ultracentrifuged at 35000 rpm for 35 min at 4°C. The supernatant was collected and filtered through a 0.45 μm filter. A 1 ml column Bio-Scale mini profinity cartridge was used to purify arrestin. Upon equilibration of the column by using 10 volumes of arrestin buffer, the filtered sample was loaded by means of a syringe at a flow rate of 3 ml/min. Finally the cartridge was washed with 40 ml arrestin buffer. The total time for the binding and washing steps ranges between 30 min to 40 min, a period in which cleavage of arrestin from the prodomain/profinity eXact™ fusion tag by immobilized S189 subtilisin BPN' is negligible. Arrestin was released and eluted from the column bound prodomain/profinity eXact™ fusion tag by initially injecting 3 ml arrestin elution buffer followed by a 20-30 min incubation at RT, and then an addition of 2 ml arrestin elution buffer again. Samples of unbound protein, washes and elutions were loaded onto an SDS-PAGE gel and Coomassie blue staining was used to observe the protein bands (see section 3.6.4.1).

Buffers:

- Arrestin buffer: 10 mM MOPS pH 7.2 containing 50 mM NaCl and 0.1 mM PMSF and protease inhibitor (filtered before use).
- Arrestin elution buffer: Arrestin buffer containing 0.1 M NaF

3.6.7 Arrestin R175E interaction with rhodopsin

In this thesis, two experiments were carried out to determine arrestin binding to rhodopsin. One is the pulling down assay which is used to detect the interaction between arrestin and rhodopsin in membranes. Another is the Meta II decay measurement by fluorescence detection to show arrestin inhibition of retinal release from Meta II.

3.6.7.1 Arrestin R175E binding to light-activated rhodopsin

In the dark state, 1.55 μM purified arrestin was mixed with 1.1 μM Rho in ROS membrane in 800 μl arrestin buffer, and separated into two samples (400 μl/each). One sample named "dark state" was kept in the dark at RT. Another sample called "light state" was illuminated (> 495 nm) for 5 min at RT under a light of 150 W. These samples were pelleted by centrifugation in the dark

at 6000 rpm for 30 min at 4°C. The supernatant was removed, and washed with 500 μl of arrestin buffer. These washing steps were repeated six times. Finally the pellets from dark state and light state were solubilized in 20 μl of arrestin buffer and subject to SDS-PAGE (described in section 3.6.4.1).

3.6.7.2 Meta II decay measurement by fluorescence spectroscopy

Purified rhodopsin and arrestin R175E were mixed in arrestin buffer at different ratios, 1:0, 1:2 and 1:4 respectively, and the fluorescence intensity was measured until stabilization. Then, the sample was illuminated for 30 s and the fluorescence increase was measured as described in section 3.6.2.1.

3.6.8 M3R and mutants membrane protein preparation

M3R WT and M3R mutants named M3R-N132G, M3R-D518N, M3R-D518K and M3R-K523Q were separately transfected or cotransfected with tau protein into HEK293S-GNTI$^-$ cells and HEK293T cells. Here, HEK293S-GNTI$^-$ cells was used for further detection by WB, and HEK293T cells were used to detect the protein trafficking by immunocytochemistry. After 48 h incubation, samples were harvested and re-suspended with 200 μl PBS for each sample. 1 μl sample was dissolved in 100 μl PBS to detect the amount of cells under $A_{540\ nm}$ by spectrophotometry. Absorbance of the samples was adjusted to the same value diluting with PBS. 10 μl 10% DM was added to each sample which was agitated for 1 h at 4°C and then centrifuged at 6000 rpm for 30 min. The supernatants including proteins were collected and detected by WB.

3.6.9 Immunocytochemistry detection

To detect the interaction between M3R and mutants and tau protein in cells, immunofluorescence was used by checking different fluorescence signals. The cells were cultured in 6 well plates, transfected by PEI reagent and incubated for 24 h. The medium was removed and cells were rinsed twice with PBS. 1 ml 3.7% formaldehyde fixative was added into each well and incubated at 37°C for 20 min to fix the cells onto the coverslips. Cells were gently washed with TBS 3 times, 5 min per time. To avoid unspecific binding, cells expressing M3R and the mutants were blocked directly with 5% milk in TBS for 30 min at RT. Cells expressing IC tau protein were incubated with the permeation buffer, to increase membrane permeability, before blocking.

Briefly, each well was washed three times with the permeation buffer, for 4 min each, with agitation. After permeation, cells were washed with TBS 3 times, 5 min per time, and blocked with 5% milk in TBS for 30 min at RT and agitation.

Cells were incubated for 1h with the corresponding primary antibody. TTBS was used to wash the cells three times for 5 min each. Then the secondary antibody conjugated to fluorescein was used for 1 h, followed by three times washing with TTBS for 5 min. Two types of protein samples have been used in the immunofluorescence experiments and the corresponding antibodies are listed in Table 3.4. Antibodies were dissolved in TBS buffer. In co-transfection experiments, primary and secondary antibodies were used for 1 h separately. In our experiments, tetramethylrhodamine (TRITC) and fluorescein isothiocyanate (FITC) fluorescent dyes were used for conjugation to the different secondary antibodies for cellular imaging.

Table 3.4 Immunocytochemistry samples and antibody classification.

M3R WT, M3R mutants and tau protein were detected by immunofluorescence. All the samples were incubated with their corresponding antibodies.

Samples	M3R and mutants	Tau protein
Source and expression	COS-1, HEK293T cells	COS-1, HEK293T cells
Primary antibody	mAChR M3R rabbit polyclonal IgG	Tau-5 mouse monoclonal IgG
Primary antibody dilution	1:1000	1:5000
Secondary antibody	TRITC anti-rabbit IgG	FITC anti-mouse IgG
Secondary antibody dilution	1:200	1:200
Absorption spectrum	550 nm	490 nm - 495 nm
Emission spectrum	620 nm	525 nm - 530 nm
Color on immunofluorescence	Orange fluorescence	Yellow-green fluorescence

After the incubation with antibodies finished, the coverslips were taken out and mounted on a glass slide with a mounting medium for fluorescence with 4’, 6-diamidino-2-phenylindole (DAPI) stain (Vector Laboratories, Inc), which stains the nucleus to blue. A fluorescence microscope was used to detect the fluorescence signals.

3.6.10 Lowry protein assay

The Lowry protein assay is a biochemical assay for determining the total concentration of protein in a solution. It is used to detect the protein concentration. Different concentrations of bovine serum albumin (BSA) were prepared to construct a standard calibration line (Table 3.5). The protein sample (20 µl) and buffer (blank) (20 µl) were also prepared at the same time.

Table 3.5 Standard BSA samples preparation.

Six different concentrations of BSA samples diluted in water were used as a standard.

	BSA1	**BSA2**	**BSA3**	**BSA4**	**BSA5**	**BSA6**
Final C_{BSA}	0.9 µg/µl	0.8 µg/µl	0.7 µg/µl	0.6 µg/µl	0.5 µg/µl	0
0.1% BSA (1 µg/µl)	18 µl	16 µl	14 µl	12 µl	10 µl	0 µl
H_2O	2 µl	4 µl	6 µl	8 µl	10 µl	20 µl

9.8 ml Lowry solution A and 0.2 ml Lowry solution B were mixed together and 0.9 ml of this mixture was added to 20 µl of each sample (BSA 1-6, protein sample and blank) and mixed thoroughly. After 15 min incubation at RT, 0.1 ml 1.0 N Folin and Ciocalteu's phenol reagent was added to each sample, subject to vortex and incubated for 5 min at RT. Measurement of $A_{660\ nm}$ was used to determine protein concentration from the BSA standard concentration line.

Buffers:

- Lowry solution A (10 ml): 0.1 M NaOH (40 mg) and 0.2 g Na_2CO_3 dissolved in 10 ml ddH_2O
- Lowry solution B (10 ml): 0.1 g potassium sodium tartrate tetrahydrate and 50 mg $CuSO_4$ dissolved in 10 ml ddH_2O. $CuSO_4$ was dissolved first to avoid any aggregation.

4. RESULTS AND DISCUSSION

4.1 Increased conformational stability of rhodopsin mutants associated with RP in phospholipid bicelles

Rhodopsin WT and two RP mutants, G90V and N55K, were studied for spectroscopic and functional characterization under artificial membrane DMPC/DHPC bicelles condition. G90V showed very low thermal stability in the dark state [70,157]. On the other side, N55K, associated with sector RP, also showed structural instability in the dark and thermal sensitivity [79]. Herein, 9-*cis*-retinal was used as an exogenous retinal analog [69,79,158], in the regeneration of rhodopsin and subsequent mutants purification. Considerable efforts have been done to increase the stability of rhodopsin mutants in the past, such using salts, detergents and phospholipids [91,94,97]. All the characterized parameters of the rhodopsin WT and G90V, N55K mutants can be compared in DMPC/DHPC bicelles and DM detergent and can be responsible for inherited retinal disorders.

4.1.1 Stability of Rho in DMPC/DHPC bicelles

DMPC/DHPC bicelles have been used to increase the thermal stability of purified rhodopsin obtained from ROS membranes [33,35,94]. In this case, ROS rhodopsin, solubilized in DM (Rho_{DM}), was used to confirm the effectiveness of DMPC/DHPC bicelles in maintaining protein stability.

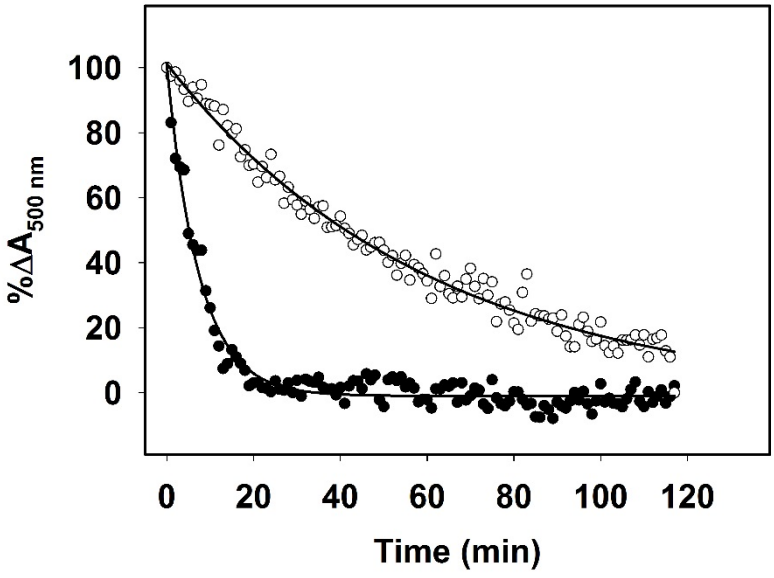

Figure 4.1 DMPC/DHPC stabilization of rhodopsin from ROS.

Thermal stability, in the dark, of Rho_{DM} (•) or $Rho_{bicelles}$ (o) at 55°C was characterized as explained in section 3.5.1. Spectra were recorded and normalized absorption maximum (Amax) were plotted over time per min (see section 3.6.1.2). At the end of the thermal decay, 50 mM hydroxylamine (pH 7.0) was added to confirm complete decay. Curves were fit to an exponential decay function.

The decay of the visible band (500 nm) was followed for Rho_{DM} and rhodopsin in bicelles ($Rho_{bicelles}$) at 55ºC (Figure 4.1) and the $t_{1/2}$ for the processes were determined. $t_{1/2}$ for $Rho_{bicelles}$,

at 55ºC (41.2 ± 2.5 min) was about 9 fold larger than $t_{1/2}$ for Rho_{DM} (4.7 ± 0.4 min) indicating that DMPC/DHPC bicelles remarkably increased the thermal stability of rhodopsin in comparison to the detergent-solubilized samples, in agreement with previous reports [35,70].

4.1.2 UV-Vis spectral characterization of purified WT, G90V, and N55K mutants

WT and G90V, N55K mutants were purified from transfected COS-1 cells and their UV-Vis spectral properties were compared in either DM buffer (Figure 4.2) or bicelles buffer (Figure 4.3). A summary of the spectral features of the DM buffer samples, including λ_{max} value of the visible chromophoric band, molar extinction coefficient (ε) and spectral ratio ($A_{280}/A_{\lambda max}$) is shown in Table 4.1. The band with a maximum at $\lambda_{280\ nm}$ is related to the total protein and includes the regenerated protein, misfolded protein and opsin species that may have lost the chromophore during the purification process [159]. The UV-Vis characterization of WT, N55K and G90V (regenerated with 9-*cis*-retinal) in DM detergent and in DMPC/DHPC bicelles was performed (Figure 4.2 and 4.3). The 9-*cis* isomer was used because it has been shown to improve chromophore regeneration of rhodopsin mutants [21]. The visible bands of the WT and the mutants appear blue-shifted, with regard to the 11-*cis*-retinal containing samples [158], due to the specific differential interaction of 9-*cis*-retinal with the amino acids in the binding pocket. The WT, G90V and N55K mutants showed visible absorbance bands at 486 nm, 480 nm and 480 nm respectively.

Table 4.1 Spectroscopic properties of WT and RP mutants with 9-*cis*-retinal purified in DM buffer.

[a]Mean values of the visible λ_{max} of WT and RP mutants G90V, N55K in DM buffer. [b]Each ε value was calculated with the equation: $\varepsilon = (A / A_{Rho})(A_{440\ Rho} / A_{440})\ \varepsilon_{Rho}$, where A is the absorbance at the λ_{max} value, A_{440} is the absorbance at 440 nm after acid denaturation, and the ε_{Rho} is the molar extinction of rhodopsin ($43.2\times10^3\ M^{-1}cm^{-1}$) [70]. [c]The A_{280} / A_{max} ratio reflects the extent of chromophore regeneration. All values were determined as averages from 3 independent experiments.

Opsin	[a]λ_{max} (nm)	[b]ε x 10^3 ($M^{-1}cm^{-1}$)	[c]A_{280} / A λ_{max}
WT	486 ± 3	43.2 ± 0.1	2.4 ± 0.1
G90V	480 ± 3	34.1 ± 0.5	3.0 ± 0.3
N55K	480 ± 2	35.5 ± 0.3	5.1 ± 1.6

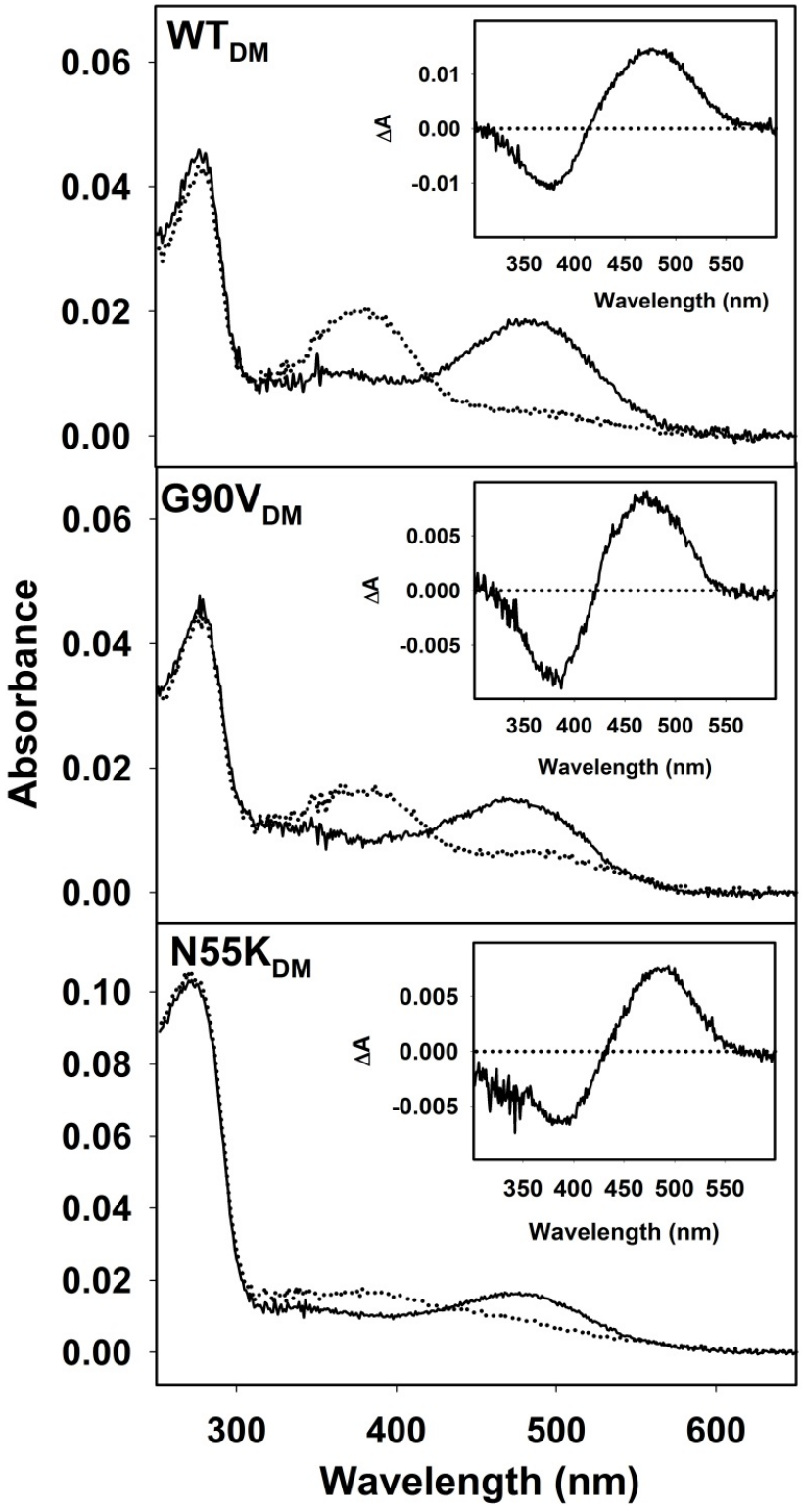

Figure 4.2 UV-Vis characterization of WT, N55K and G90V (regenerated with 9-*cis*-retinal) in DM buffer.

WT and G90V and N55K mutants were immunopurified in 0.05% DM buffer. The spectra were obtained at 20ºC. Illumination was carried out for 30 s with a 150 W power source equipped with an optic fiber guide using a > 495 nm cut-off filter. (—) Dark state. (⋯) photobleached state; inset, difference spectrum (dark-light).

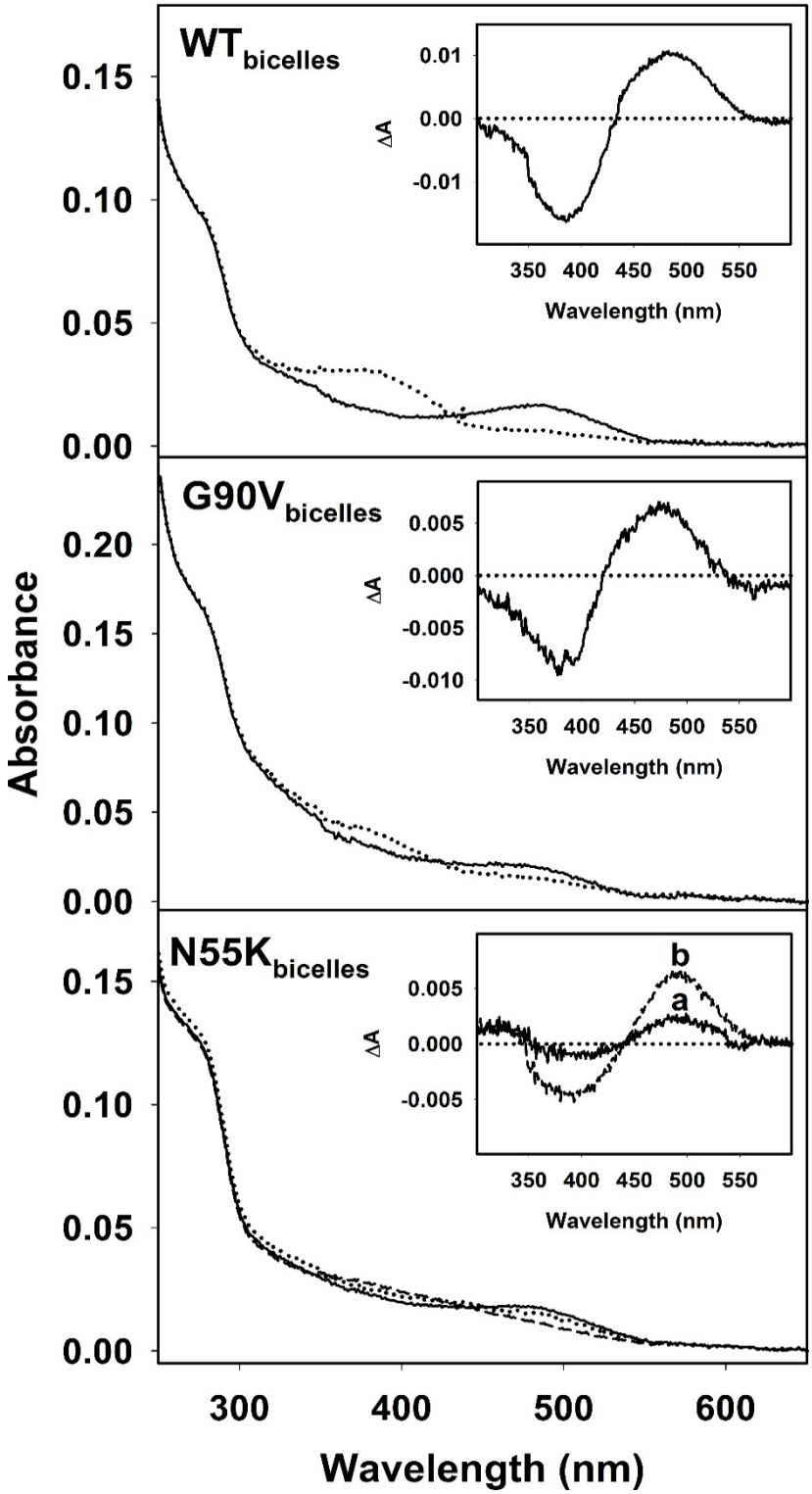

Figure 4.3 UV-Vis characterization of WT, N55K and G90V in bicelles.

WT, G90V, and N55K were purified and inserted into DMPC/DHPC bicelles. The spectra were measured at 20ºC. Illumination was carried out with a 150 W power source equipped with an optic fiber guide using a > 495 nm cut-off filter. (—) Dark state; (⋯) photobleached state after 30 s illumnation; (---) photobleached state after 60 s illumination. Inset, difference spectrum (dark-light). Notably, $N55K_{bicelles}$ showed only 20% photobleaching (a), and illumination for a further 30 s caused further decay of the visible band (b).

In DM buffer (Figure 4.2, Table 4.1), G90V and N55K mutants showed a higher $A_{280}/A_{\lambda max}$ ratio than WT, especially N55K, which showed a 2-fold larger ratio than WT. The high $A_{280}/A_{\lambda max}$ ratio implies lower chromophore regeneration. Besides, N55K showed much lower purification yield which is nearly 30% of G90V and only 15% of WT during the purification process which likely indicates some misfolding effect due to the mutation [79].

Upon illumination, $G90V_{DM}$ and $N55K_{DM}$ mutants showed incomplete conversion of the visible band to the 380 nm absorbing species with ~25% remaining absorbance at this wavelength indicating partial trapping of a photointermediate with a protonated SB linkage (Figure 4.2) [70,79]. WT and G90V showed similar behavior upon illumination in DM buffer and in bicelles buffer (Figure 4.2 and 4.3). While $N55K_{bicelles}$ showed an altered photobleaching pattern and double illumination time which was required to shift most of the visible band to 380 nm compared with $N55K_{DM}$ (Figure 4.3).

During the purification, the WT and mutants were purified by the process as described in section 3.4.2 by which the proteins were dissolved in DM detergent, or inserted into DMPC/DHPC bicelles as described in section 3.5.1. Compared with WT_{DM}, the ratio $A_{280}/A_{\lambda max}$ of $G90V_{DM}$ and $N55K_{DM}$ is 3.0 and 5.1 respectively which approximately is 1.2 and 3.2 fold. This could be interpreted as $N55K_{DM}$ mutant showing lower chromophore stability during the purification process than the other proteins (Figure 4.2) [79]. Upon illumination, $G90V_{DM}$ and $N55K_{DM}$ also showed abnormal photobleaching behavior, with incomplete conversion of the visible band (Figure 4.2) which is a behavior also seen for other rhodopsin mutants [70,79].

The DM detergent forms micelles to stabilize the protein (see section 1.3.1) [70,106] whereas the DMPC/DHPC bicelles provide a lipid bilayer mimic membrane for protein stabilization (see section 1.4.1) [35,121]. The schematic models for these arrangements were shown in Figure 1.9. Upon purification of WT and mutant rhodopsins in bicelles environment, misfolding cannot be determined by the ratio $A_{280}/A_{\lambda max}$ due to the high background detected on the spectrum (Figure 4.3). However, the illumination shift at the visible band can be clearly characterized for both WT and the mutants (Figure 4.3). In bicelles environment, $WT_{bicelles}$ showed nearly complete illumination and the peak shifted from 486 nm to 380 nm. $G90V_{bicelles}$ depicted $G90V_{DM}$-like character, with incomplete but similar photobleaching conversion from 480 nm to 380 nm as in

DM conditions. $N55K_{bicelles}$ showed an altered illumination pattern. Upon two illumination times, the $N55K_{bicelles}$ mutant only showed 1/5 photoconversion at the first time (Figure 4.3 N55K line a) and about 1/2 illumination at the second time (Figure 4.3 N55K line b). The visible band of $N55K_{bicelles}$ appears to be more stable than $N55K_{DM}$, indicating that bicelles stabilized its dark state (Figure 4.3).

4.1.3 WB of WT and G90V and N55K mutants in DM and in bicelles

Purified proteins were electrophoretically characterized by means of WB analysis (Figure 4.4).

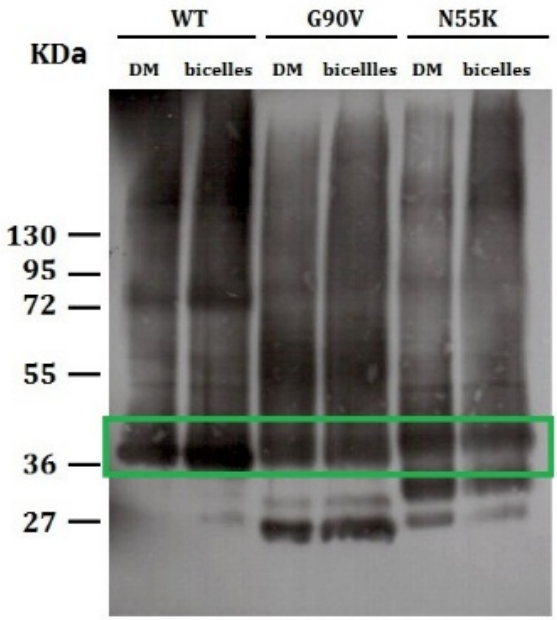

Figure 4.4 WB of WT and G90V, N55K in either DM detergent or bicelles conditions.

WT, G90V and N55K mutants were purified from COS-1 cells either in DM buffer or bicelles buffer respectively (as explained in section 3.6.5). The same amount of protein was loaded onto a SDS-PAGE gel, subject to electrophoresis and subsequently transferred to a nitrocellulose membrane for detection. Below the main opsin band (green rectangle), G90V and N55K mutants also showed bands, associated to truncated forms of the protein, or to non-glycosylated species.

$WT_{bicelles}$ showed more dimer bands and high-mobility species than WT_{DM} which can be tentatively assigned to oligomeric species of rhodopsin although the contribution of protein aggregation cannot be ruled out. G90V showed a prominent characteristic 27 kDa lower band that has been attributed to a truncated form of rhodopsin [50,51]. This band was detected both in

DM and in bicelles. In the case of N55K mutant, $N55K_{bicelles}$ showed a less intense 27 kDa and an apparent increase in the high molecular mass species band when compared to the $N55K_{DM}$ pattern.

Therefore, the electrophoretic analysis of the purified mutant proteins revealed differences in the intensities of bands that would correspond to dimeric (or higher-order oligomeric) conformations that appeared to be favored in bicelles. This behavior suggests that the mutants may have increased susceptibility to protein truncation, associated to a decreased conformational stability during protein purification, and/or linked to the molecular phenotype underlying the pathological nature of the mutations.

4.1.4 Characterization of WT, G90V and N55K in DM and in DMPC/DHPC bicelles by means of thermal stability, chromophore regeneration and Meta II decay assays

4.1.4.1 Thermal stability of WT, G90V and N55K in DM and DMPC/DHPC bicelles

WT, G90V and N55K were eluted in either DM buffer or bicelles buffer and their thermal stability was determined at 37ºC (Figure 4.5). WT in DM and bicelles showed high thermal stability which decreased only less than 10% in 2.5 h. $G90V_{bicelles}$ and $N55K_{bicelles}$ showed enhanced thermal stability when compared to the DM-solubilized samples. Thermal decay process involves protein conformational changes, retinal isomerization and eventually hydrolysis of SB and chromophore release [34,94,160]. The $t_{1/2}$ of $G90V_{bicelles}$ and $N55K_{bicelles}$ suffered a 3 and 4 fold increase respectively when compared to those of the detergent-solubilized samples (Figure 4.5 and Table 4.2A).

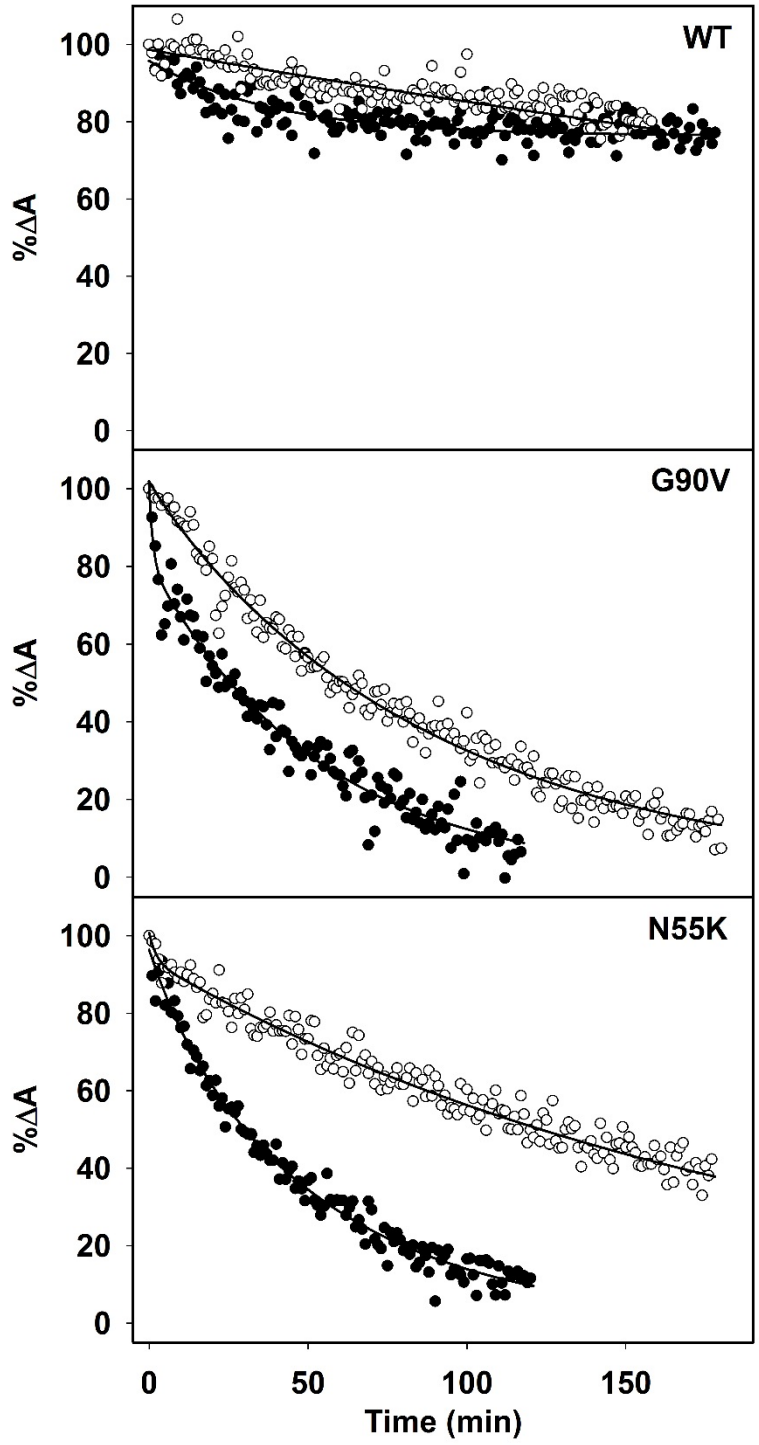

Figure 4.5 Thermal stability of WT, G90V and N55K in both DM and bicelles conditions.

The panel shows the thermal decay process of WT and G90V and N55K mutants in buffer A containing DM detergent (•) and in the bicelles buffer (o) described in section 3.5.1. The experiments were run at 37°C and normalized absorbance values at the A_{max}, in the visible region, were plotted over time. The spectra were recorded every minute. At the end of the thermal decay, 50 mM hydroxylamine (pH 7.0) was added to confirm the complete decay. Curves were fit to an exponential decay function.

4.1.4.2 Chromophore regeneration of WT and G90V and N55K mutants in DM and DMPC/DHPC bicelles

The effect of DMPC/DHPC bicelles on pigment regeneration after photobleaching was analyzed for the purified proteins. The maximal extent of regeneration and the regeneration rate were the main factors analyzed (Figure 4.6).

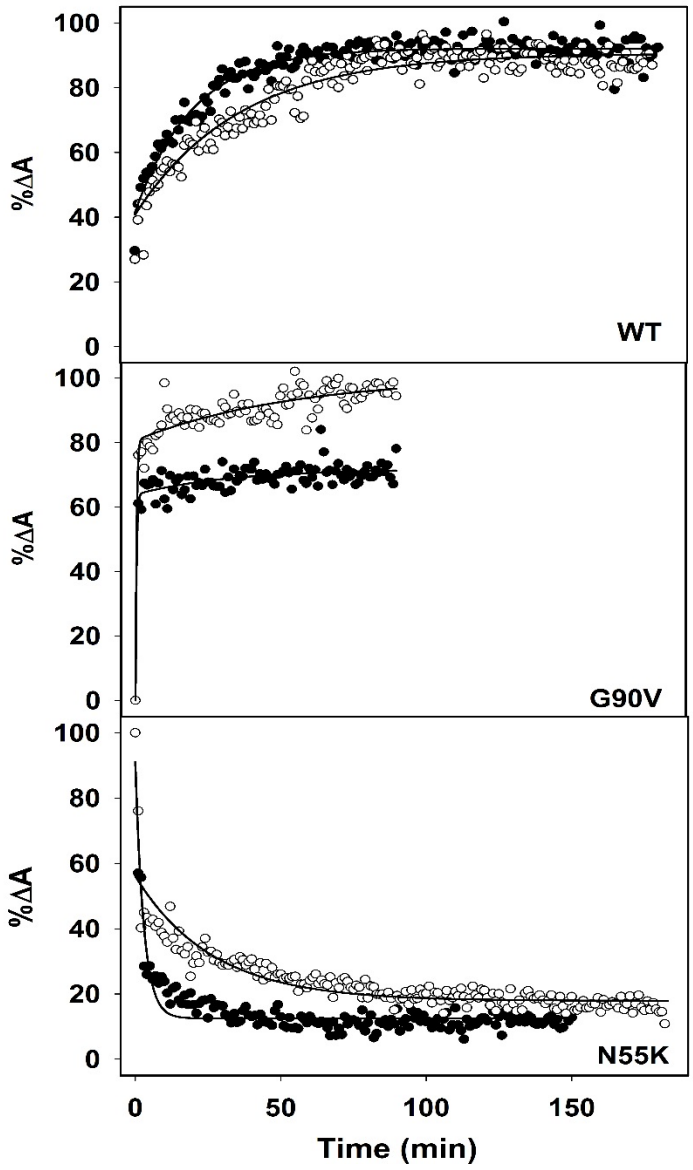

Figure 4.6 Chromophore regeneration of WT and opsin mutant pigments in bicelles.

The chromophore regeneration rates for bleached WT, G90V and N55K mutant were measured in buffer A containing (•) DM detergent and (o) bicelles buffer. 9-*cis*-retinal was added to the samples, and regeneration rates were determined by measuring the absorbance increase at the visible A_{max} after pigment illumination with a cut-off filter of $\lambda > 495$ nm. The experiments were run at RT and normalized absorbance values at the A_{max}, of the visible band, were plotted over time. The spectra were recorded every minute.

The rate of regeneration was clearly faster in the bicelles system. The 9-*cis*-retinal regeneration

extent was similar both for WT_{DM} and $WT_{bicelles}$. $G90V_{bicelles}$ showed 20% more chromophore regeneration than $G90V_{DM}$. In contrast, N55K exhibited a special behavior. Upon the illumination with 30 s, $N55K_{DM}$ and $N55K_{liposomes}$ only caused 30-40% photoconversion of the visible absorbance band. After 9-*cis*-retinal addition, N55K did not show apparent chromophore regeneration but a decrease on A_{max} suggesting a consistently retinal release possibly due to an impaired retinal entrance. Even though, DMPC/DHPC bicelles still helped N55K kept 5% more chromophore in the binding pocket than in DM detergent (Figure 4.6 and Table 4.2B).

4.1.4.3 Meta II decay of WT, and G90V and N55K mutants, in DM and DMPC/DHPC bicelles

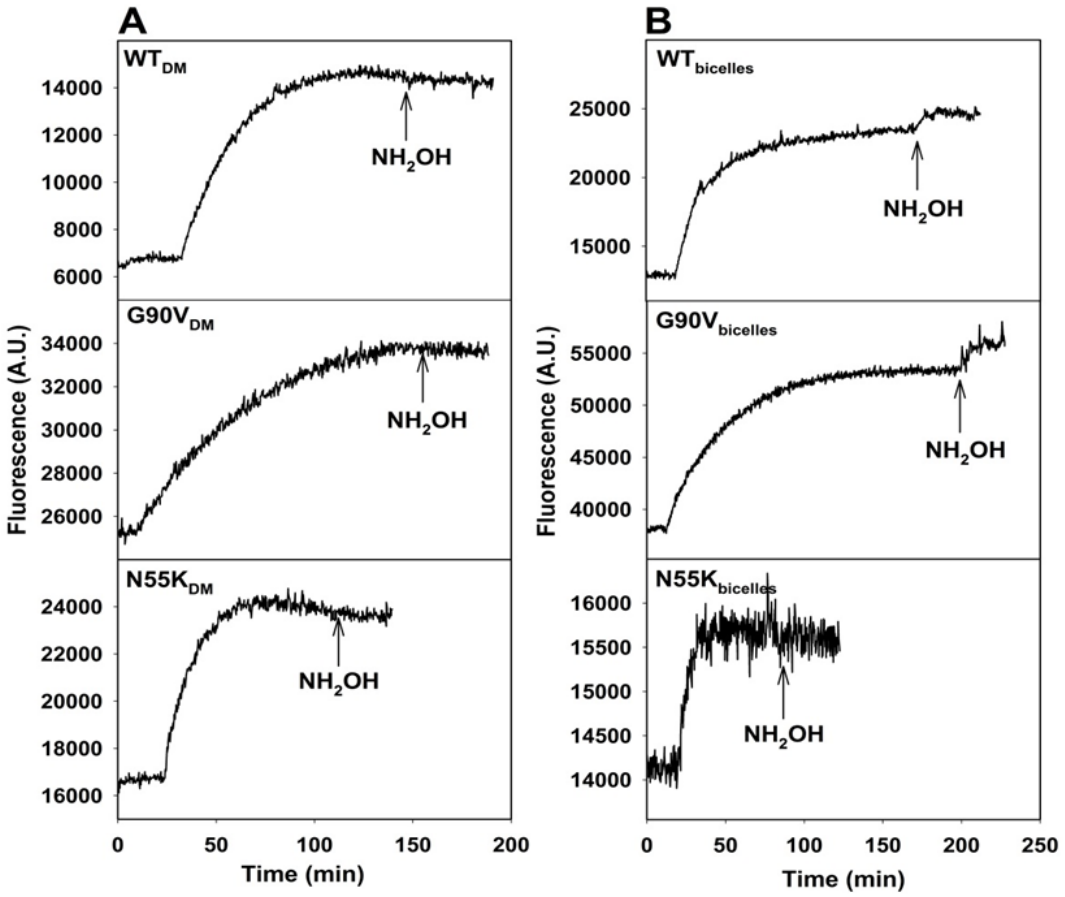

Figure 4.7 Meta II decay for WT and G90V, N55K mutants.

WT, G90V and N55K were purified in either DM buffer (panel A) or in bicelles buffer (panel B). The samples were illuminated for 30 s (λ > 495 nm) after the dark-state fluorescence intensity was stabilized. After Meta II decay and once the fluorescence intensity reached plateau, 50 mM hydroxylamine, pH 7.0, was added to confirm complete retinal release.

Meta II stability was studied by fluorescence spectroscopy, which measures retinal release upon sample illumination [155]. Overall, the retinal release process was faster in bicelles than in DM

samples. Under both conditions, $t_{1/2}$ values for retinal release followed the order G90V >> WT > N55K, being G90V the slowest (Figure 4.7 and Table 4.2C). This behavior could be tentatively associated with the clinical phenotypes caused by these mutations.

In all cases, bicelles have shorten $t_{1/2}$ of the retinal release process for WT (25.4%), G90V (39.8%), and N55K (7.9%) compared with the same process in DM buffer (Figure 4.7 and Table 4.2C). Hydroxylamine was added in order to confirm complete retinal release. No changes were detected for WT and G90V and N55K mutants in DM buffer (Figure 4.7A), but in bicelles environment both WT and G90V mutant showed a slight additional increase of Trp fluorescence emission which suggested additional retinal release from the binding pocket (Figure 4.7B). On the other hand, after hydroxylamine addition, N55K did not show increase on fluorescence intensity either in DM or in bicelles. This result was in contrast to that obtained in a previous study in which hydroxylamine did cause the fluorescence signal increase of N55K dissolved in PBS (pH 7.4) and containing 0.05% DM, pointing out to a strong effect of buffer in the spectrofluorimetric measurements [79]. In addition, different fluorescence intensities can be observed between DM (Figure 4.7A) and bicelles (Figure 4.7B) because of potential contribution from the DMPC/DHPC bicelles to the fluorescence signal.

Overall, the data from thermal stability, chromophore regeneration and Meta II decay experiments is summarized in Table 4.2 and further analyzed in Figure 4.8 to determine the conformational properties of WT, G90V and N55K in both DM and DMPC/DHPC bicelles.

The thermal stability for the mutants at 37ºC was clearly improved in the bicelles system. WT in DM and in DMPC/DHPC bicelles was stable for hours at 37ºC. On the other hand, a 3-fold of $G90V_{bicelles}$ and a 4-fold of $N55K_{bicelles}$ increase in the thermal stability were determined compared with $G90V_{DM}$ and $N55K_{DM}$ respectively, meaning that bicelles provide conformational stability, and a better environment to protect the SB linkage from hydrolysis (Figure 4.5, 4.8A and Table 4.2A) [160].

Table 4.2 WT and RP mutants thermal stability (A), chromophore regeneration (B) and Meta II decay (C) in DM and bicelles.

[A]$t_{1/2}$ of WT and G90V and N55K mutants in thermal bleaching experiments, as explained in section 3.6.1.2. Thermal decay experiments were run at 37°C. At the end of the thermal decay, 50 mM hydroxylamine (pH 7.0) was added to confirm complete decay. Curves were fit to an exponential decay function. [B]Regeneration percentage of WT and G90V and N55K mutants. Retinal was added before illumination and spectra were recorded every min after illuminating the samples for 30 s using a > 495 nm cut-off filter. These experiments were run at 20ºC. [C]Retinal release $t_{1/2}$ of WT, G90V and N55K mutants. Samples were stabilized for 10 min in the dark and subsequently illuminated for 30 s using a > 495 nm cut-off filter. Fluorescence increase was measured until the signal reached a plateau. 50 mM hydroxylamine pH 7.0 was added to confirm complete retinal release. The $t_{1/2}$ of the retinal release was determined from the exponential curves.

`	Buffer	WT	G90V	N55K
[A]Thermal bleaching	DM	> 180 min	22.5 ± 3.1 min	30.1 ± 1.7 min
	bicelles	> 180 min	64.1 ± 3.7 min	123.5 ± 2.6 min
[B]Regeneration	DM	91.8 ± 3.2%	70.8 ± 3.3%	11.7 ± 1.9%
	bicelles	88.9 ± 3.2%	96.2 ± 2.3%	16.9 ± 2.1%
[C]Meta II decay	DM	19.3 ± 0.5 min	34.9 ± 1.0 min	10.1 ± 1.5min
	bicelles	14.4 ± 1.7 min	21.0 ± 2.6 min	9.3 ± 2.1 min

Chromophore regeneration is an important index of structural preservation for rhodopsin mutants (Figure 4.6, 4.8B and Table 4.2B). WT in DM and in DMPC/DHPC bicelles presented similar regeneration of 90% indicating that WT was stable and not significantly affected by the DM or DMPC/DHPC environment. $G90V_{bicelles}$ showed 96% regeneration with 9-*cis*-retinal which is 20% more increase than compared to $G90V_{DM}$ with 70% regeneration, suggesting that lipids play a role in the regeneration process by helping stabilize its optimal ligand-binding conformation (Figure 4.6, 4.8B and Table 4.2B). In contrast, N55K mutant did not show any chromophore regeneration. The retinal release trend of N55K, in DM and in DMPC/DHPC bicelles, indicated that N55K had a low ability to bind 9-*cis*-retinal. It is likely that the N55K mutation impaired retinal release by interfering in the retinal release pathway [161]. In spite of this, DMPC/DHPC bicelles helped N55K in keeping 5% more retinal than in DM detergent (Figure 4.2B).

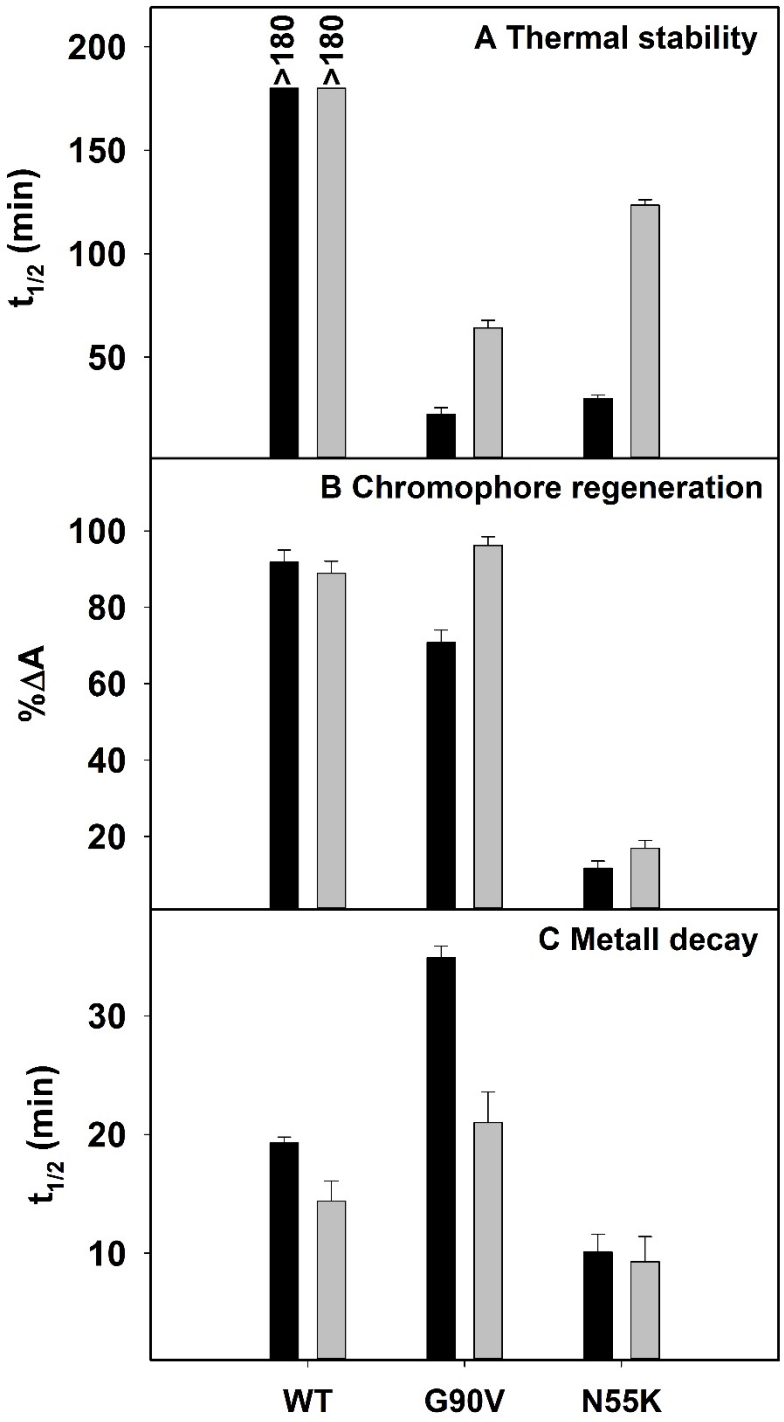

Figure 4.8 Characterization of WT and RP mutant phenotypes by means of thermal stability, chromophore regeneration and Meta II decay assays.

WT, G90V and N55K were purified in DM buffer (black bar) and bicelles buffer (gray bar). A. $t_{1/2}$ of WT, G90V and N55K mutants from thermal bleaching experiments at 37°C; B. Chromophore regeneration percentage of WT, G90V and N55K mutants; C. $t_{1/2}$ of WT, G90V and N55K mutants from the Meta II decay experiments. The numerical values for the measured times are displayed in Table 4.2. The mean and error bars of three independent measurements are represented.

In the Meta II decay experiment (Figure 4.7), the fluorescence of WT and the mutants was allowed to stabilize in the dark, and increased upon illumination. After the fluorescence signal reaching a plateau, hydroxylamine was added to confirm complete retinal release. In DM detergent, there was no fluorescence change upon hydroxylamine addition (Figure 4.7A). On the other hand, after active Meta II decay, subsequent hydroxylamine addition, in bicelles, resulted in an additional fluorescence increase for $WT_{bicelles}$ and $G90V_{bicelles}$. The decreased $t_{1/2}$ of Meta II decay in bicelles meaning Meta II state could stay longer time. The hydroxylamine results indicated that after Meta II decay there is still some retinal in $WT_{bicelles}$ and $G90V_{bicelles}$ (Figure 4.7B) [31]. On the contrary, $N55K_{bicelles}$ did not show any intensity change upon hydroxylamine addition. Figure 4.8 showed the decrease of $t_{1/2}$ of Meta II in WT bicelles and G90V bicelles, N55K did not depict obvious differences between DM and bicelles.

4.1.5 Opsin conformational stability after retinal release

WT and G90V and N55K mutants, in DM buffer or bicelles buffer, were analyzed by fluorescence spectroscopy in order to follow the potential ability of 9-*cis*-retinal to enter the opsin pocket after complete Meta II decay. Thus, 2.5 fold exogenous 9-*cis*-retinal was added, after complete retinal release (plateau in the fluorescence curve), in order to test whether this ligand could enter the binding pocket. Upon retinal addition, WT_{DM} showed only a minor reduction of Trp fluorescence suggesting that the retinal significantly could not enter the binding pocket. A clear decrease in fluorescence was detected in the case of $WT_{bicelles}$, indicating that the exogenous chromophore could enter the binding pocket thus quenching Trp fluorescence. This result indicated that bicelles help to maintain a stable opsin structure for a long time, after the complete retinal release process, thus favoring retinal binding to the protein (Figure 4.9). The structurally unstable mutants G90V and N55K showed a clear distinct behavior. Exogenous addition of 9-*cis*-retinal resulted in an important decrease of the fluorescence signal for $G90V_{DM}$ and a further decrease for $G90V_{bicelles}$ suggesting that lipids play a role in the regeneration process by stabilizing its optimal ligand-binding conformation (Figure 4.9). Compared with WT, G90V appears to have a more open binding pocket that could bind more retinal both in DM and bicelles. However, addition of 9-*cis*-retinal did not cause any changes of $N55K_{DM}$ or $N55K_{bicelles}$ after complete Meta II decay, suggesting that the binding pocket of N55K opsin presented an impaired entrance [76]. This unique N55K behavior may provide new clues that would guide us into deciphering the molecular

mechanism of sector RP. We have previously associated this mechanism to a different response behavior upon light exposure to this mutant [30].

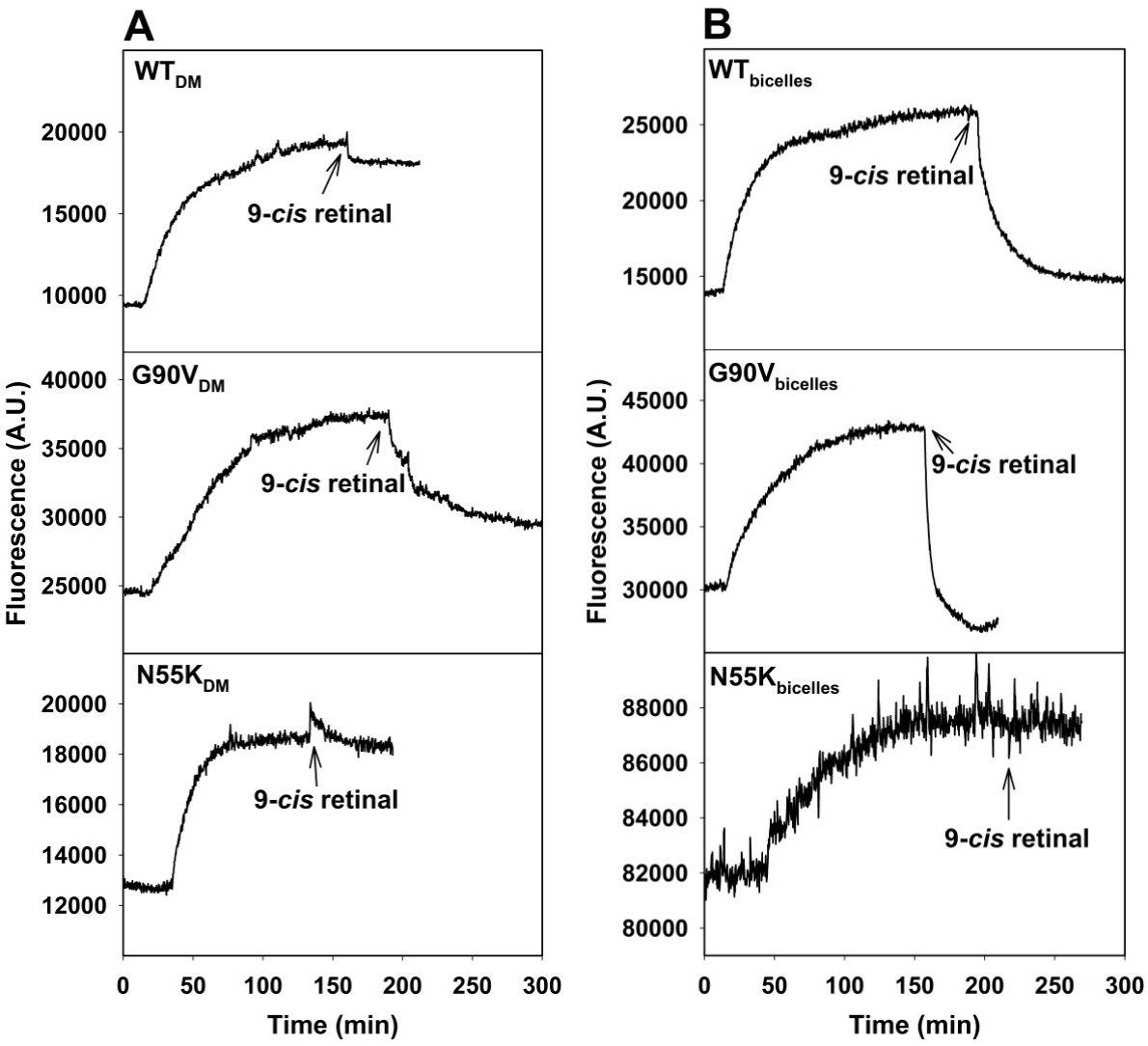

Figure 4.9 Chromophore 9-*cis*-retinal entry in photoactivated opsin.

After fluorescence signal reached a plateau, in the Meta II decay experiment, WT, N55K and G90V pigments purified either in DM buffer (panel A) or bicelles buffer (panel B), retinal was added (2.5 fold of exogenous retinal to the concentration of pigment) to detect retinal entry into the binding pocket (as described in section 3.6.2.2). $WT_{bicelles}$ and $G90V_{bicelles}$ showed more fluorescence decrease compared to the DM samples, whereas $N55K_{bicelles}$ did not show any change upon retinal addition in any condition.

Similar results were obtained when the experiments were carried out by using 11-*cis*-retinal (Figure 4.10). Upon addition of 11-*cis*-retinal (Figure 4.10B), $WT_{bicelles}$ and $G90V_{bicelles}$ could bind more retinal than with 9-*cis*-retinal addition (Figure 4.9B). In contrast, N55K opsin in bicelles remained stable both upon 9-*cis*-retinal and 11-*cis*-retinal exposure. The Y axis data, between A and B in Figure 4.9 and 4.10, is different possible due to bicelles contribution in the background.

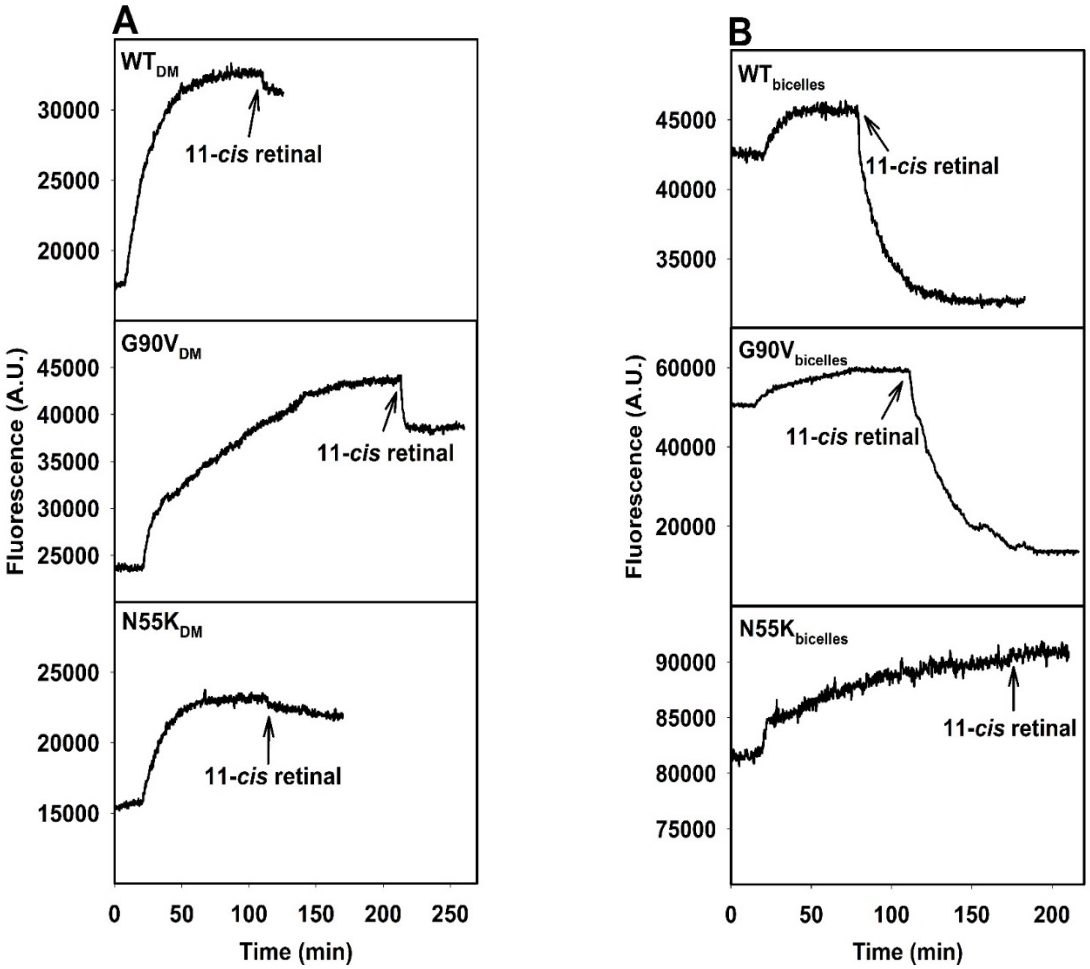

Figure 4.10 Photoactivated visual opsin reconstitution with 11-*cis*-retinal.

After the fluorescence signal reached a plateau, 11-*cis*-retinal was added (2.5 fold of exogenous retinal to the concentration of pigment) and mixed well to determine retinal entrance into the binding pocket. Compared with DM, $WT_{bicelles}$ and $G90V_{bicelles}$ showed a higher decrease in fluorescence. $N55K_{bicelles}$ did not show any change upon 11-*cis*-retinal addition.

In order to analyze accurately the different accessibility of retinal to G90V in DM and bicelles environment, the post-bleached regenerated sample was illuminated again and only the sample in bicelles showed a slight increase in fluorescence which was not apparent in the DM sample. This effect is probably due to hydroxylamine addition that confirmed the entrance of retinal in the binding pocket of photobleached opsin (Figure 4.11).

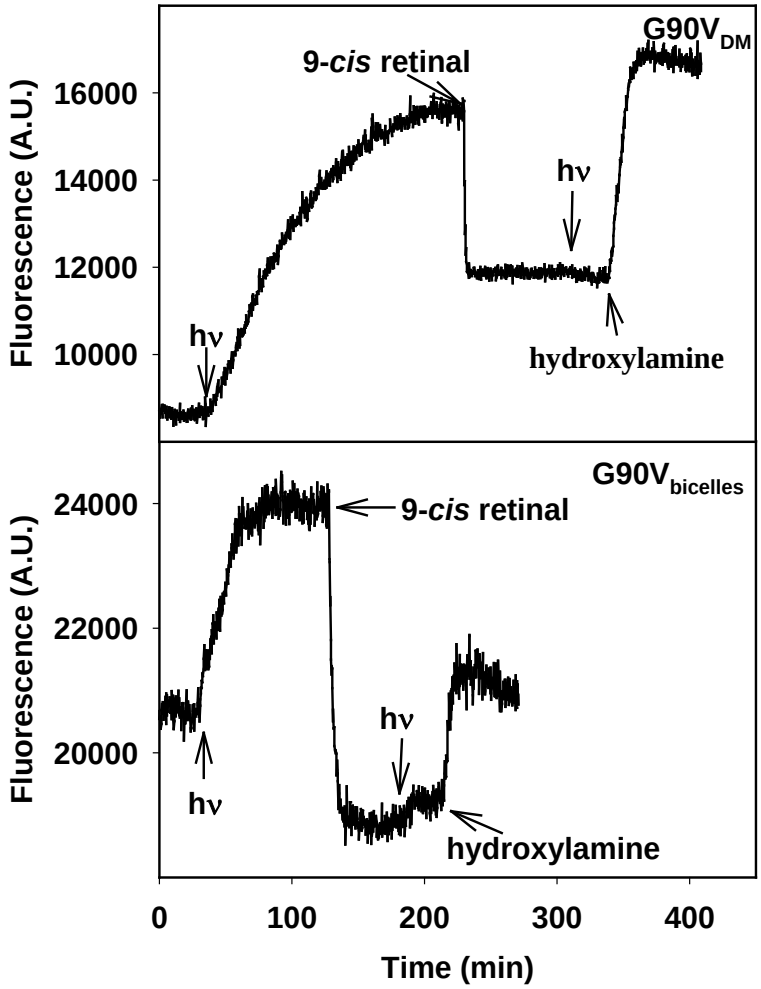

Figure 4.11 Accessibility retinal to the binding site in G90V opsin.

G90V either in buffer A containing DM or in bicelles was illuminated for 30 s using a λ > 495 nm cut-off filter, and the increase in fluorescence intensity was monitored to detect 9-*cis*-retinal release. Once the fluorescence was stable, meaning that Meta II decay was complete, exogenous 9-*cis*-retinal was added to test retinal binding to photobleached opsin. Subsequent second illumination and hydroxylamine addition were done as indicated.

4.1.6 Structural analysis of the rhodopsin mutants

Both mutations, N55K and G90V, are facing inside the protein and are involved in helix-helix interations. Thus, residues at 55 and 90 are not facing the lipid or involved in monomer-monomer interactions (Figure 4.12). Furthermore, the residues do not appear to significantly alter their orientation (or interactions) in the activated state of the receptor [12].

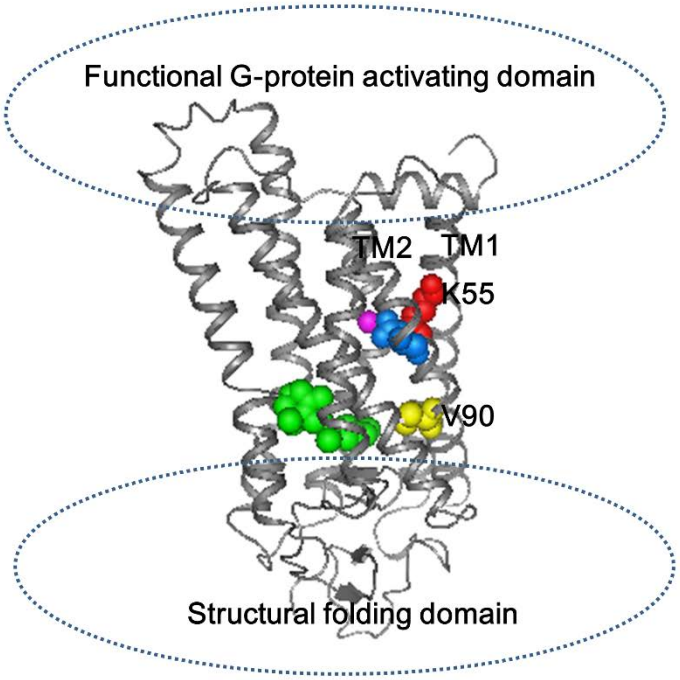

Figure 4.12 Structural model of rhodopsin showing the sites of mutations.

Lys at position 55 (red) and Val at position 90 (yellow) are shown together with other relevant molecules, like retinal (green), Asp83 (blue) and water (magenta). Although the two mutations are located at the transmembrane domain of the protein, Lys55 is closer to the cytoplasmic domain where the G-protein activating function of the receptor takes place, whereas Val90 is closer to the retinal binding site and the intradiscal domain, a region of the protein that governs its folding and stability. Rhodopsin dark-state crystal structure (PDB id 3C9L) was used and the image was created using PyMol (Schrodinger, LLC. The PyMOL Molecular Graphics System, Version 1.5).

In the case of N55K, this mutation is located at transmembrane H1 in a region closer to the cytoplasmic side of the protein where the G-protein activation process takes place. Three highly conserved residues, throughout the GPCRs superfamily, towards the cytoplasmic side of the receptor, N55 (98%), D83 (92%) and N302 (77%), define a region with intimate contact between H1, H2 and H7, which involves also various highly conserved water molecules. In the N55K substitution, the Lys side-chain would interfere with these contacts and could form a salt bridge with D83 (Figure 4.12). The G90V mutation affects an amino acid, at transmembrane H2, which is located towards the intradiscal domain of the protein that plays a structural role in the folding of the receptor and in the retinal binding process. The reported G90V mutant behavior suggests an important role for a functional water molecule present in the vicinity of E113 and the SB in

the dark-state crystal structure of rhodopsin [21]. This water molecule binds to both the carbonyl backbone and one of the carboxyl oxygens of E113. The lack of a side-chain at G90 gives an empty volume that is filled with such a water molecule, whereas the hydrophobic chain in G90V would either not allow the water molecule to be accommodated or result in a smaller affinity. The lack of the water molecule would alter the Meta I to Meta II transition energy landscape and would also decrease dark-state stability [21].

4.2 DHA liposomes effects on the conformational stability of rhodopsin G90V and N55K mutants

To stabilize rhodopsin mutants associated with RP disease, G90V and N55K, and to study the molecular mechanism in more native conditions, DDHA-PC liposomes were used to mimic the bilayer environment. Here, G90V and N55K mutants, with thermal instability and fast decay defect, were purified from COS-1 cells by immunoaffinity chromatography with 11-*cis*-retinal in DM detergent and reconstituted into DDHA-PC liposomes system. A series of techniques were used to detect the conformational stability and the DDHA-PC liposomes function for rhodopsin WT and mutants.

4.2.1 UV-Vis spectrophotometry of immunopurified WT and mutants in DDHA-PC liposomes

The UV-Vis spectral properties of WT and G90V and N55K mutants in detergent have been well characterized previously (Figure 4.13) [70,79]. The proteins were removed from DM detergent to DDHA-PC liposomes (Figure 4.14). The measured spectra showed two main characteristic bands for all opsins: the $\lambda_{280\,nm}$ value of the opsin apoprotein band and the λ_{max} value of the visible chromophoric band [159]. The λ_{max} value of the visible chromophoric band of WT, G90V and N55K mutant is 499 ± 1 nm, 489 ± 1 nm and 495 ± 2 nm respectively, and it does not change under DM detergent and DDHA-PC liposomes environment. In DM detergent (Figure 4.13), the ratio A_{280}/A_{max} of rhodopsin WT is around 1.9, while the ratio of G90V and N55K were 3.5 and 6.3 respectively which is much higher than WT. The high A_{280}/A_{max} ratio is related to the misfolding, aggregation and regeneration problem of mutants. With the presence of DDHA-PC liposomes, the ratio A_{280}/A_{max} of WT and mutants increased largely compared with the proteins in DM detergent. The higher A_{280}/A_{max} ratio in liposomes is mainly caused by the liposomes background absorption rather than by an increase on protein misfolding or aggregation (Figure 4.14).

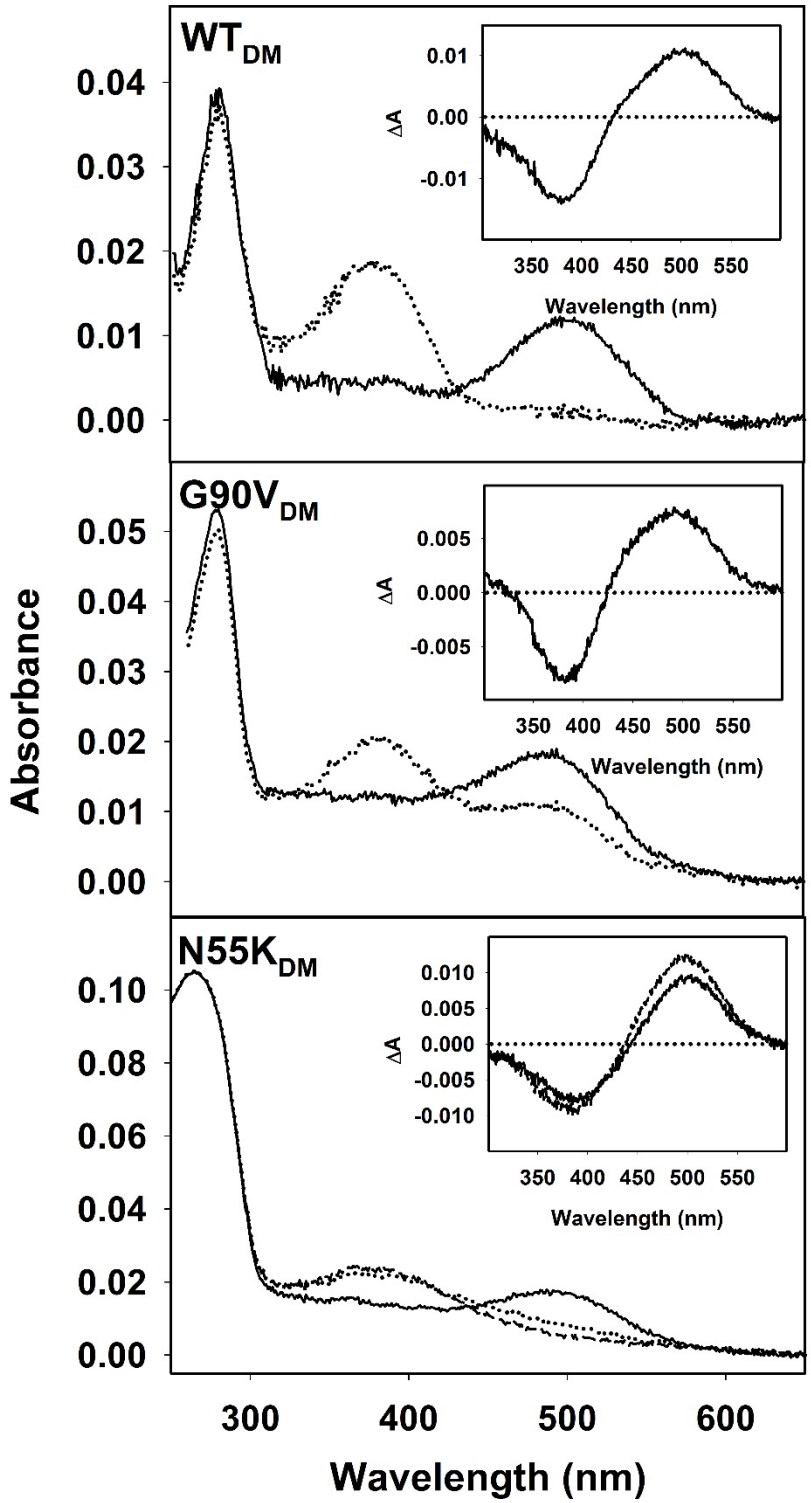

Figure 4.13 UV-Vis characterization of purified WT and N55K and G90V regenerated with 11-*cis*-retinal in DM buffer.

WT, G90V and N55K mutants were expressed in HEK293T cells and were immunopurified in PBS buffer with 0.05% DM. Spectra were recorded at 20ºC. Illumination was carried out for 30 s with a 150 W power source equipped with an optic fiber guide using a $\lambda > 495$ nm cut-off filter. (—) Dark state. (⋯) photobleached state; inset, difference spectrum (dark-light).

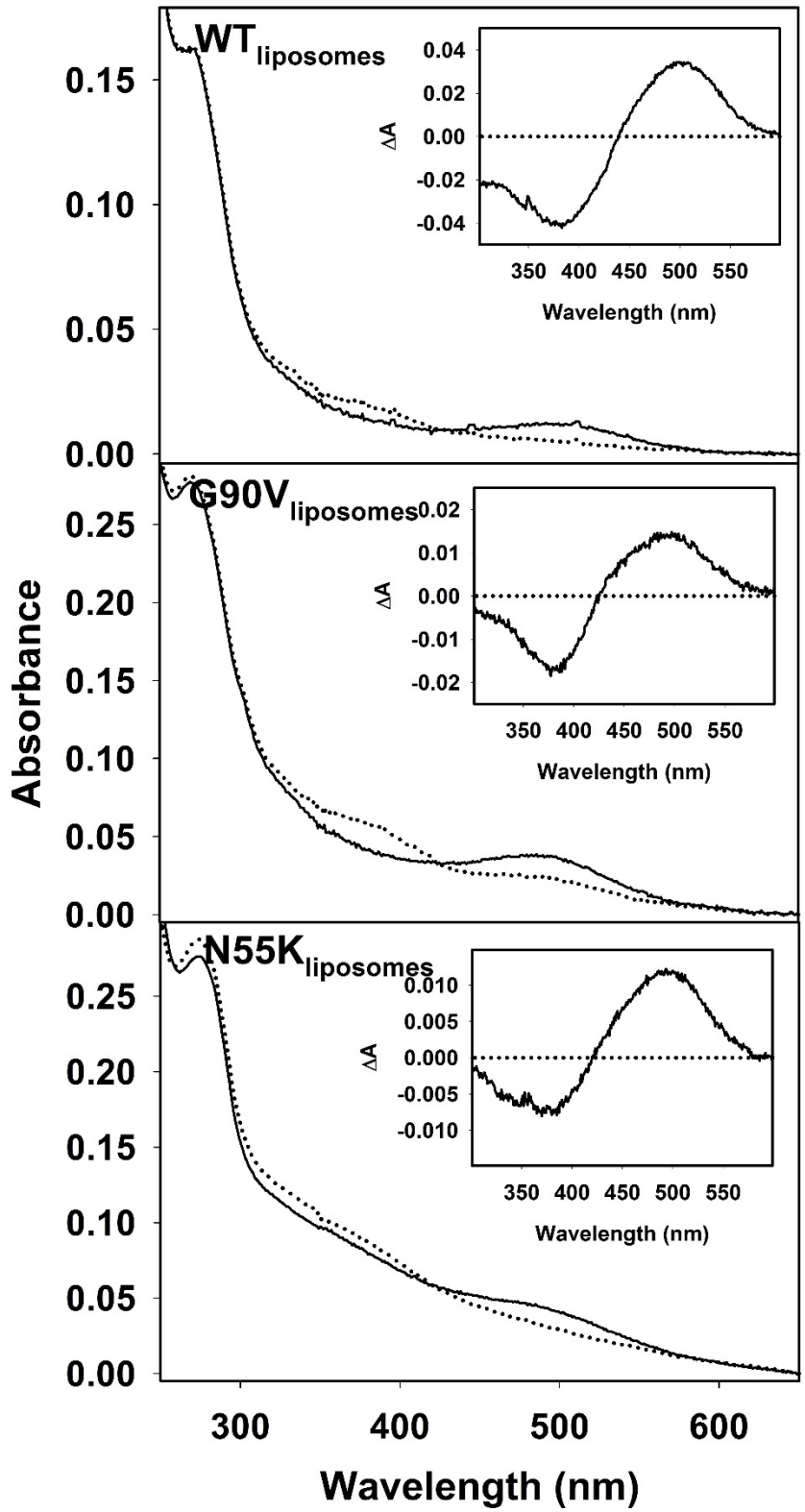

Figure 4.14 UV-Vis characterization of purified WT, N55K and G90V regenerated with 11-cis-retinal in DDHA-PC liposomes.

WT and G90V and N55K mutants were purified and reconstituted into DDHA-PC liposomes. Spectra were recorded at 20ºC. Illumination was carried out for 30 s with a 150 W power source equipped with an optic fiber guide using a λ > 495 nm cut-off filter. (—) Dark state. (⋯) photobleached state; inset, difference spectrum (dark-light).

UV-Vis spectroscopy was used to characterize rhodopsin photobleaching. After 30 s illumination, photoactived WT and the mutants showed the typical shift of the visible absorbance band to 380 nm (Figure 4.13). WT rhodopsin displayed complete conversion of the visible band to the 380 nm absorbing species. G90V and N55K showed incomplete conversion [70] suggesting formation of a photointermediate with a protonated SB linkage in the liposomes system [79]. This spectral characterization of WT, G90V, N55K in DDHA-PC liposomes, in the dark and after, is shown in Figure 4.14.

4.2.2 Rhodopsin electrophoretic behavior in DDHA-PC liposomes

Rhodopsin oligomerization status can be studied by a number of different biochemical and biophysical techniques [10,11]. Monomeric rhodopsin has the ability to activate the Gt [22,113,162]. Rhodopsin was shown to be arranged as dimers in disc membranes by infrared-laser atomic-force microscopy [163,164] and these dimeric structures were proposed to affect the ligand binding pharmacology, signal transduction and cellular trafficking [11]. Other oligomeric states, like tetramers, were detected and presumed to play important functional roles [165].

BN-PAGE was conducted to compare the oligomeric status of rhodopsin in DM detergent and in DDHA-PC liposomes. WT_{DM} clearly displayed the predominant presence of monomer and dimer bands. On the contrary, rhodopsin appears to exist in monomeric, dimeric and tetrameric forms in DDHA-PC liposomes. Liposomes increased the presence of high molecular weight bands compatible with tetramers (Figure 4.15). The appearance of tetrameric WT rhodopsin in liposomes may contribute to the increase thermal stability detected in liposomes.

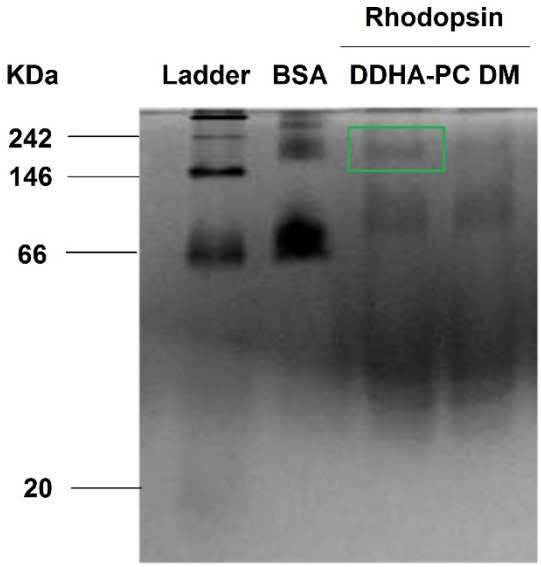

Figure 4.15 BN-PAGE of WT in PBS with DM and DDHA-PC liposomes.

BN-PAGE was performed to detect the oligomerization state of WT in DM and in DDHA-PC liposomes. Lane 1, standard protein ladder; lane 2, BSA used as an internal marker; lane 3, WT in DDHA-PC liposomes; Lane 4, WT in DM. WT was expressed in HEK293S-GNTI$^-$ cells and purified in DM and DDHA-PC liposomes. Monomer (40 kDa) and dimer bands (80 kDa) presented similar band intensity in WT_{DM} and $WT_{liposomes}$. However $WT_{liposomes}$ sample showed a more intense band corresponding to the tetramer state (160 kDa) (green box) than WT_{DM}.

4.2.3 DDHA-PC liposomes increase WT, G90V and N55K thermal stability

G90V and N55K mutants in PBS containing DM or DDHA-PC liposomes were prepared, and thermal stability was studied at 48ºC [70]. The thermal decay process is associated with the protein irreversible denaturation, breakage of the protonated SB and retinal chromophore isomerization [160,166].

We have previously reported that DDHA-PC liposomes improve the thermal stability of rhodopsin dissolved in PBS with DM at 48ºC and 55ºC [97]. Here, at 48ºC, $G90V_{liposomes}$ (2.8 ± 0.2 min) increased the $t_{1/2}$ of thermal stability 4 times more than $t_{1/2}$ of $G90V_{DM}$ (0.7 ± 0.1 min), indicating that the mutant structure was protected by the DDHA-PC liposomes bilayer [160]. $N55K_{liposomes}$ only showed a slight increase in stability (Figure 4.16). These results confirm that DDHA-PC liposomes improve the thermal stability of WT and the G90V mutant (Figure 4.16). The comparison between the G90V and N55K results indicate that the mutants show different

molecular phenotypes that could be linked to their different clinical phenotypes.

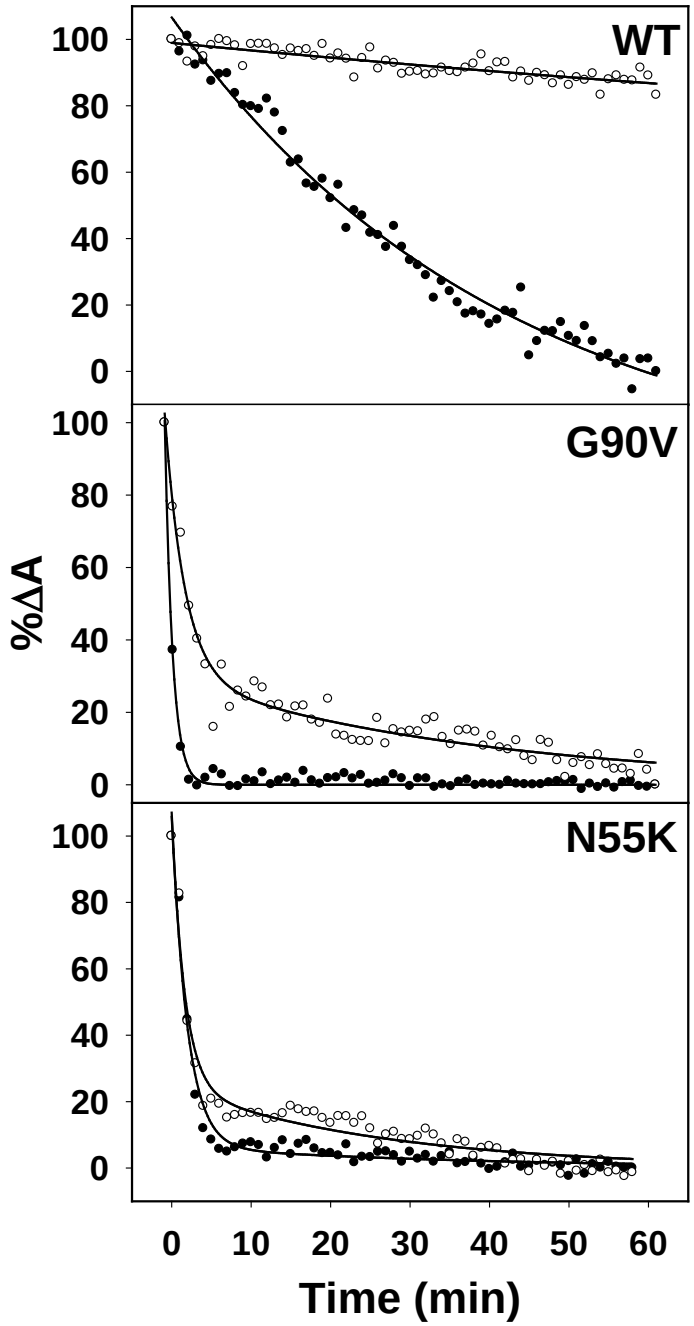

Figure 4.16 Thermal stability of WT, G90V and N55K mutants in PBS containing DM (•) or liposomes (o) at 48°C.

WT and G90V and N55K mutants were purified from COS-1 cells and dissolved in PBS containing DM (•) or liposomes (o), and the thermal stability was determined by UV-Vis spectra (as described on section 3.6.1). All the data were recorded at 48°C in the dark. Curves were fit to an exponential decay function.

4.2.4 Retinal release kinetics and opsins conformational stability

WT_{DM} or $WT_{liposomes}$ fluorescence spectra in the dark were measured until the fluorescence

intensity stabilized. Upon illumination, the fluorescence signal started to increase, due to the retinal release process (related to the decay of Meta II process). After the complete Meta II decay, exogenous 11-*cis*-retinal was added to test whether it could enter the binding pocket. The $t_{1/2}$ of retinal release for WT and G90V and N55K mutants dissolved in PBS containing DM or DDHA-PC liposomes were determined (Figure 4.17 and Table 4.3).

Table 4.3 $t_{1/2}$ for the retinal release and the uptake for WT, G90V and N55K mutants dissolved in PBS buffer containing DM or DDHA-PC liposomes.

The $t_{1/2}$ of retinal release and uptake were determined from the fluorescence curves. The $t_{1/2}$ of retinal release clearly decreased in DDHA-PC liposomes in all cases.

	Buffer	WT	G90V	N55K
$t_{1/2}$ of retinal release (min)	DM	14.3±0.9	23.4±0.3	9.5±0.1
	Liposomes	4.4±0.4	15.3±0.3	4.7±0.3
$t_{1/2}$ of retinal uptake (min)	DM	none	1.1±0.1	none
	Liposomes	2.4±0.3	16.3±0.3	none

The retinal release process in DDHA-PC liposomes, after illumination, is faster than in DM detergent. The retinal release $t_{1/2}$ of WT decreased from 14.3 min in DM to 4.4 min in liposomes becoming 10 min shorter. G90V also decreased $t_{1/2}$ of retinal release from 23.4 min for $G90V_{DM}$ to 15.3 min for $G90V_{liposomes}$. The $t_{1/2}$ of N55K retinal release decreased from 9.5 min in DM to 4.7 min in liposomes.

After completely decay of Meta II and additional retinal addition, Trp fluorescence of WT_{DM} remained unaffected, indicating that the retinal did not reenter the binding pocket. On the other hand, a decrease in the fluorescence signal for $WT_{liposomes}$ was detected, meaning that the chromophore was partially able to enter to the protein thus quenching the Trp fluorescence. Interestingly, both $G90V_{DM}$ and $G90V_{liposomes}$ showed a decrease in Trp fluorescence signal after exogenous retinal addition, but a larger decrease was observed in the case of $G90V_{liposomes}$ indicating that $G90V_{liposomes}$ may have more retinal entrance capacity. N55K displayed a completely different behavior. Exogenously retinal addition did not cause any decrease in the fluorescence signal either for $N55K_{DM}$ or for $N55K_{liposomes}$ (Figure 4.17). Compared with the WT structure, G90V may have a more open binding pocket conformation which favor retinal

entrance particularly in liposomes.

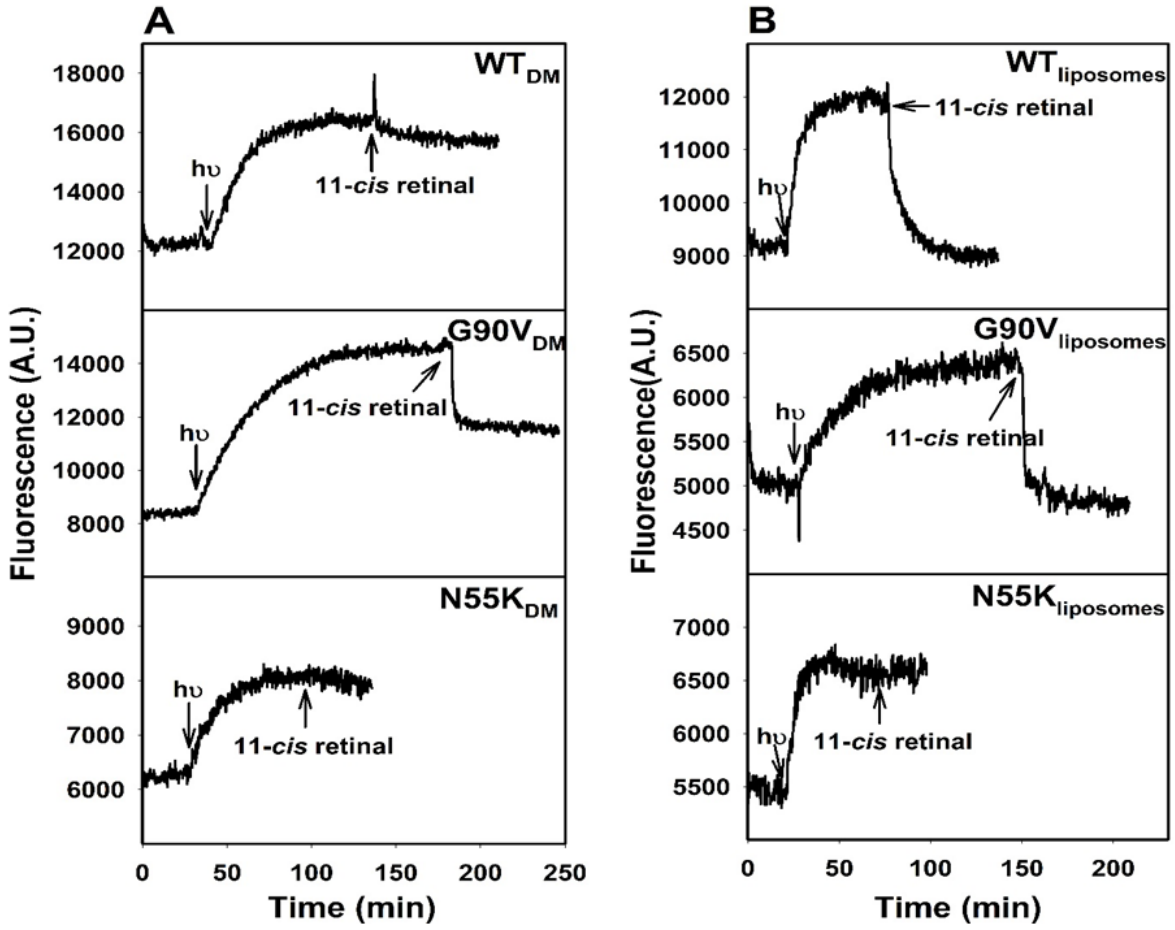

Figure 4.17 Meta II decay and chromophore uptake kinetics for WT and G90V and N55K mutant in PBS containing (A) DM or (B) DDHA-PC liposomes.

Purified WT and mutants were allowed to stabilize at 20°C in the dark and subsequently illuminated for 30 s. The exogenous 11-*cis*-retinal was added after the fluorescence signal had reached a plateau. All fluorescence spectra were measured by exciting the samples for 2 s at 295 nm and a bandwidth slit of 0.5 nm.

4.2.5 Gt purification by sucrose density gradient

Gt was purified by a sucrose density gradient and concentrated by dialysis (see section 3.4.4). SDS-PAGE was carried out to check the Gt protein yield and purity [167]. In Figure 4.18, Gt samples of 10 μl (lane 1) and 20 μl (lane 2) were loaded onto the SDS-PAGE. Lane 4 corresponded to the total protein at the beginning of the purification process and lane 5 was the solution used for dialysis. To determine the Gt concentration, lanes 6 to 9 contain different amounts of BSA: 1 μg, 2 μg, 3 μg and 5 μg. From lane 1 and lane 2, the concentration of Gt was estimated as 12.8 μM. This concentration was used for the Gt activation assay.

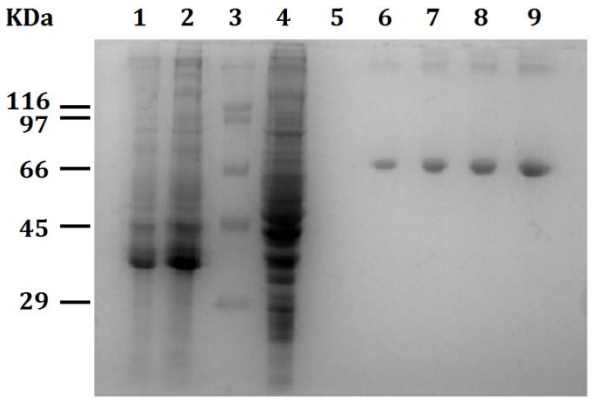

Figure 4.18 Gt purification and concentration determination by SDS-PAGE.

After Gt purification, Gt sample was loaded onto an SDS-PAGE gel to check its purity and to determine its concentration. Lanes 1, 10 µl of purified Gt sample; lane 2, 20 µl of purified Gt sample; lane 3, protein ladder; lane 4, total protein in ROS of retina; lane 5, dialysis wash; lane 6, 1 µg of BSA; lane 7, 2 µg of BSA; lane 8, 3 µg of BSA; lane 9, 5 µg of BSA.

4.2.6 Gt activation assays for WT, and G90V and N55K mutants

Gt activation was determined by calculating the amount of GTPγS^{35} bound upon WT, G90V and N55K mutants photoactivation by means of a radioactive binding assay [70,79]. Rhodopsin activity was measured in the dark and illumination state. In DM detergent environment the amount of GTPγS^{35} bound to Gt for WT and G90V and N55K was low in the dark and increased after illumination. On the other hand, WT and G90V and N55K in DDHA-PC liposomes showed comparatively low Gt activation upon illumination (Figure 4.19).

Rhodopsin reconstituted into liposomes can adopt different orientations, outside-out and inside-out, in the proteoliposomes. Considering the possible existance of monomer, dimer and tetramer states of rhodopsin, different permutations are possible with different orientations. The low Gt activation in liposomes of WT and mutants can be a consequence of a non-productive orientation of the receptor in the proteoliposomes (Figure 4.19).

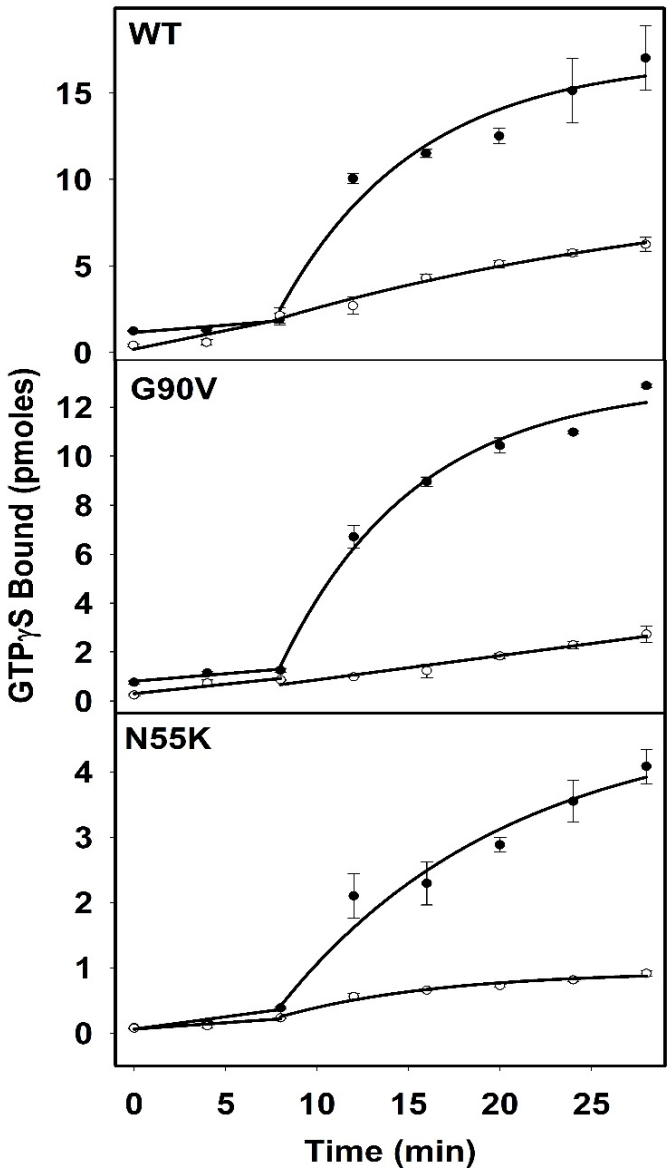

Figure 4.19 Gt activation by WT and G90V and N55K mutants in DM and DDHA-PC liposomes.

In order to test the WT and G90V and N55K mutants functional activity in PBS containing DM detergent (•) and in DDHA-PC liposomes (o), WT and G90V and N55K mutants were purified and eluted in DM detergent and then reconstituted into DDHA-PC liposomes separately (as described in section 3.6.3). Then the activity of rhodopsin in the dark and after illumination was measured by means of a radioactive filter-binding assay. The assay was carried out in the dark by mixing 10 nM rhodopsin and 500 nM Gt in 25 mM Tris, pH 7.5, 100 mM NaCl, 5 mM magnesium acetate, 5% glycerol, 2.5 mM DTT and 5 μM [^{35}S]GTPγS. The reaction was started by the addition of WT or G90V, N55K mutants to the reaction mixture at RT. At different incubation time points, the samples were filtered to wash off the unbound free [^{35}S]GTPγS. The assay was done in the dark (0 min, 4 min, 8 min) and after illumination (12 min, 16 min, 20 min, 24 min and 28 min) to determine the amount of bound [^{35}S]GTPγS by Gt.

4.2.7 Gt activation by fluorescence spectroscopy

Fluorescence spectroscopy was also used to detect Gt activation by photoactivated rhodopsin. The rate of GTPγS uptake by Gα can be followed by monitoring the increase in intrinsic

fluorescence of a Trp, which is conserved in all G proteins [156]. Initially, excitation and emission wavelengths were determined by emission and excitation scans (Figure 4.20). The excitation wavelength was found at λ = 285 nm and the emission wavelength at λ = 338 nm.

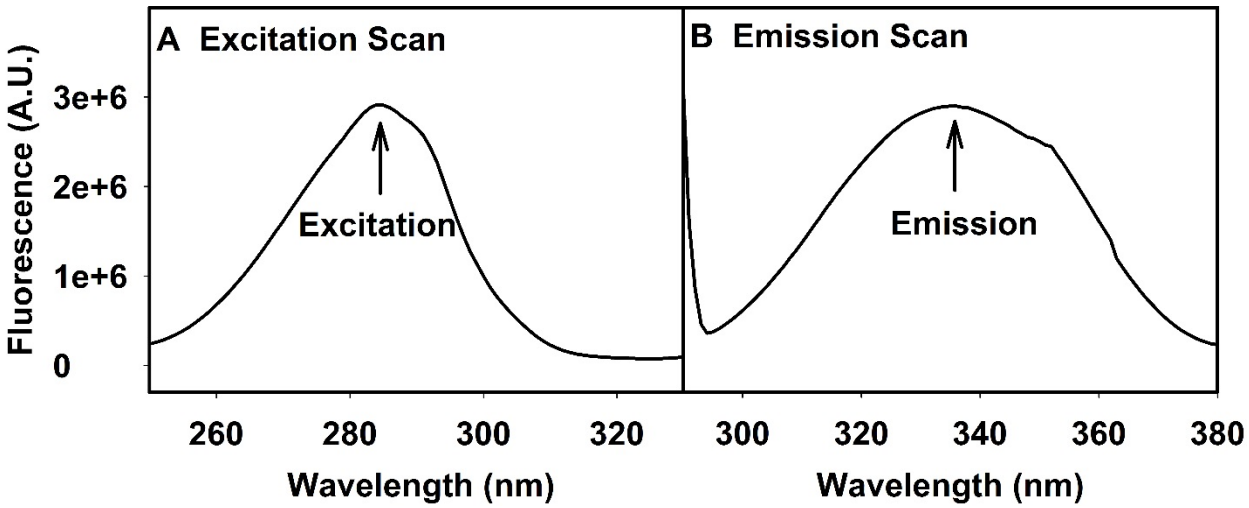

Figure 4.20 Excitation and emission spectra were monitored to determine the optimal excitation and emission wavelengths.

The sample was prepared with WT and Gt (as explained in section 3.6.3.2). Excitation and emission scans were carried out to determine the excitation and emission wavelengths with maximum intensity. Finally excitation was determined at λ = 285 nm and the emission wavelength at λ = 338 nm.

Gt activation was carried out as explained in detail in section 3.6.3.2. Fluorescence spectroscopy can directly monitor the interaction between rhodopsin and Gt. In the dark state, rhodopsin cannot activate Gt. Upon illumination, rhodopsin activated Meta II conformation can bind and activate the Gt protein. The change in Trp fluorescence reflects a conformational change in the α-subunit and the exchange between GDP inside the pocket and the exogenous GTPγS. In WT_{DM}, a fluorescence intensity increase was observed due to activation of Gt. However, in $WT_{liposomes}$, no increase of fluorescence was observed (Figure 4.21) in agreement with the radioactive assay results indicating that DDHA-PC liposomes impede somehow the interaction between rhodopsin and Gt.

Two different methods such as fluorescence spectroscopy and radioactivity filter assay, showed similar results on $WT_{liposomes}$ confirming that liposomes formation may interfere on Gt activation possibly due to the different orientation of WT in liposomes [102].

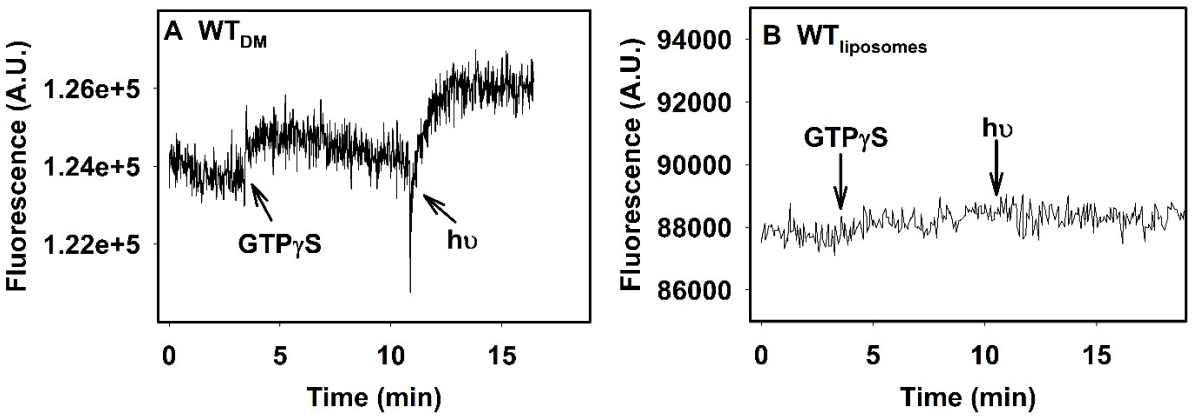

Figure 4.21 Gt activation of WT in DM and DDHA-PC liposomes followed by fluorescence spectroscopy.

Gt activation of WT in (A) DM detergent and in (B) DDHA-PC liposomes. After the fluorescence intensity stabilization, GTPγS was added until fluorescence signal stabilization. Then, 1 min illumination was carried out at 25°C. Increase of fluorescence was monitored until a plateau was reached. WT_{DM} showed an increase of Trp fluorescence intensity whereas no change could be detected in the case of $WT_{liposomes}$.

4.2.8 Rhodopsin structural consequences of the chemical structure of DHA

The effects observed can be associated with the chemical nature of the DHA lipid. Different from saturated and monounsaturated hydrocarbon chains, the neutral polyunsaturated DHA has a unique chemical structure with six cis-locked double bounds. The number of freedom degrees of DHA chains is substantially lower which could be indicative of rigidity. Polyunsaturated chains in crystals form highly ordered, elongated structures with angle-iron or helical arrangement of double bonds. The experimental results clearly indicated that the low order in bilayers with high DHA content is a direct consequence of high conformational flexibility and of rapid structural conversions of DHA chains themselves without significant energetic penalty [131]. NMR data proved that the photointermediate Meta III had stronger contact with DHA compared with dark rhodopsin, Meta I and Meta II states. DHA enrichment may alter protein function both by a change of general membrane properties as well as by specific interactions with particular regions of the protein [131]. DHA interacts with rhodopsin and tends to weaken the interhelical packing. N55K, mutation in an amino acid located in helix 1, and G90V located in helix 2, are structurally located near residues 48, 50, 92, 95, 96 which are tightly packed with DHA [130]. DHA increased the thermal stability of WT and G90V but not N55K mutant. In the Meta II decay experiment. DHA speeded up the retinal release and allowed more retinal uptake by $G90V_{liposomes}$. On the other hand, N55K mutant did not uptake retinal upon Meta II decay. DDHA-PC decreased the Gt

activation of WT and mutants which could be mainly attributed to the receptor orientation in liposomes [102]. Therefore, DDHA-PC lipids could be used in combination with other lipids and/or preparative protocols in order to achieve artificial membranes that could circumvent the orientation problem [121,124,168].

4.3 GPCRs interactions with other proteins

In this section, the interaction between GPCRs and other proteins was studied to understand GPCRs structural mechanism. For this purpose, two GPCRs, rhodopsin and M3R were used.

- In the visual system, activated rhodopsin recruits Gt and cellular signal transduction starts. Among the signals, the activation of rhodopsin kinase that phosphorylates rhodopsin increases the affinity towards visual arrestin [137]. As a GPCR transducer, arrestin binds rhodopsin blocking its interaction with Gt leading to desensitization. The binding of arrestin to rhodopsin also initiates other cellular signaling pathways that are G-protein independent. Mutant arrestin R175E was expressed and purified from BL21-RP cells. The pull-down assay and Meta II decay experiments were carried out to study the rhodopsin-arrestin interaction.
- In the mAChRs family, the M3R mutants could be associated with AD through its interaction with tau protein. Previous studies also show the EC tau protein interacts with M3R. The M3R WT and mutants protein and tau protein were co-expressed in mammalian cells and their interaction was detected by both WB and immunofluorescence in order to pinpoint the potential M3R-tau interacting sites.

4.3.1 Arrestin R175E mutant purification

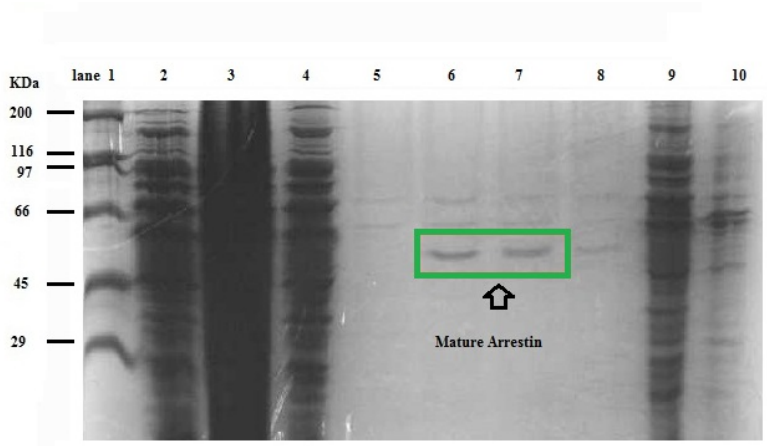

Figure 4.22 SDS-PAGE of arrestin R175E purification.

Lane 1, protein marker; lane 2, total BL21-RP cells induced by IPTG; lane 3, cell debris of IPTG induced cells after sonication; lane 4, soluble protein of IPTG induced cells after sonication; lane 5, column wash; lane 6, elution 1 (E1); lane 7, elution 2 (E2); lane 8, elution 3 (E3); lane 9, total un-induced cells; lane 10, cell debris of un-induced cells. Purified arrestin can be seen in E1 and E2 (green box).

As described in section 3.6.6, arrestin R175E was overexpressed in *E.coli* BL21-RP cells by

ITPG induction [133]. Then, R175E mutant arrestin was purified by affinity chromatography using Bio-scale mini profinity cartridges and detected by SDS-PAGE and Coomassie blue staining. Figure 4.22 (green box) showed the purified R175E arrestin by means of SDS-PAGE.

In order to determine purified arrestin concentration, BSA dilutions were prepared for a Lowry protein assay (explained in section 3.6.10) to obtain a protein standard line (Figure 4.23) and the following equation;

$$\mathbf{Abs = 3.3 \cdot \rho}$$

Where Abs corresponds to the absorbance at 600 nm on the UV-Vis scanned and ρ is the protein concentration (in μg/μl).

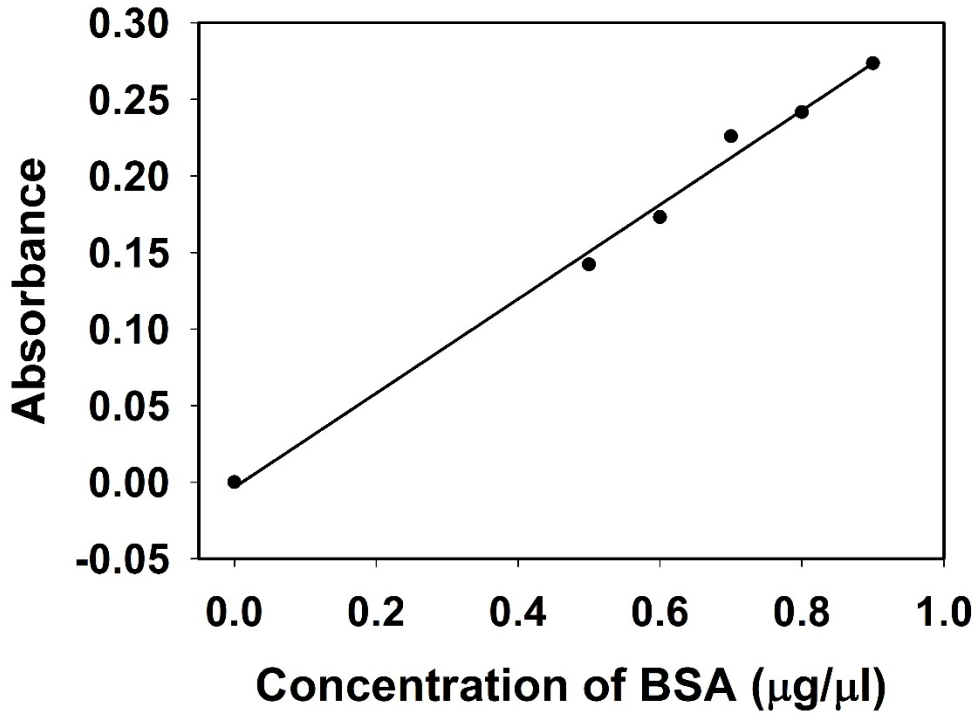

Figure 4.23 BSA standard line.

Different BSA concentrations were used to determine an equation to calculate arrestin.

$Abs_{600\ nm}$ of purified arrestin was measured to be 0.027 Abs and consequently the final concentration determined from the formula was 0.09 μg/μl. Finally, the molar concentration of arrestin was calculated by the formula:

$$\mathbf{C} = \frac{\boldsymbol{n}}{\boldsymbol{V}} = \frac{\boldsymbol{m}}{\boldsymbol{M} \cdot \boldsymbol{V}} = \frac{\boldsymbol{\rho}}{\boldsymbol{M}}$$

Where C is the molar concentration of arrestin; ρ is the protein concentration (0.09 μg/μl); and M is the molar mass of arrestin (48000 g/mol). Finally the arrestin concentration was determined to be 1.9 μM.

4.3.2 Pulling down assay between arrestin R175E and rhodopsin in ROS

Pull down assay is an established centrifugation process to exam the light dependent binding to nonphosphorylated rhodopsin in ROS membranes (explained in section 3.6.7.1). As shown in Figure 4.24, arrestin R175E remained in the supernatant after incubation with ROS membranes in the dark (lane 2); arrestin R175E was pulled down by the ROS membrane upon illumination after centrifugation (lane 3). In previous studies [133], different stoichiometry of rhodopsin and arrestin were used. The structural models suggested activated rhodopsin interact with arrestin in a 2:1 stoichiometry; while 1 activated rhodopsin: 1 arrestin was also suggested by the functional assay. Docking modes were discussed with arrestin binding to both monomeric and dimeric rhodopsin [169]. The photoactivation density is also associated with the activated rhodopsin-arrestin binding ratio, with 1:1 at low photoactivation density and 2:1 binding at high photoactivation density linearly [170,171]. Different from the previous results, Figure 4.24 showed that lower arrestin (green box) was pulled down by ROS. This decreased bound rate were associated with many factors such as purification, arrestin activity and buffer [133].

Studies on the interaction of rhodopsin with arrestin could provide keen insights into the rhodopsin conformational changes and the signaling pathways started upon arrestin binding. Arrestin is composed of two β-strand domains, N and C domains with similar sizes, and is able to interact with photoactivated rhodopsin [172]. Arrestin first binds to specific phosphorylated serine and threonine residues located at the C-terminus of light activated rhodopsin, and the cytoplasmic loops, major sites of G protein interaction, to quench further signaling [133,173]. The interaction between RP mutatns and arrestin will be deeply studied for the molecular mechanisms.

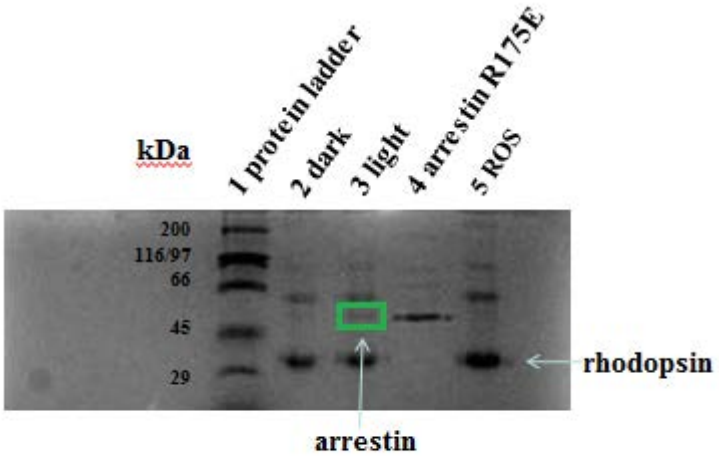

Figure 4.24 Arrestin R175E pull down assay with ROS membrane by SDS-PAGE.

Lane 1, Protein ladder. Lane 2, ROS and arrestin R175E in the dark. Lane 3, ROS and arrestin R175E after illumination. Lane 4, Arrestin R175E; Lane 5, ROS.

4.3.3 Influence of arrestin binding on rhodopsin Meta II decay

Fluorescence spectroscopy was used to detect the interaction between arrestin R175E and rhodopsin and its mutants as indicated in section 3.6.7.2. Figure 4.25A shows the retinal release from rhodopsin at different rhodopsin/arrestin R175E ratios. Rhodopsin and arrestin R175E were mixed with different stoichiometries, as 1:0 (pink), 1:2 (light blue) and 1:4 (light green) of rhodopsin: arrestin. After illumination, the fluorescence caused by retinal release increased till to the plateau on which state opsin was separated from 11-*cis*-retinal. The pink curve shows the completely chromophore release from rhodopsin and was used as a control of the total retinal release. The amount of retinal release in the presence of 2 fold concentration of arrestin R175E to rhodopsin (light blue) resulted in a decrease of 37% compared with the control (pink). At a 1:4 ratio (light green), the decrease observed was 56%. The reduction of retinal release is represented in Figure 4.25B. Increase in the arrestin R175E/rhodopsin ratio resulted in increased Meta II interaction with the arrestin R175E and forming Meta II/arrestin R175E complex that decreased the retinal release which paralleled with the opsin product. It can be concluded that R175E stabilized the Meta II state. Previous work has proved that arrestin could also bind to Meta III, a post Meta II photodecay product, and reverted back to Meta II like species. It was suggested that arrestin would regulate the level of free retinal in the rod cell controling the formation of

damaging oxidative retinal adducts under light conditions [139].

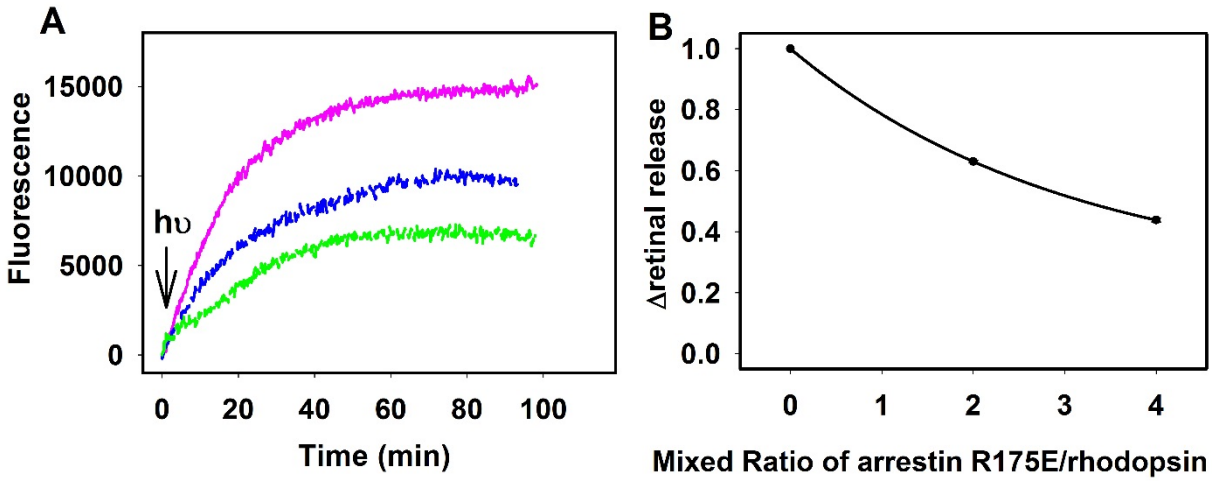

Figure 4.25 Arrestin R175E stabilized the Meta II state and inhibited retinal release.

A, the effect of arrestin on retinal release was investigated by fluorescence spectroscopy. Purified rhodopsin was mixed with arrestin R175E with different stoichiometries 1:0 (pink), 1:2 (light blue) and 1:4 (light green). The samples were photobleached and the fluorescence increased to plateau. B, the retinal release decreased because of the increased ratio of arrestin R175E/rhodopsin. With the increased ratio of arrestin R175E/rhodopsin, more Meta II was combined with arrestin R175E.

The crystal structure of rhodopsin-arrestin complex shows a 1:1 stoichiometry. The binding activity is lower than that published but is in accordance with the pull down assay result (section 4.3.2).

Rhodopsin signaling involves interacting with Gt, rhodopsin kinase, arrestin and other proteins. Structural and modeling studies have proved that the competition on the binding surfaces is a major regulatory mechanism for signal processing [174,175]. Some indirect evidence suggested that the rhodopsin/arrestin complex may be a pathogenic mechanism for certain types of RP in human patients. One rhodopsin mutant K296E, associated with ADRP, forms a stable complex with arrestin that is toxic to mouse rod photoreceptors [176]. The complex of rhodopsin mutant G90D and visual arrestin could offset the effect of abnormal rhodopsin signaling without light and retinal isomerization. The subsequent docking of polyphenol antioxidant cyanidin 3-rutinoside with G90V rhodopsin initiates its activation and regeneration to trigger normal visual transduction cascade to cure night blindness [177]. The interaction between arrestin R175E and rhodopsin mutants such as G90V, N55K could be studied to further dissect the details of the molecular mechanisms underlying RP. Figure 4.26 showed rhodopsin interaction with the

cytoplasmic partners, Gt, arrestin R75E and rhodopsin kinase. Different from the arrestin WT, arrestin R175E has been shown to bind non-phosphorylated activated rhodopsin. As such, this R175E arrestin bypasses the need to bind the phosphorylated rhodopsin [139,174,178,179].

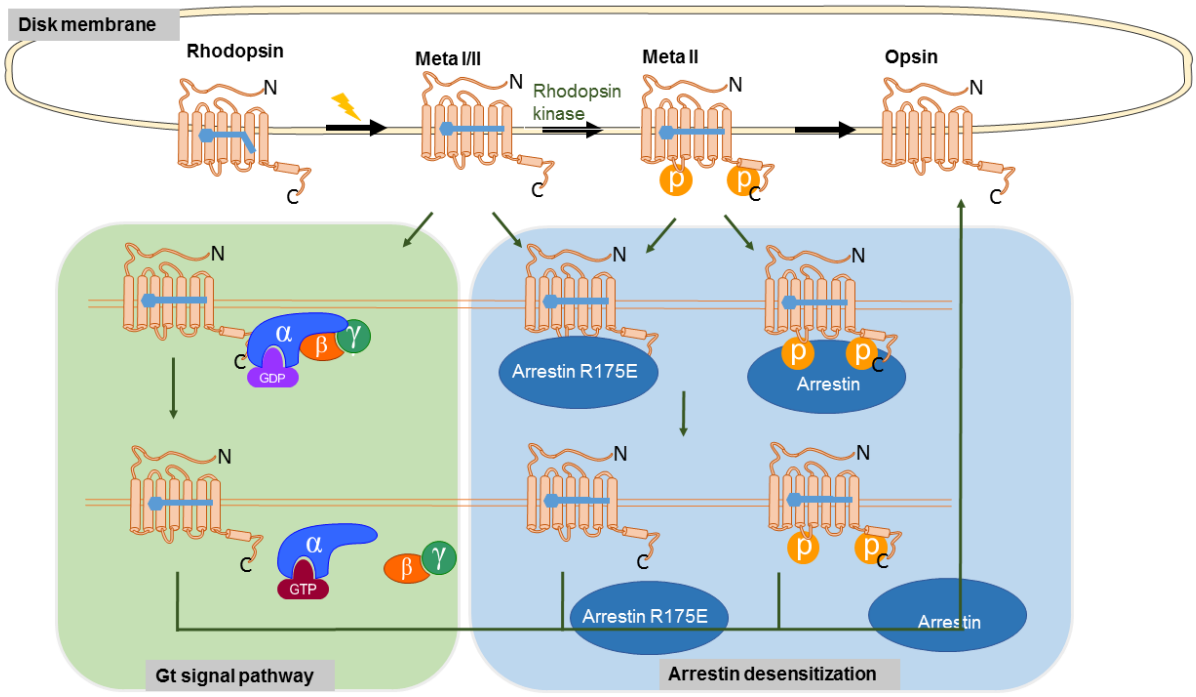

Figure 4.26 Rhodopsin interaction with cytoplasmic Gt, arrestin/arrestin R175E and rhodopsin kinase.

The figure illustrates the relative activation and desensitization pathways of vision. Gt and arrestin are the rhodopsin partners in the signal transmission. Arrestin R175E is used to interact with light activated rhodopsin.

4.3.4 M3R and the mutants expression and purification

M3R WT and M3R mutants (M3R-N132G, M3R-D518N, M3R-D518K and M3R-K523Q) were first cloned by Dr Laura Iarriccio [149]. DNA agarose gel was run as previously described in section 3.3.2.2 to check the plasmids state being stored after several years. Figure 4.27 shows a gel containing the five plasmid vectors.

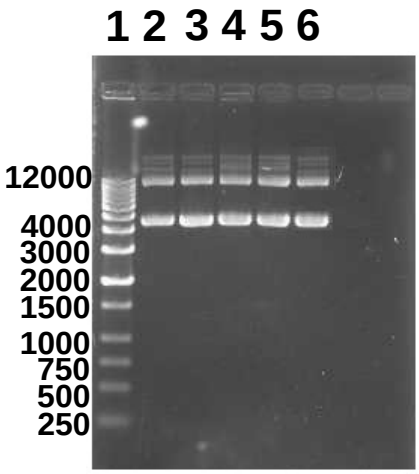

Figure 4.27 M3R WT and mutants DNA agarose gel electrophoresis.

Plasmids containing M3R WT and mutants were analyzed by means of agarose gel electrophoresis. Lane 1, DNA ladder. Lane 2, M3R-N132G. Lane 3, M3R-D518N. Lane 4, M3R-D518K. Lane 5, M3R-K523Q. Lane 6, M3R-WT plasmid.

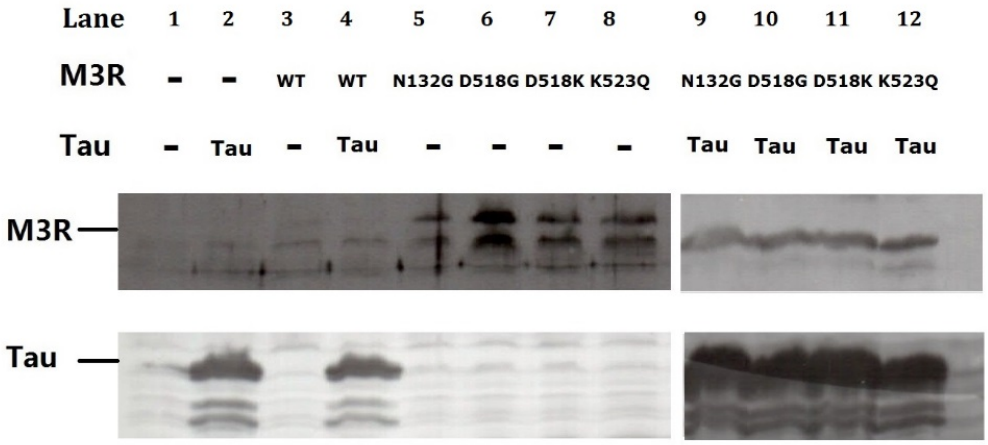

Figure 4.28 WB of M3R WT and mutants coexpressed with or without tau.

The different M3R WT and mutants and tau were transfected into HEK293S-GNTI$^-$ cells. Lane 1, blank without plasmid transfection; lane 2, tau transfection; lane 3, M3R WT transfection; lane 4, M3R WT and tau cotransfection; lane 5, M3R-N132G transfection; lane 6, M3R-D518G transfection; lane 7, M3R-D518K transfection; lane 8, M3R-K523Q transfection; lane 9, M3R-N132G and tau cotransfection; lane 10, M3R-D518G and tau cotransfection; lane 11, M3R-D518K and tau cotransfection; lane 12, M3R-K523Q and tau cotransfection. When M3R mutants were expressed, two bands of M3R mutants proteins were shown. When M3R mutants and tau were coexpressed in cells, the M3R mutants only showed one main band with higher intensity.

M3R and M3R mutants were coexpressed with tau protein in mammalian cell HEK293S-GNTI$^-$. The cells were collected as described in section 3.6.8 and the proteins were detected by WB using M3R ant tau antibodies (Figure 4.28).

Tau protein exists in mammalian cells as a microtubule associated protein. Tau is not only a microtubule associated protein but also appears to play a key role in dementia. It has focused on the role of tau proteins in microtubule dynamics and its dysfunctions [180,181]. Figure 4.28 clearly showed that tau overexpression changed the conformational status of EC M3R mutants expressed in HEK293S-GNTI$^-$ cells. In the absence of tau cotransfection, the four M3R mutants displayed different expression levels with two main bands in their electrophoretic pattern. Upon tau coexpression, however, each M3R mutant showed only a single main band.

4.3.5 Detection of M3R and mutants expression by immunofluorescence

Twelve samples (sample A to L) of M3R WT and mutants were transfected alone or cotransfected with tau as described in Table 4.4. The double immunofluorescence analysis using antibodies against tau and M3R were performed as described (in section 3.6.9) to colocalize both tau and M3R WT and mutants in the cells (Figure 4.29).

Table 4.4 Combination of M3R WT and mutant samples transfected alone or cotransfected with tau that used in the immunofluorescence assay.

	A	B	C	D	E	F	G	H	I	J	K	L
tau	--	tau	--	tau	--	tau	--	Tau	--	tau	--	tau
M3R	--	--	WT	WT	N132G	N132G	D518N	D518N	D518K	D518K	K523Q	K523Q

There is not endogenous M3R expression in HEK293T cells but tau protein, as a soluble endogenous protein, is expressed in all living cells to stabilize microtubule polymers, suppresses microtubule dynamics and promote cytoplasmic extension or neuritogenesis [144,181]. Figure 4.29A shows the sample blank without any transfection. Tau was overexpressed in a soluble form in the cells cytoplasm and showed high FITC fluorescence (Figure 4.29B). Figure 4.29C shows the result of only M3R WT transfection where M3R WT was overexpressed and located correctly to the cell membrane. Cotransfection of M3R WT with tau cause mislocation of tau from the soluble in the cytoplasm to the cell membrane while M3R kept its location on the membrane. The changes location of tau may be associated to hyperphosphorylation (Figure 4.29D) [147,148]. Tau hyperphosphorylation can not only cause tau mislocalization but also trigger β-amyloid aggregation associated with AD [182]. M3R mutants N132G and D518N showed a similar behavior: when the two M3R mutants were coexpressed with tau, N132G and D518N were located in the

membrane (Figure 4.29E, G), whereas tau mainly changed the location from the cytoplasm to-

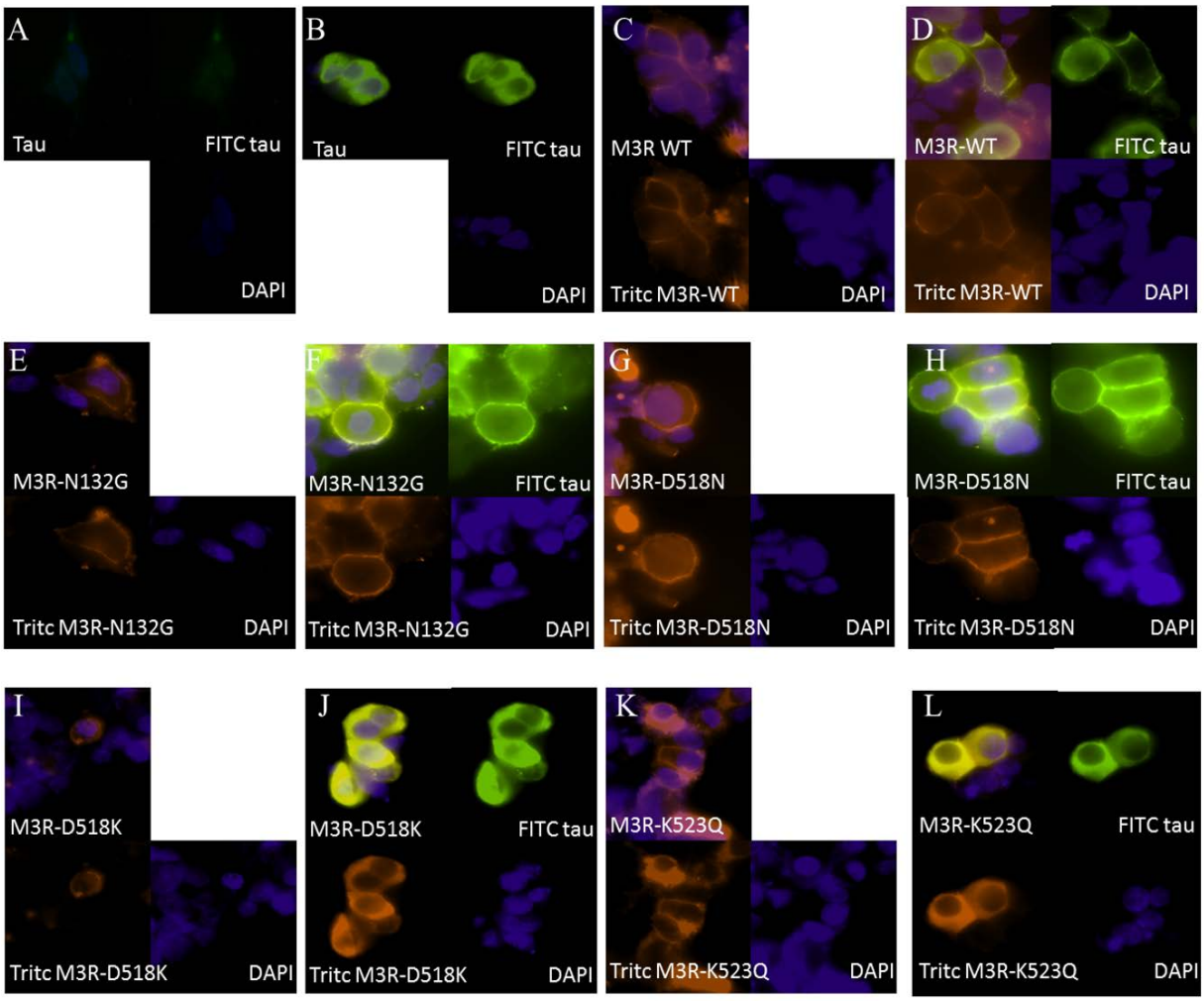

Figure 4.29 Immunofluorescence of M3R and mutants coexpressed with/without tau in HEK293T cells.

M3R WT and mutants and tau were transfected into HEK293S-GNTI$^-$ cells. Samples from A to L were detected by immunofluorescence. Tau was detected by the FITC fluorescence; M3R and mutants were detected by the TRITC fluorescence. M3R WT, N132G and D518N caused tau mislocalization from cytoplasm to the membrane. While M3R D518K and K523Q mislocalized from membrane to the cytoplasm because of the tau coexpression.

-the membrane (Figure 4.29F, H). Different from M3R WT, N132G and D518N, the M3R mutants D518K and K523Q changed their locations from the membrane (Figure 4.29I, K) to the cytoplasm (Figure 4.29J, L) and tau overexpression did not change their location (still in the cytoplasm).

Overall, M3R WT, N132G and D518N mutants changed the location of tau, from the cytoplasm to membrane, suggesting that M3R WT, N132G and D518N mutants increase M3R affinity to

tau (Table 4.5).

Table 4.5 The locations of tau and M3R WT and mutants transfections.

Blue color showed the protein on the membrane. The pink showed the protein in the cytoplasm. Because of the cotransfection of M3R WT and mutants with tau, the locations of protein changed. M3R WT and N132G and D518N caused the tau location from cytoplasm to the membrane. While M3R D518K and K523Q located from membrane to the cytoplasm.

Sample	Protein	M3R transfection without tau	M3R cotransfection with tau
M3R WT	WT	Membrane	Membrane
	Tau	Cytoplasm	Membrane
M3R N132G	N132G	Membrane	Membrane
	Tau	Cytoplasm	Membrane
M3R D518N	D518N	Membrane	Membrane
	Tau	Cytoplasm	Membrane
M3R D518K	D518K	Membrane	Cytoplasm
	Tau	Cytoplasm	Cytoplasm
M3R K523Q	K523Q	Membrane	Cytoplasm
	Tau	Cytoplasm	Cytoplasm

The tau mislocalization also occurred by the decreased affinity between tau and microtubules which associated with the phosphorylation/ hyper-phosphorylation and resulted the movement of tau proteins from microtubule to the membrane space [180,183,184]. Compared with the location of M3R WT under tau presence, M3R D518K and K523Q mutants changed the location from membrane to the cytosol by the overexpression of tau (Table 4.5). The overexpressed tau could be hyperphosphorylated and toxic for newborn neurons [144,185] and result the secretion of tau via membrane vesicles in cells [186]. The EC tau interacts with the cell membrane receptors such as M1R and M3R receptors and cause toxic to the cells that increase the risk of AD [144]. The tau phosphorylation and tau mislocalization have been proved as an intermediate signaling molecules between β-amyloid initiation and eventual synaptic dysfunction early in AD pathogenesis [140,187,188].

4.3.6 Physiological analysis of the M3R mutants and AD

M3R-N132G is located in EC2 while M3R-D518G, M3R-D518K and M3R-K523Q are located in EC6 (Figure 4.30). EC tau could bind with M3R and promote IC calcium changes which was present in tauopathies such as AD [90]. These mutants may interact with tau and this interaction may alter the M3R mutants expression, at least in the HEK293T cells used in these experiments.

In neurons, the increased phosphorylation of tau destabilized tau-microtubule interactions, leading to microtubule instability, transport defects along microtubules, and ultimately neuronal death [189]. The tau and microtubule binding plays essential roles in polarity axon and dentrite formation of neuronal cells [190].

The axon terminal contains synapses, specialized structures where neurotransmitter chemicals are released to communicate with target neurons. The results in HE293T cells showed that tau can not only interact with microtubules but also with M3R WT and the four mutants. The mutants D518K and K523Q appear to interact with tau by a different mechanism that the other two mutants and result in different cell location. Different tau-M3R mutant complex arrangements could be envisaged and this could cause the different protein localization. Tau is co-transported with microtubule fragments from cell bodies into axons and the M3R-tau complexes could interfere in this process altering the normal function of neurons.

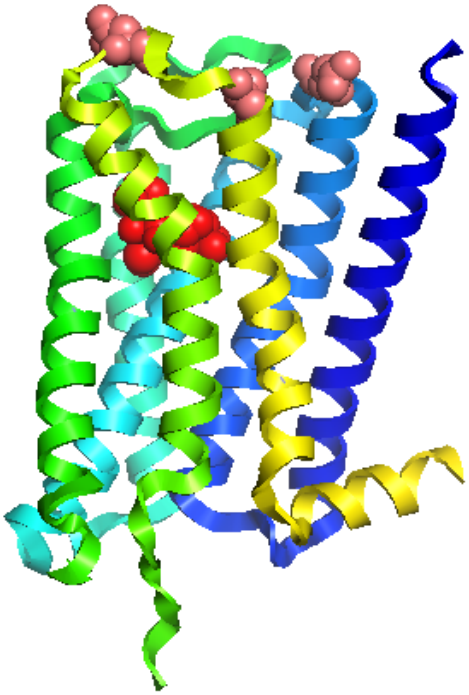

Figure 4.30 Structural model of M3R with the sites of mutations.

The N132, D518 and K523 residues (pink) are shown in the figure. These three sites are all located in the EC loops where the G-protein binding and activation of the receptor take place. M3R crystal structure (PDB ID 4U14) was used and the image was created using PyMol (Schrodinger, LLC. PyMOL Molecular Graphics System, Version 1.5).

5. GENERAL DISCUSSION

Signal transduction is a fundamental biological process to maintain cellular homeostasis and relevant cellular activity in all organisms. GPCRs, representing the largest and most diverse membrane proteins family, serve as the communication interface between the external and internal environments. By responding to a wide spectrum of EC signals such as photons, ions, small organic molecules and entire proteins, GPCRs undergo conformational changes which cause the activation of complex cytosolic signaling networks and result in a variety of cellular responses [5,25]. Thus, GPCRs are responsible for the proper operation of many physiological processes such as vision, intercellular communication, neuronal transmission, hormonal signaling, and they are involved in many pathological processes. Mutations in GPCRs, which represent about 4% of the human genome, are associated with a broad spectrum of diseases of diverse etiology. Such mutations can alter the process of ligand binding and significantly affect signaling transduction pathways [5]. This can lead to two degenerative diseases such as RP and AD. Determining the structure-function relationships of GPCRs mutants and understanding the molecular mechanisms of RP and AD can be of fundamental importance in treating these conditions and promoting human health.

Rhodopsin, a receptor of Class A GPCRs, is responsible for the vision process. Among the ~700 identified members of Class A, more than twenty receptors have been crystalized and the structures have been solved at atomic resolution [97]. Rhodopsin mutations lead to visual disorders associated with impaired vision including the retinal degenerative disease RP. The RP condition refers to a group of heterogeneous inherited disorders associated with degeneration and loss of photoreceptor retinal cells [5]. Here, two artificial membrane systems, DMPC/DHPC bicelles and DDHA-PC liposomes, were used in an attempt to stabilize rhodopsin mutants and to unravel the molecular mechanism of RP associated with structural instability. G90V (causing RP) and N55K (causing sectorial RP) were chosen as model mutations to investigate their molecular properties in artificial membranes compared to the DM detergent system, which is commonly used. The advances to underlying the stability and function properties of rhodopsin mutants could provide novel mechanistic insights that can open novel therapeutic strategies for the treatment of congenital retinal disorders.

Purified WT rhodopsin, and the G90V and N55K mutants, regenerated with 9-*cis*-retinal were purified in both DM detergent [70,79] and DMPC/DHPC bicelles environment. The UV-Vis spectra

of WT, G90V and N55K in DM detergent was in agreement with previous studies [70,79,94]. The most interesting result was that $N55K_{bicelles}$ required double illumination time for complete photoconversion (Figures 4.2 and 4.3). This result showed that the light sensitivity of N55K is altered especially in the DMPC/DHPC bicelles environment. WB results demonstrated that DMPC/DHPC bicelles decreased the N55K truncated protein band intensity and increased the tetramer band which also was observed for the G90V mutant but not for the WT (Figure 4.4). The increase of tetrameric formation or other oligomerization states caused by bicelles could affect the conformational stability.

DMPC/DHPC bicelles increased the thermal stability of WT rhodopsin, and the G90V and N55K mutants to various degrees (Figure 4.5) indicating that bicelles can provide conformational stability by protecting the SB and preventing protein aggregation at 37ºC [34,94,160]. WT in DM and bicelles showed similar 9-*cis*-retinal regeneration, at nearly 90%, even though the $t_{1/2}$ of the regeneration process was slightly slowed down in bicelles. The trend of G90V retinal regeneration was in agreement with WT whereas N55K showed a completely different trend. $G90V_{bicelles}$ showed 96% retinal regeneration which was 20% higher than in the case of $G90V_{DM}$. On the contrary, N55K did not show regeneration but displayed a retinal release at the visible band under the exogenous retinal. In spite of this abnormal behavior for N55K mutant, bicelles appeared to slow down the absorbance band decrease suggesting that the protein was stabilized in some way. The novel retinal regeneration behavior of N55K in bicelles may be associated with the clinical phenotype of sectorial RP [79,191]. Compared with the $t_{1/2}$ of retinal release in the Meta II decay process, the bicelles not only decrased the $t_{1/2}$ of retinal regeneration of WT, G90V and N55K, but also speeded up the retinal release during the Meta II decay process (Figure 4.6 and 4.7). Hydroxylamine addition, after Meta II decay, was used to confirm complete retinal release. No changes were detected for WT and G90V in DM after hydroxylamine addition, whereas a novel behavior could be observed in bicelles, WT and G90V showed additional increase of Trp fluorescence emission indicating that after Meta II decay some retinal was still present in the binding pocket of $WT_{bicelles}$ and $G90V_{bicelles}$ (Figure 4.7) [31]. On the other hand, N55K did not show increase in fluorescence intensity either in DM or in bicelles environment. This result was in contrast with the previous study in which N55K was dissolved in PBS (pH 7.4) containing 0.05% DM [79]. This previous study showed that hydroxylamine did cause an increase in the

fluorescence signal of N55K highlighting the importance of buffer conditions on the fluorescence spectroscopic behavior. In addition, different fluorescence intensity was observed between DM and bicelles likely due to the background fluorescence contribution of the DMPC/DHPC bicelles (Figure 4.7).

After Meta II decay, 9-*cis*-retinal was added to test the retinal entrance to the opsin binding pocket. Bicelles could help stabilizing WT and G90V opsins obtained by Meta II complete decay (Figure 4.9 and 4.10). The results indicated that the exogenously added retinal chromophore could enter the binding pocket thus quenching Trp fluorescence, and that bicelles preserved the opsin stability allowing retinal binding after illumination [70]. N55K opsin did not show any change either in DM or in bicelles suggesting that the accessibility to the binding pocket of N55K opsin had been impaired due to the mutation [76] which is in agreement with the regeneration result (Figure 4.9 and 4.10). This unique N55K behavior may provide new clues that would guide us in deciphering the molecular mechanism of sector RP. Compared to the occluded structure of N55K, the G90V mutant appears to have a more open structure with a more accessible binding pocket that could explain its retinal binding capacity both in DM and in bicelles.

In DDHA-PC liposomes environment, the purified WT rhodopsin, and the G90V and N55K mutants, regenerated with 11-*cis*-retinal, were studied the properties compared with those in DM detergent [70,79]. Interestingly, the UV-Vis spectral behavior of WT, G90V and N55K in DDHA-PC liposomes (Figure 4.14) were similar to that in DMPC/DHPC bicelles which can be correlated with the bilayer conformation [118,121]. $WT_{liposomes}$ also showed presumed tetrameric state character which was also observed in $WT_{bicelles}$. Thermal stability at 48ºC in DDHA-PC liposomes increased for both WT and G90V thus prolonging the $t_{1/2}$ of the thermal decay curves (Figure 4.16) [70]. Therefore, both bilayer systems of DMPC/DHPC bicelles and DDHA-PC liposomes can protect the molecular structure of WT and G90V regenerated with 9-*cis*-retinal as well as with 11-*cis*-retinal. At 48ºC, DDHA-PC liposomes did not increase the thermal stability of N55K compared to DM control. At a later stage of the N55K thermal decay process, $N55K_{liposomes}$ appeared to provide higher stability suggesting that DDHA-PC liposomes efficiently protected the N55K opsin structure. The temperature used for the thermal stability studies, 37ºC, was chosen because rhodopsin mutants showed thermal sensitive character which prevents their study

at higher temperatures.

WT, G90V and N55K revealed faster retinal release kinetics, from Meta II decay assays, in DDHA-PC liposomes than in DM detergent (Figure 4.17). This performance in liposomes was consistent with the behavior of WT rhodopsin and the mutants in DMPC/DHPC bicelles. Both states of DMPC/DHPC bicelles and DDHAPC liposomes accelerated retinal release in experiments. This performance may be associated with the specific interactions between DHA and rhodopsin [130,131]. Accordingly, the DDHA-PC liposomes helped WT and G90V opsins, produced upon Meta II decay, bind more retinal by stabilizing opsin and preserving its correctly folded (ligand-binding) conformation. Gt activation was carried out in order to detect the functionality of WT rhodopsin, G90V and N55K mutants (Figure 4.19 and 4.21). DDHA-PC liposomes decreased the Gt activation capacity of rhodopsin WT, and particularly the mutants confirming that liposomes formation may interfere with Gt activation possibly due to the non-productive orientation of rhodopsin reconstituted in liposomes [102]. Considering this drawback in liposomes formation, DDHA-PC lipids can be used to form other artificial membranes types such as bicelles to circumvent the orientation problem [35,121,168].

The interaction between rhodopsin and visual arrestin R175E was studied by a pulling down assay (Figure 4.24) and by Meta II decay assay (Figure 4.25) showing that arrestin R175E could bind with activated rhodopsin (Meta II) and inhibit retinal release. The rhodopsin-arrestin interaction probably regulates the level of free retinal in the rod cell and control formation of damaging oxidative retinal adducts under light conditions [139]. It would be interesting to investigate other specific features of the complex formed between rhodopsin mutants and arrestin R175E for a deeper knowledge of the RP molecular mechanisms [176,177].

In AD, the accumulation of neurofibrillary tangles and cholinergic deficiency are the two prominent features [80,84]. The interaction between tau protein composing neurofibrillary tangles and the M3R WT has been previously described. The study of mutations at the EC domain of the M3R receptor can provide novel clues on the role of the M3R-tau interaction in the molecular mechanism causing AD. This study may help in understanding how the interaction between neurofibrillary tangles associated with tau and mAChRs may contribute to the pathophysiology and cognitive impairment in AD [80,83,192].

The WB analysis of M3R WT and M3R mutants coexpressed with tau (Figure 4.28) indicated that the M3R mutants displayed different expression yields and molecular bands indicating that the overexpressed tau affected the expression of M3R and mutants. Immunofluorescence analysis was carried out to obtain more clues on the interaction between tau and M3R mutants (Figure 4.29), particularly on the trafficking alterations and cell localization of the two interacting proteins. The coexpression of tau and M3R WT and mutants caused the mislocation of tau and/or M3R (WT and mutants). The tau mislocalization may be associated to the phosphorylated/ hyperphosphorylated states by disturbing the homeostasis among microtubule and tau. This may correspond to a signaling intermediate complex that would trigger β-amyloid initation and the eventual synaptic dysfunction found early in AD pathogenesis [140,180,182–184,188]. The M3R mutants mislocalization indicated that the membrane protein trafficking was affected, directly or indirectly, by tau overexpression in agreement with the known interaction of M3R with EC tau [144,185,186]. In this thesis, the specific sites N132, D518 and K523 at the EC site of M3R had important effects on the tau-M3R interaction suggesting that they may be involved in the physical interacting site.

6. CONCLUSIONS

The structural and folding properties of WT rhodopsin, and RP mutants, were analyzed in artificial DMPC/DHPC bicelles and DDHA-PC liposomes separately, using biochemical and biophysical approaches.

Properties of WT, and G90V and N55K mutants, regenerated with 9-*cis*-retinal in DMPC/DHPC bicelles

- DMPC/DHPC bicelles provide an artificial membrane environment for rhodopsin and G90V and N55K mutants being more stable than the DM environment.

- DMPC/DHPC bicelles increase the stability of the sector RP N55K mutant by showing an obvious light desensitization effect compared with the behavior in DM detergent. The light desensitization character of N55K in DMPC/DHPC bicelles may be associated with the peculiar sector RP phenotype.

- In DM environment, G90V and N55K mutants show increased opsin truncation which can be associated with conformational instability. In contrast, electrophoretic analysis reveals that DMPC/DHPC bicelles would decrease the amount of truncated opsin.

- DMPC/DHPC bicelles stabilize the folded opsin conformation and provide higher thermal stability for WT, G90V and N55K in the dark state at 37ºC. This means the bicelles provide conformational stability and protect the SB linkage from hydrolysis.

- In chromophore regeneration experiments, G90V shows a more stable structure in bicelles that allows enhanced retinal entry into the binding pocket. On the other hand, N55K does not have the capability of retinal regeneration under the same experimental conditions.

- In the Meta II decay experiment, the retinal release processes of WT rhodopsin, and G90V and N55K mutants, in DMPC/DHPC bicelles and DDHA-PC liposomes, are faster than in DM detergent. Hydroxylamine addition, after Meta II complete decay, to WT and G90V in bicelles could increase fluorescence intensity, suggesting that some retinal was still in the binding pocket after Meta II decay.

- The $WT_{bicelles}$ and $G90V_{bicelles}$ opsins produced after Meta II decay could bind more 9-*cis*-retinal and 11-*cis*-retinal than in DM detergent. This is likely due to the stabilization effect of the lipid bicelles on the opsin conformation. Contrarily, neither $N55K_{DM}$ nor $N55K_{bicelles}$ could bind 9-*cis*-retinal or 11-*cis*-retinal after complete Meta II decay, suggesting that the binding pocket of N55K opsin suffered a conformational change impairing retinal entrance (possibly retaining isomerized retinal within the binding pocket).

Characterization of WT rhodopsin, and the G90V and N55K mutants, regenerated with 11-*cis*-retinal, in DDHA-PC liposomes

- DDHA-PC liposomes are a stable and effective lipid system to preserve WT and mutants structural features. Rhodopsin in DDHA-PC liposomes apparently shows higher oligomeric conformational states than in DM detergent.

- DDHA-PC liposomes increase WT, G90V thermal stability, at 48ºC, by delaying protein denaturation and protecting the protonated SB. $N55K_{liposomes}$ does not show an increase in $t_{1/2}$ compared to $N55K_{DM}$. However, at later stage $N55K_{liposomes}$ appears to be more stable than $N55K_{DM}$.

- DDHA-PC liposomes could accelerate the retinal release from the binding pocket of WT, G90V and N55K mutants (upon Meta II state) compared with the samples in DM detergent.

- WT opsin, obtained from the Meta II decay, could bind the exogenously retinal in DDHA-PC liposomes. Both $G90V_{DM}$ and $G90V_{liposomes}$ showed a decrease in the Trp fluorescence signal after exogenous retinal was added. A deeper decrease signal is detected in $G90V_{liposomes}$ indicating higher retinal binding capacity in the liposomes condition. On the contrary, N55K Meta II decay opsin could not incorporate the added retinal neither in DM nor in DDHA-PC liposomes.

- WT, G90V and N55K in DDHA-PC liposomes show low Gt activation possibly due to different protein orientations in liposomes.

Mechanism of GPCRs interaction with other proteins

- Arrestin R175E not only binds and stabilizes the Meta II state of rhodopsin, but also slows down the retinal release from the binding pocket of rhodopsin. The interaction between arrestin R175E and rhodopsin mutants associated with RP can be the objective of future studies.

- Tau protein and M3R WT and mutants are coexpressed in HEK293T cells. M3R WT and mutants N132G and D518N change the locations of tau from the cytoplasm to the membrane. M3R mutants D518K and K523Q are mislocalized to the cytoplasm (and not to the membrane) upon coexpression with tau protein. The location changes observed could be explained by the specific interactions between tau and M3R mutants. The mutation sites may contribute to the binding/recognition of tau on M3R and play a role in the pathophysiology of AD.

7. REFERENCES

(1) Stevens, R. C., Cherezov, V., Katritch, V., Abagyan, R., Kuhn, P., Rosen, H., and Wuthrich, K. (2013) The GPCR Network: a large-scale collaboration to determine human GPCR structure and function. *Nat. Rev. Drug Discov. 12*, 25–34.

(2) Lagerstrom, M. C., and Schioth, H. B. (2008) Structural diversity of G protein-coupled receptors and significance for drug discovery. *Nat. Rev. Drug Discov. 7*, 339–357.

(3) Lander, E. S., Linton, L. M., Birren, B., Nusbaum, C., Zody, M. C., Baldwin, J., Devon, K., Dewar, K., Doyle, M., FitzHugh, W., Funke, R., Gage, D., Harris, K., Heaford, A., Howland, J., Kann, L., Lehoczky, J., LeVine, R., McEwan, P., McKernan, K., Meldrim, J., Mesirov, J. P., Miranda, C., Morris, W., Naylor, J., Raymond, C., Rosetti, M., Santos, R., Sheridan, A., Sougnez, C., Stange-Thomann, Y., Stojanovic, N., Subramanian, A., Wyman, D., Rogers, J., Sulston, J., Ainscough, R., Beck, S., Bentley, D., Burton, J., Clee, C., Carter, N., Coulson, A., Deadman, R., Deloukas, P., Dunham, A., Dunham, I., Durbin, R., French, L., Grafham, D., Gregory, S., Hubbard, T., Humphray, S., Hunt, A., Jones, M., Lloyd, C., McMurray, A., Matthews, L., Mercer, S., Milne, S., Mullikin, J. C., Mungall, A., Plumb, R., Ross, M., Shownkeen, R., Sims, S., Waterston, R. H., Wilson, R. K., Hillier, L. W., McPherson, J. D., Marra, M. A., Mardis, E. R., Fulton, L. A., Chinwalla, A. T., Pepin, K. H., Gish, W. R., Chissoe, S. L., Wendl, M. C., Delehaunty, K. D., Miner, T. L., Delehaunty, A., Kramer, J. B., Cook, L. L., Fulton, R. S., Johnson, D. L., Minx, P. J., Clifton, S. W., Hawkins, T., Branscomb, E., Predki, P., Richardson, P., Wenning, S., Slezak, T., Doggett, N., Cheng, J. F., Olsen, A., Lucas, S., Elkin, C., Uberbacher, E., Frazier, M., Gibbs, R. A., Muzny, D. M., Scherer, S. E., Bouck, J. B., Sodergren, E. J., Worley, K. C., Rives, C. M., Gorrell, J. H., Metzker, M. L., Naylor, S. L., Kucherlapati, R. S., Nelson, D. L., Weinstock, G. M., Sakaki, Y., Fujiyama, A., Hattori, M., Yada, T., Toyoda, A., Itoh, T., Kawagoe, C., Watanabe, H., Totoki, Y., Taylor, T., Weissenbach, J., Heilig, R., Saurin, W., Artiguenave, F., Brottier, P., Bruls, T., Pelletier, E., Robert, C., Wincker, P., Smith, D. R., Doucette-Stamm, L., Rubenfield, M., Weinstock, K., Lee, H. M., Dubois, J., Rosenthal, A., Platzer, M., Nyakatura, G., Taudien, S., Rump, A., Yang, H., Yu, J., Wang, J., Huang, G., Gu, J., Hood, L., Rowen, L., Madan, A., Qin, S., Davis, R. W., Federspiel, N. A., Abola, A. P., Proctor, M. J., Myers, R. M., Schmutz, J., Dickson, M., Grimwood, J., Cox, D. R., Olson, M. V, Kaul, R., Raymond, C., Shimizu, N., Kawasaki, K., Minoshima, S., Evans, G. A., Athanasiou, M., Schultz, R., Roe, B. A., Chen, F., Pan, H., Ramser, J., Lehrach, H., Reinhardt, R., McCombie, W. R., de

la Bastide, M., Dedhia, N., Blocker, H., Hornischer, K., Nordsiek, G., Agarwala, R., Aravind, L., Bailey, J. A., Bateman, A., Batzoglou, S., Birney, E., Bork, P., Brown, D. G., Burge, C. B., Cerutti, L., Chen, H. C., Church, D., Clamp, M., Copley, R. R., Doerks, T., Eddy, S. R., Eichler, E. E., Furey, T. S., Galagan, J., Gilbert, J. G., Harmon, C., Hayashizaki, Y., Haussler, D., Hermjakob, H., Hokamp, K., Jang, W., Johnson, L. S., Jones, T. A., Kasif, S., Kaspryzk, A., Kennedy, S., Kent, W. J., Kitts, P., Koonin, E. V, Korf, I., Kulp, D., Lancet, D., Lowe, T. M., McLysaght, A., Mikkelsen, T., Moran, J. V, Mulder, N., Pollara, V. J., Ponting, C. P., Schuler, G., Schultz, J., Slater, G., Smit, A. F., Stupka, E., Szustakowki, J., Thierry-Mieg, D., Thierry-Mieg, J., Wagner, L., Wallis, J., Wheeler, R., Williams, A., Wolf, Y. I., Wolfe, K. H., Yang, S. P., Yeh, R. F., Collins, F., Guyer, M. S., Peterson, J., Felsenfeld, A., Wetterstrand, K. A., Patrinos, A., Morgan, M. J., de Jong, P., Catanese, J. J., Osoegawa, K., Shizuya, H., Choi, S., Chen, Y. J., and Szustakowki, J. (2001) Initial sequencing and analysis of the human genome. *Nature 409*, 860–921.

(4) Fredriksson, R., Lagerstrom, M. C., Lundin, L.-G., and Schioth, H. B. (2003) The G-protein-coupled receptors in the human genome form five main families. Phylogenetic analysis, paralogon groups, and fingerprints. *Mol. Pharmacol. 63*, 1256–1272.

(5) Zalewska, M., Siara, M., and Sajewicz, W. (2014) G protein-coupled receptors: abnormalities in signal transmission, disease states and pharmacotherapy. *Acta Pol. Pharm. 71*, 229–243.

(6) Di Pizio, A., and Niv, M. Y. (2014) Computational Studies of Smell and Taste Receptors. *Isr. J. Chem. 54*, 1205–1218.

(7) Sarramegna, V., Talmont, F., Demange, P., and Milon, A. (2003) Heterologous expression of G-protein-coupled receptors: comparison of expression systems from the standpoint of large-scale production and purification. *Cell. Mol. Life Sci. 60*, 1529–1546.

(8) Katritch, V., Cherezov, V., and Stevens, R. C. (2013) Structure-function of the G protein-coupled receptor superfamily. *Annu. Rev. Pharmacol. Toxicol. 53*, 531–556.

(9) Insel, P. A., Wilderman, A., Zambon, A. C., Snead, A. N., Murray, F., Aroonsakool, N., McDonald, D. S., Zhou, S., McCann, T., Zhang, L., Sriram, K., Chinn, A. M., Michkov, A. V, Lynch, R. M., Overland, A. C., and Corriden, R. (2015) G Protein-Coupled Receptor (GPCR) Expression in Native Cells: "Novel" endoGPCRs as Physiologic Regulators and Therapeutic Targets. *Mol. Pharmacol. 88*, 181–187.

(10) Reggio, P. H. (2006) Computational methods in drug design: modeling G protein-coupled receptor monomers, dimers, and oligomers. *AAPS J. 8*, E322–36.

(11) Hiller, C., Kuhhorn, J., and Gmeiner, P. (2013) Class A G-protein-coupled receptor (GPCR) dimers and bivalent ligands. *J. Med. Chem. 56*, 6542–6559.

(12) Grigoriadis, D. E., Hoare, S. R. J., Lechner, S. M., Slee, D. H., and Williams, J. A. (2009) Drugability of extracellular targets: discovery of small molecule drugs targeting allosteric, functional, and subunit-selective sites on GPCRs and ion channels. *Neuropsychopharmacology 34*, 106–125.

(13) Trzaskowski, B., Latek, D., Yuan, S., Ghoshdastider, U., Debinski, A., and Filipek, S. (2012) Action of molecular switches in GPCRs--theoretical and experimental studies. *Curr. Med. Chem. 19*, 1090–1109.

(14) Tuteja, N. (2009) Signaling through G protein coupled receptors. *Plant Signal. Behav. 4*, 942–947.

(15) Harmar, A. J. (2001) Family-B G-protein-coupled receptors. *Genome Biol. 2*, REVIEWS3013.

(16) Gao, Q.-B., and Wang, Z.-Z. (2006) Classification of G-protein coupled receptors at four levels. *Protein Eng. Des. Sel. 19*, 511–516.

(17) Katritch, V., Cherezov, V., and Stevens, R. C. (2012) Diversity and modularity of G protein-coupled receptor structures. *Trends Pharmacol. Sci. 33*, 17–27.

(18) Bermudez, M., and Wolber, G. (2015) Structure versus function-The impact of computational methods on the discovery of specific GPCR-ligands. *Bioorg. Med. Chem. 23*, 3907–3912.

(19) Miyano, K., Sudo, Y., Yokoyama, A., Hisaoka-Nakashima, K., Morioka, N., Takebayashi, M., Nakata, Y., Higami, Y., and Uezono, Y. (2014) History of the G protein-coupled receptor (GPCR) assays from traditional to a state-of-the-art biosensor assay. *J. Pharmacol. Sci. 126*, 302–309.

(20) Chen, L., Jin, L., and Zhou, N. (2012) An update of novel screening methods for GPCR in drug discovery. *Expert Opin. Drug Discov. 7*, 791–806.

(21) Ferre, S. (2015) The GPCR heterotetramer: challenging classical pharmacology. *Trends*

Pharmacol. Sci. 36, 145–152.

(22) (2000) Crystal structure of rhodopsin: a G protein-coupled receptor. Palczewski K,*(1) kumasaka T, hori T, behnke CA, motoshima H, fox BA, trong IL, teller DC, okada T, stenkamp RE, yamamoto M, miyano M. Science 2000;289:739-745. *Am. J. Ophthalmol. 130*, 865.

(23) Tesmer, J. J. G. (2010) The quest to understand heterotrimeric G protein signaling. *Nat Struct Mol Biol 17*, 650–652.

(24) Rosenbaum, D. M., Rasmussen, S. G. F., and Kobilka, B. K. (2009) The structure and function of G-protein-coupled receptors. *Nature 459*, 356–363.

(25) Venkatakrishnan, a J., Deupi, X., Lebon, G., Tate, C. G., Schertler, G. F., and Babu, M. M. (2013) Molecular signatures of G-protein-coupled receptors. *Nature 494*, 185–94.

(26) Tautermann, C. S. (2014) GPCR structures in drug design, emerging opportunities with new structures. *Bioorg. Med. Chem. Lett. 24*, 4073–4079.

(27) Zocher, M., Bippes, C. A., Zhang, C., and Muller, D. J. (2013) Single-molecule force spectroscopy of G-protein-coupled receptors. *Chem. Soc. Rev. 42*, 7801–7815.

(28) Heifetz, A., Schertler, G. F. X., Seifert, R., Tate, C. G., Sexton, P. M., Gurevich, V. V, Fourmy, D., Cherezov, V., Marshall, F. H., Storer, R. I., Moraes, I., Tikhonova, I. G., Tautermann, C. S., Hunt, P., Ceska, T., Hodgson, S., Bodkin, M. J., Singh, S., Law, R. J., and Biggin, P. C. (2015) GPCR structure, function, drug discovery and crystallography: report from Academia-Industry International Conference (UK Royal Society) Chicheley Hall, 1-2 September 2014. *Naunyn. Schmiedebergs. Arch. Pharmacol. 388*, 883–903.

(29) Krumm, B. E., and Grisshammer, R. (2015) Peptide ligand recognition by G protein-coupled receptors. *Front. Pharmacol. 6*, 48.

(30) Buzhynskyy, N., Salesse, C., and Scheuring, S. (2011) Rhodopsin is spatially heterogeneously distributed in rod outer segment disk membranes. *J. Mol. Recognit. 24*, 483–489.

(31) Wang, Y., Botelho, A. V., Martinez, G. V, and Brown, M. F. (2002) Electrostatic properties of membrane lipids coupled to metarhodopsin II formation in visual transduction. *J. Am. Chem. Soc. 124*, 7690–7701.

(32) Huber, T., Rajamoorthi, K., Kurze, V. F., Beyer, K., and Brown, M. F. (2002) Structure of

docosahexaenoic acid-containing phospholipid bilayers as studied by (2)H NMR and molecular dynamics simulations. *J. Am. Chem. Soc. 124*, 298–309.

(33) Jastrzebska, B., Debinski, A., Filipek, S., and Palczewski, K. (2011) Role of membrane integrity on G protein-coupled receptors: Rhodopsin stability and function. *Prog. Lipid Res. 50*, 267–77.

(34) Fotiadis, D., Liang, Y., Filipek, S., Saperstein, D. A., Engel, A., and Palczewski, K. (2003) Atomic-force microscopy: Rhodopsin dimers in native disc membranes. *Nature 421*, 127–128.

(35) McKibbin, C., Farmer, N. A., Jeans, C., Reeves, P. J., Khorana, H. G., Wallace, B. A., Edwards, P. C., Villa, C., and Booth, P. J. (2007) Opsin stability and folding: modulation by phospholipid bicelles. *J. Mol. Biol. 374*, 1319–1332.

(36) Menon, S. T., Han, M., and Sakmar, T. P. (2001) Rhodopsin: structural basis of molecular physiology. *Physiol. Rev. 81*, 1659–1688.

(37) Morris, M. B., Dastmalchi, S., and Church, W. B. (2009) Rhodopsin: structure, signal transduction and oligomerisation. *Int. J. Biochem. Cell Biol. 41*, 721–724.

(38) Hernandez-Rodriguez, E. W., Sanchez-Garcia, E., Crespo-Otero, R., Montero-Alejo, A. L., Montero, L. A., and Thiel, W. (2012) Understanding rhodopsin mutations linked to the retinitis pigmentosa disease: a QM/MM and DFT/MRCI study. *J. Phys. Chem. B 116*, 1060–1076.

(39) Lamb, T. D., and Pugh, E. N. (2006) Phototransduction, dark adaptation, and rhodopsin regeneration the proctor lecture. *Invest. Ophthalmol. Vis. Sci. 47*, 5137–52.

(40) Hofmann, K. P., Scheerer, P., Hildebrand, P. W., Choe, H.-W., Park, J. H., Heck, M., and Ernst, O. P. (2009) A G protein-coupled receptor at work: the rhodopsin model. *Trends Biochem. Sci. 34*, 540–52.

(41) Yau, K.-W., and Hardie, R. C. (2009) Phototransduction motifs and variations. *Cell 139*, 246–264.

(42) Palczewski, K. (2012) Chemistry and biology of vision. *J. Biol. Chem. 287*, 1612–1619.

(43) Choe, H.-W., Kim, Y. J., Park, J. H., Morizumi, T., Pai, E. F., Krauss, N., Hofmann, K. P., Scheerer, P., and Ernst, O. P. (2011) Crystal structure of metarhodopsin II. *Nature 471*, 651–655.

(44) Scheerer, P., Park, J. H., Hildebrand, P. W., Kim, Y. J., Krauss, N., Choe, H.-W., Hofmann, K. P., and Ernst, O. P. (2008) Crystal structure of opsin in its G-protein-interacting conformation.

Nature 455, 497–502.

(45) Palczewski, K. (2006) G protein-coupled receptor rhodopsin. *Annu. Rev. Biochem. 75*, 743–767.

(46) Perusek, L., and Maeda, T. (2013) Vitamin A derivatives as treatment options for retinal degenerative diseases. *Nutrients 5*, 2646–2666.

(47) Saari, J. C. (2000, February) Biochemistry of visual pigment regeneration: the Friedenwald lecture. *Invest. Ophthalmol. Vis. Sci.* UNITED STATES.

(48) Boya, P., and Codogno, P. (2013, September) Cell biology: Recycling in sight. *Nature*. England.

(49) Hatori, M., and Panda, S. (2010) The emerging roles of melanopsin in behavioral adaptation to light. *Trends Mol. Med. 16*, 435–446.

(50) Bloem, B., Poorthuis, R. B., and Mansvelder, H. D. (2014) Cholinergic modulation of the medial prefrontal cortex: the role of nicotinic receptors in attention and regulation of neuronal activity. *Front. Neural Circuits 8*, 17.

(51) Eglen, R. M. (2006) Muscarinic receptor subtypes in neuronal and non-neuronal cholinergic function. *Auton. Autacoid Pharmacol. 26*, 219–233.

(52) Haga, T. (2013) Molecular properties of muscarinic acetylcholine receptors. *Proc. Jpn. Acad. Ser. B. Phys. Biol. Sci. 89*, 226–256.

(53) Bubser, M., Byun, N., Wood, M. R., and Jones, C. K. (2012) Muscarinic receptor pharmacology and circuitry for the modulation of cognition. *Handb. Exp. Pharmacol.* 121–166.

(54) Brown, D. A. (2010) Muscarinic acetylcholine receptors (mAChRs) in the nervous system: some functions and mechanisms. *J. Mol. Neurosci. 41*, 340–346.

(55) Pera, T., and Penn, R. B. (2014) Crosstalk between beta-2-adrenoceptor and muscarinic acetylcholine receptors in the airway. *Curr. Opin. Pharmacol. 16*, 72–81.

(56) Hille, B., Dickson, E., Kruse, M., and Falkenburger, B. (2014) Dynamic metabolic control of an ion channel. *Prog. Mol. Biol. Transl. Sci. 123*, 219–247.

(57) Minami, K., and Uezono, Y. (2013) The recent progress in research on effects of anesthetics and analgesics on G protein-coupled receptors. *J. Anesth. 27*, 284–292.

(58) Popova, J. S., and Rasenick, M. M. (2004) Clathrin-mediated endocytosis of m3 muscarinic

receptors. Roles for Gbetagamma and tubulin. *J. Biol. Chem. 279*, 30410–30418.

(59) Kruse, A. C., Hu, J., Pan, A. C., Arlow, D. H., Rosenbaum, D. M., Rosemond, E., Green, H. F., Liu, T., Chae, P. S., Dror, R. O., Shaw, D. E., Weis, W. I., Wess, J., and Kobilka, B. K. (2012) Structure and dynamics of the M3 muscarinic acetylcholine receptor. *Nature 482*, 552–556.

(60) Li, J. H., Hamdan, F. F., Kim, S.-K., Jacobson, K. A., Zhang, X., Han, S.-J., and Wess, J. (2008) Ligand-specific changes in M3 muscarinic acetylcholine receptor structure detected by a disulfide scanning strategy. *Biochemistry 47*, 2776–2788.

(61) Martinez-Archundia, M., Cordomi, A., Garriga, P., and Perez, J. J. (2012) Molecular modeling of the M3 acetylcholine muscarinic receptor and its binding site. *J. Biomed. Biotechnol. 2012*, 789741.

(62) Insel, P. A., Tang, C.-M., Hahntow, I., and Michel, M. C. (2007) Impact of GPCRs in clinical medicine: monogenic diseases, genetic variants and drug targets. *Biochim. Biophys. Acta 1768*, 994–1005.

(63) Ulloa-Aguirre, A., Zarinan, T., Dias, J. A., and Conn, P. M. (2014) Mutations in G protein-coupled receptors that impact receptor trafficking and reproductive function. *Mol. Cell. Endocrinol. 382*, 411–423.

(64) Rivolta, C., Sharon, D., DeAngelis, M. M., and Dryja, T. P. (2002) Retinitis pigmentosa and allied diseases: numerous diseases, genes, and inheritance patterns. *Hum. Mol. Genet. 11*, 1219–1227.

(65) Daiger, S. P., Sullivan, L. S., and Bowne, S. J. (2013) Genes and mutations causing retinitis pigmentosa. *Clin. Genet. 84*, 132–141.

(66) Krebs, M. P., Holden, D. C., Joshi, P., Clark, C. L. 3rd, Lee, A. H., and Kaushal, S. (2010) Molecular mechanisms of rhodopsin retinitis pigmentosa and the efficacy of pharmacological rescue. *J. Mol. Biol. 395*, 1063–1078.

(67) Concepcion, F., and Chen, J. (2010) Q344ter mutation causes mislocalization of rhodopsin molecules that are catalytically active: a mouse model of Q344ter-induced retinal degeneration. *PLoS One 5*, e10904.

(68) Berger, W., Kloeckener-Gruissem, B., and Neidhardt, J. (2010) The molecular basis of human retinal and vitreoretinal diseases. *Prog. Retin. Eye Res. 29*, 335–375.

(69) Srinivasan, S., Ramon, E., Cordomí, A., and Garriga, P. (2014) Binding specificity of retinal analogs to photoactivated visual pigments suggest mechanism for fine-tuning GPCR-ligand interactions. *Chem. Biol. 21*, 369–78.

(70) Toledo, D., Ramon, E., Aguilà, M., Cordomí, A., Pérez, J. J., Mendes, H. F., Cheetham, M. E., and Garriga, P. (2011) Molecular mechanisms of disease for mutations at Gly-90 in rhodopsin. *J. Biol. Chem. 286*, 39993–40001.

(71) Andres, A., Garriga, P., and Manyosa, J. (2003) Altered functionality in rhodopsin point mutants associated with retinitis pigmentosa. *Biochem. Biophys. Res. Commun. 303*, 294–301.

(72) Rayapudi, S., Schwartz, S. G., Wang, X., and Chavis, P. (2013) Vitamin A and fish oils for retinitis pigmentosa. *Cochrane database Syst. Rev. 12*, CD008428.

(73) Saliba, R. S., Munro, P. M. G., Luthert, P. J., and Cheetham, M. E. (2002) The cellular fate of mutant rhodopsin: quality control, degradation and aggresome formation. *J. Cell Sci. 115*, 2907–2918.

(74) Hartong, D. T., Berson, E. L., and Dryja, T. P. (2006) Retinitis pigmentosa. *Lancet 368*, 1795–1809.

(75) Anasagasti, A., Irigoyen, C., Barandika, O., Lopez de Munain, A., and Ruiz-Ederra, J. (2012) Current mutation discovery approaches in Retinitis Pigmentosa. *Vision Res. 75*, 117–129.

(76) Van Woerkom, C., and Ferrucci, S. (2005) Sector retinitis pigmentosa. *Optometry 76*, 309–317.

(77) Petrs-Silva, H., and Linden, R. (2014) Advances in gene therapy technologies to treat retinitis pigmentosa. *Clin. Ophthalmol. 8*, 127–136.

(78) Bosch-Presegue, L., Ramon, E., Toledo, D., Cordomi, A., and Garriga, P. (2011) Alterations in the photoactivation pathway of rhodopsin mutants associated with retinitis pigmentosa. *FEBS J. 278*, 1493–1505.

(79) Ramon, E., Cordomi, A., Aguila, M., Srinivasan, S., Dong, X., Moore, A. T., Webster, A. R., Cheetham, M. E., and Garriga, P. (2014) Differential light-induced responses in sectorial inherited retinal degeneration. *J. Biol. Chem. 289*, 35918–35928.

(80) Selkoe, D. J. (2001) Alzheimer’s disease: genes, proteins, and therapy. *Physiol. Rev. 81*, 741–766.

(81) Jiang, S., Li, Y., Zhang, C., Zhao, Y., Bu, G., Xu, H., and Zhang, Y.-W. (2014) M1 muscarinic acetylcholine receptor in Alzheimer's disease. *Neurosci. Bull. 30*, 295–307.

(82) Pakaski, M., and Kalman, J. (2008) Interactions between the amyloid and cholinergic mechanisms in Alzheimer's disease. *Neurochem. Int. 53*, 103–111.

(83) Tanzi, R. E., and Bertram, L. (2005) Twenty years of the Alzheimer's disease amyloid hypothesis: a genetic perspective. *Cell 120*, 545–555.

(84) Chen, G.-J., Xiong, Z., and Yan, Z. (2013) Aβ impairs nicotinic regulation of inhibitory synaptic transmission and interneuron excitability in prefrontal cortex. *Mol. Neurodegener. 8*, 3.

(85) Fisher, A. (2012) Cholinergic modulation of amyloid precursor protein processing with emphasis on M1 muscarinic receptor: perspectives and challenges in treatment of Alzheimer's disease. *J. Neurochem. 120 Suppl 1*, 22–33.

(86) Jakob-Roetne, R., and Jacobsen, H. (2009) Alzheimer's disease: from pathology to therapeutic approaches. *Angew. Chem. Int. Ed. Engl. 48*, 3030–3059.

(87) Buee, L., Bussiere, T., Buee-Scherrer, V., Delacourte, A., and Hof, P. R. (2000) Tau protein isoforms, phosphorylation and role in neurodegenerative disorders. *Brain Res. Brain Res. Rev. 33*, 95–130.

(88) Avila, J., Lucas, J. J., Perez, M., and Hernandez, F. (2004) Role of tau protein in both physiological and pathological conditions. *Physiol. Rev. 84*, 361–384.

(89) Simon, D., Hernandez, F., and Avila, J. (2013) The involvement of cholinergic neurons in the spreading of tau pathology. *Front. Neurol. 4*, 74.

(90) Gomez-Ramos, A., Diaz-Hernandez, M., Rubio, A., Miras-Portugal, M. T., and Avila, J. (2008) Extracellular tau promotes intracellular calcium increase through M1 and M3 muscarinic receptors in neuronal cells. *Mol. Cell. Neurosci. 37*, 673–681.

(91) Reyes-Alcaraz, A., Martinez-Archundia, M., Ramon, E., and Garriga, P. (2011) Salt effects on the conformational stability of the visual G-protein-coupled receptor rhodopsin. *Biophys. J. 101*, 2798–2806.

(92) Vogel, R., Fan, G. B., Sheves, M., and Siebert, F. (2001) Salt dependence of the formation and stability of the signaling state in G protein-coupled receptors: evidence for the involvement of the Hofmeister effect. *Biochemistry 40*, 483–493.

(93) Park, P. S.-H., Sapra, K. T., Kolinski, M., Filipek, S., Palczewski, K., and Muller, D. J. (2007) Stabilizing effect of Zn2+ in native bovine rhodopsin. *J. Biol. Chem. 282*, 11377–11385.

(94) Ramon, E., Marron, J., del Valle, L., Bosch, L., Andrés, A., Manyosa, J., and Garriga, P. (2003) Effect of dodecyl maltoside detergent on rhodopsin stability and function. *Vision Res. 43*, 3055–3061.

(95) Bubis, J. (1998) Effect of detergents and lipids on transducin photoactivation by rhodopsin. *Biol. Res. 31*, 59–71.

(96) Sengupta, D., and Chattopadhyay, A. (2015) Molecular dynamics simulations of GPCR-cholesterol interaction: An emerging paradigm. *Biochim. Biophys. Acta 1848*, 1775–1782.

(97) Sanchez-Martin, M. J., Ramon, E., Torrent-Burgues, J., and Garriga, P. (2013) Improved conformational stability of the visual G protein-coupled receptor rhodopsin by specific interaction with docosahexaenoic acid phospholipid. *Chembiochem 14*, 639–644.

(98) Boesze-Battaglia, K., and Schimmel, R. J. (1997) Cell membrane lipid composition and distribution: implications for cell function and lessons learned from photoreceptors and platelets. *J. Exp. Biol. 200*, 2927–2936.

(99) Gibson, N. J., and Brown, M. F. (1991) Membrane lipid influences on the energetics of the metarhodopsin I and metarhodopsin II conformational states of rhodopsin probed by flash photolysis. *Photochem. Photobiol. 54*, 985–992.

(100) Cho, H. S., Dominick, J. L., and Spence, M. M. (2010) Lipid domains in bicelles containing unsaturated lipids and cholesterol. *J. Phys. Chem. B 114*, 9238–9245.

(101) Ujwal, R., and Abramson, J. (2012) High-throughput crystallization of membrane proteins using the lipidic bicelle method. *J. Vis. Exp.* e3383.

(102) Niu, L., Kim, J.-M., and Khorana, H. G. (2002) Structure and function in rhodopsin: asymmetric reconstitution of rhodopsin in liposomes. *Proc. Natl. Acad. Sci. U. S. A. 99*, 13409–13412.

(103) Lambert, O., Levy, D., Ranck, J. L., Leblanc, G., and Rigaud, J. L. (1998) A new “gel-like” phase in dodecyl maltoside-lipid mixtures: implications in solubilization and reconstitution studies. *Biophys. J. 74*, 918–930.

(104) Kim, T. H., Chung, K. Y., Manglik, A., Hansen, A. L., Dror, R. O., Mildorf, T. J., Shaw, D. E., Kobilka, B. K., and Prosser, R. S. (2013) The role of ligands on the equilibria between functional states of a G protein-coupled receptor. *J. Am. Chem. Soc. 135*, 9465–9474.

(105) Kubicek, J., Block, H., Maertens, B., Spriestersbach, A., and Labahn, J. (2014) Expression and purification of membrane proteins. *Methods Enzymol. 541*, 117–140.

(106) Chattopadhyay, A., Rao, B. D., and Jafurulla, M. (2015) Solubilization of G protein-coupled receptors: a convenient strategy to explore lipid-receptor interaction. *Methods Enzymol. 557*, 117–134.

(107) Sarramegn, V., Muller, I., Milon, A., and Talmont, F. (2006) Recombinant G protein-coupled receptors from expression to renaturation: a challenge towards structure. *Cell. Mol. Life Sci. 63*, 1149–1164.

(108) Vukoti, K., Kimura, T., Macke, L., Gawrisch, K., and Yeliseev, A. (2012) Stabilization of functional recombinant cannabinoid receptor CB(2) in detergent micelles and lipid bilayers. *PLoS One 7*, e46290.

(109) Thompson, A. A., Liu, J. J., Chun, E., Wacker, D., Wu, H., Cherezov, V., and Stevens, R. C. (2011) GPCR stabilization using the bicelle-like architecture of mixed sterol-detergent micelles. *Methods 55*, 310–317.

(110) Albert, A. D., Young, J. E., and Paw, Z. (1998) Phospholipid fatty acyl spatial distribution in bovine rod outer segment disk membranes. *Biochim. Biophys. Acta 1368*, 52–60.

(111) Paila, Y. D., and Chattopadhyay, A. (2010) Membrane cholesterol in the function and organization of G-protein coupled receptors. *Subcell. Biochem. 51*, 439–466.

(112) Albert, A. D., and Boesze-Battaglia, K. (2005) The role of cholesterol in rod outer segment membranes. *Prog. Lipid Res. 44*, 99–124.

(113) Tsukamoto, H., Szundi, I., Lewis, J. W., Farrens, D. L., and Kliger, D. S. (2011) Rhodopsin in nanodiscs has native membrane-like photointermediates. *Biochemistry 50*, 5086–5091.

(114) Marsh, D. (2008) Protein modulation of lipids, and vice-versa, in membranes. *Biochim. Biophys. Acta 1778*, 1545–1575.

(115) Soubias, O., Niu, S.-L., Mitchell, D. C., and Gawrisch, K. (2008) Lipid-rhodopsin

hydrophobic mismatch alters rhodopsin helical content. *J. Am. Chem. Soc. 130*, 12465–12471.

(116) Mansoor, S. E., Palczewski, K., and Farrens, D. L. (2006) Rhodopsin self-associates in asolectin liposomes. *Proc. Natl. Acad. Sci. U. S. A. 103*, 3060–3065.

(117) Torchilin, V. P. (2006) Multifunctional nanocarriers. *Adv. Drug Deliv. Rev. 58*, 1532–1555.

(118) Serebryany, E., Zhu, G. A., and Yan, E. C. Y. (2012) Artificial membrane-like environments for in vitro studies of purified G-protein coupled receptors. *Biochim. Biophys. Acta 1818*, 225–233.

(119) Garavito, R. M., and Ferguson-Miller, S. (2001) Detergents as tools in membrane biochemistry. *J. Biol. Chem. 276*, 32403–32406.

(120) Sanders, C. R., and Prosser, R. S. (1998) Bicelles: a model membrane system for all seasons? *Structure 6*, 1227–34.

(121) Kaya, A. I., Thaker, T. M., Preininger, A. M., Iverson, T. M., and Hamm, H. E. (2011) Coupling efficiency of rhodopsin and transducin in bicelles. *Biochemistry 50*, 3193–3203.

(122) Temprana, C. F., Duarte, E. L., Femia, A. L., Alonso, S. del V, and Lamy, M. T. (2012) Structural effect of cationic amphiphiles in diacetylenic photopolymerizable membranes. *Chem. Phys. Lipids 165*, 589–600.

(123) Ujwal, R., and Bowie, J. U. (2011) Crystallizing membrane proteins using lipidic bicelles. *Methods 55*, 337–341.

(124) McKibbin, C., Farmer, N. a, Jeans, C., Reeves, P. J., Khorana, H. G., Wallace, B. a, Edwards, P. C., Villa, C., and Booth, P. J. (2007) Opsin stability and folding: modulation by phospholipid bicelles. *J. Mol. Biol. 374*, 1319–32.

(125) Botelho, A. V., Gibson, N. J., Thurmond, R. L., Wang, Y., and Brown, M. F. (2002) Conformational energetics of rhodopsin modulated by nonlamellar-forming lipids. *Biochemistry 41*, 6354–6368.

(126) Botelho, A. V., Gibson, N. J., Thurmond, R. L., Wang, Y., and Brown, M. F. (2002) Conformational energetics of rhodopsin modulated by nonlamellar-forming lipids. *Biochemistry 41*, 6354–6368.

(127) Mitchell, D. C., Niu, S.-L., and Litman, B. J. (2003) Enhancement of G protein-coupled

signaling by DHA phospholipids. *Lipids 38*, 437–443.

(128) Oates, J., and Watts, A. (2011) Uncovering the intimate relationship between lipids, cholesterol and GPCR activation. *Curr. Opin. Struct. Biol. 21*, 802–807.

(129) Gawrisch, K., and Soubias, O. (2008) Structure and dynamics of polyunsaturated hydrocarbon chains in lipid bilayers-significance for GPCR function. *Chem. Phys. Lipids 153*, 64–75.

(130) Grossfield, A., Feller, S. E., and Pitman, M. C. (2006) A role for direct interactions in the modulation of rhodopsin by omega 3 polyunsaturated lipids. *Natl. Acad. Sci. 103*, 4888–4893.

(131) Gawrisch, K., Soubias, O., and Mihailescu, M. (2008) Insights from biophysical studies on the role of polyunsaturated fatty acids for function of G-protein coupled membrane receptors. *Prostaglandins. Leukot. Essent. Fatty Acids 79*, 131–134.

(132) Zhang, P., Kofron, C. M., and Mende, U. (2015) Heterotrimeric G protein-mediated signaling and its non-canonical regulation in the heart. *Life Sci. 129*, 35–41.

(133) Huang, L., Mao, X., Abdulaev, N. G., Ngo, T., Liu, W., and Ridge, K. D. (2012) One-step purification of a functional, constitutively activated form of visual arrestin. *Protein Expr. Purif. 82*, 55–60.

(134) Sommer, M. E., Farrens, D. L., McDowell, J. H., Weber, L. A., and Smith, W. C. (2007) Dynamics of arrestin-rhodopsin interactions: loop movement is involved in arrestin activation and receptor binding. *J. Biol. Chem. 282*, 25560–25568.

(135) Hirsch, J. A., Schubert, C., Gurevich, V. V, and Sigler, P. B. (1999) The 2.8 A crystal structure of visual arrestin: a model for arrestin's regulation. *Cell 97*, 257–269.

(136) Moller, D., and Gmeiner, P. (2015) Arrestin-Bound Rhodopsin: A Molecular Structure and its Impact on the Development of Biased GPCR Ligands. *Angew. Chem. Int. Ed. Engl. 54*, 13166–13168.

(137) Luttrell, L. M., and Lefkowitz, R. J. (2002) The role of beta-arrestins in the termination and transduction of G-protein-coupled receptor signals. *J. Cell Sci. 115*, 455–465.

(138) Kirchberg, K., Kim, T.-Y., Moller, M., Skegro, D., Dasara Raju, G., Granzin, J., Buldt, G., Schlesinger, R., and Alexiev, U. (2011) Conformational dynamics of helix 8 in the GPCR rhodopsin controls arrestin activation in the desensitization process. *Proc. Natl. Acad. Sci. U. S.*

A. 108, 18690–18695.

(139) Sommer, M. E., Smith, W. C., and Farrens, D. L. (2005) Dynamics of arrestin-rhodopsin interactions: arrestin and retinal release are directly linked events. *J. Biol. Chem. 280*, 6861–6871.

(140) Ittner, L. M., and Gotz, J. (2011) Amyloid-beta and tau--a toxic pas de deux in Alzheimer's disease. *Nat. Rev. Neurosci. 12*, 65–72.

(141) Andreadis, A. (2005) Tau gene alternative splicing: expression patterns, regulation and modulation of function in normal brain and neurodegenerative diseases. *Biochim. Biophys. Acta 1739*, 91–103.

(142) Johnson, G. V. W., and Stoothoff, W. H. (2004) Tau phosphorylation in neuronal cell function and dysfunction. *J. Cell Sci. 117*, 5721–5729.

(143) Scholz, T., and Mandelkow, E. (2014) Transport and diffusion of Tau protein in neurons. *Cell. Mol. Life Sci. 71*, 3139–3150.

(144) Avila, J., de Barreda, E. G., Fuster-Matanzo, A., Simon, D., Llorens-Martin, M., Engel, T., Lucas, J. J., Diaz-Hernandez, M., and Hernandez, F. (2012) Looking for novel functions of tau. *Biochem. Soc. Trans. 40*, 653–655.

(145) Garcia, M. L., and Cleveland, D. W. (2001) Going new places using an old MAP: tau, microtubules and human neurodegenerative disease. *Curr. Opin. Cell Biol. 13*, 41–48.

(146) Mandelkow, E.-M., and Mandelkow, E. (2012) Biochemistry and cell biology of tau protein in neurofibrillary degeneration. *Cold Spring Harb. Perspect. Med. 2*, a006247.

(147) Medina, M., Montejo de Garcini, E., and Avila, J. (1995) The role of tau phosphorylation in transfected COS-1 cells. *Mol. Cell. Biochem. 148*, 79–88.

(148) Avila, J. (2009) The tau code. *Front. Aging Neurosci. 1*, 1.

(149) Silva, L. I. (2008) Allosteric interactions at the M 3 muscarinic acetylcholine receptor.

(150) Oprian, D. D., Molday, R. S., Kaufman, R. J., and Khorana, H. G. (1987) Expression of a synthetic bovine rhodopsin gene in monkey kidney cells. *Proc. Natl. Acad. Sci. U. S. A. 84*, 8874–8878.

(151) Blankenship, E., and Lodowski, D. T. (2015) Rhodopsin purification from dark-adapted bovine retina. *Methods Mol. Biol. 1271*, 21–38.

(152) Fukada, Y., Matsuda, T., Kokame, K., Takao, T., Shimonishi, Y., Akino, T., and Yoshizawa, T. (1994) Effects of carboxyl methylation of photoreceptor G protein γ-subunit in visual transduction. *J. Biol. Chem. 269*, 5163–5170.

(153) Merino, S., Domenech, O., Vinas, M., Montero, M. T., and Hernandez-Borrell, J. (2005) Effects of lactose permease on the phospholipid environment in which it is reconstituted: a fluorescence and atomic force microscopy study. *Langmuir 21*, 4642–4647.

(154) Rigaud, J. L., Levy, D., Mosser, G., and Lambert, O. (1998) Detergent removal by non-polar polystyrene beads: Applications to membrane protein reconstitution and two-dimensional crystallization. *Eur. Biophys. J. 27*, 305–319.

(155) Farrens, D. L., and Khorana, H. G. (1995) Structure and function in rhodopsin. Measurement of the rate of metarhodopsin II decay by fluorescence spectroscopy. *J. Biol. Chem. 270*, 5073–5076.

(156) Faurobert, E., Otto-Bruc, A., Chardin, P., and Chabre, M. (1993) Tryptophan W207 in transducin T alpha is the fluorescence sensor of the G protein activation switch and is involved in the effector binding. *EMBO J. 12*, 4191–4198.

(157) Neidhardt, J., Barthelmes, D., Farahmand, F., Fleischhauer, J. C., and Berger, W. (2006) Different amino acid substitutions at the same position in rhodopsin lead to distinct phenotypes. *Invest. Ophthalmol. Vis. Sci. 47*, 1630–1635.

(158) Sekharan, S., and Morokuma, K. (2011) Why 11-cis-retinal? Why not 7-cis-, 9-cis-, or 13-cis-retinal in the eye? *J. Am. Chem. Soc. 133*, 19052–19055.

(159) Reeves, P. J., Hwa, J., and Khorana, H. G. (1999) Structure and function in rhodopsin: kinetic studies of retinal binding to purified opsin mutants in defined phospholipid-detergent mixtures serve as probes of the retinal binding pocket. *Proc. Natl. Acad. Sci. U. S. A. 96*, 1927–1931.

(160) Liu, J., Liu, M. Y., Nguyen, J. B., Bhagat, A., Mooney, V., and Yan, E. C. Y. (2009) Thermal decay of rhodopsin: role of hydrogen bonds in thermal isomerization of 11-cis retinal in the binding site and hydrolysis of protonated Schiff base. *J. Am. Chem. Soc. 131*, 8750–8751.

(161) Lamb, T. D., and Pugh, E. N. J. (2004) Dark adaptation and the retinoid cycle of vision. *Prog. Retin. Eye Res. 23*, 307–380.

(162) Ernst, O. P., Gramse, V., Kolbe, M., Hofmann, K. P., and Heck, M. (2007) Monomeric G protein-coupled receptor rhodopsin in solution activates its G protein transducin at the diffusion limit. *Proc. Natl. Acad. Sci. U. S. A. 104*, 10859–10864.

(163) Duft, D., Achtzehn, T., and Müller, R. (2003) Rhodopsin dimers in native disc membranes *421*, 127–128.

(164) Smith, A. W. (2015) Detection of rhodopsin dimerization in situ by PIE-FCCS, a time-resolved fluorescence spectroscopy. *Methods Mol. Biol. 1271*, 205–219.

(165) Shukolyukov, S. A. (2010) Proof of oligomeric state of frog rhodopsin: visualization of dimer and oligomers on gels after BN- and HRCN-PAGE using antibodies to rhodopsin and by retinylopsin fluorescence. *Biochemistry. (Mosc). 75*, 1045–1051.

(166) Landin, J. S., Katragadda, M., and Albert, A. D. (2001) Thermal destabilization of rhodopsin and opsin by proteolytic cleavage in bovine rod outer segment disk membranes. *Biochemistry 40*, 11176–11183.

(167) Dhanasekaran, N., Wessling-Resnick, M., Kelleher, D. J., Johnson, G. L., and Ruoho, A. E. (1988) Mapping of the carboxyl terminus within the tertiary structure of transducin's alpha subunit using the heterobifunctional cross-linking reagent, 125I-N-(3-iodo-4-azidophenylpropionamido-S-(2-thiopyridyl) cysteine. *J. Biol. Chem. 263*, 17942–17950.

(168) Corley, S. C., Sprangers, P., and Albert, A. D. (2011) The bilayer enhances rhodopsin kinetic stability in bovine rod outer segment disk membranes. *Biophys. J. 100*, 2946–2954.

(169) Sinha, A., Jones Brunette, A. M., Fay, J. F., Schafer, C. T., and Farrens, D. L. (2014) Rhodopsin TM6 can interact with two separate and distinct sites on arrestin: evidence for structural plasticity and multiple docking modes in arrestin-rhodopsin binding. *Biochemistry 53*, 3294–3307.

(170) Sommer, M. E., Hofmann, K. P., and Heck, M. (2011) Arrestin-rhodopsin binding stoichiometry in isolated rod outer segment membranes depends on the percentage of activated receptors. *J. Biol. Chem. 286*, 7359–7369.

(171) Hanson, S. M., Cleghorn, W. M., Francis, D. J., Vishnivetskiy, S. A., Raman, D., Song, X., Nair, K. S., Slepak, V. Z., Klug, C. S., and Gurevich, V. V. (2007) Arrestin mobilizes signaling

proteins to the cytoskeleton and redirects their activity. *J. Mol. Biol. 368*, 375–387.

(172) Kang, Y., Gao, X., Zhou, X. E., He, Y., Melcher, K., and Xu, H. E. (2015) A structural snapshot of the rhodopsin-arrestin complex. *FEBS J.*

(173) Raman, D., Osawa, S., Gurevich, V. V, and Weiss, E. R. (2003) The interaction with the cytoplasmic loops of rhodopsin plays a crucial role in arrestin activation and binding. *J. Neurochem. 84*, 1040–1050.

(174) Yanamala, N., Gardner, E., Riciutti, A., and Klein-Seetharaman, J. (2012) The cytoplasmic rhodopsin-protein interface: potential for drug discovery. *Curr. Drug Targets 13*, 3–14.

(175) Sommer, M. E., Smith, W. C., and Farrens, D. L. (2006) Dynamics of arrestin-rhodopsin interactions: acidic phospholipids enable binding of arrestin to purified rhodopsin in detergent. *J. Biol. Chem. 281*, 9407–9417.

(176) Sommer, M. E., Hofmann, K. P., and Heck, M. (2012) Distinct loops in arrestin differentially regulate ligand binding within the GPCR opsin. *Nat. Commun. 3*, 995.

(177) Kanwal, S., Nishat, S., and Khan, M. I. (2012) Docking of human rhodopsin mutant (Gly90-->Asp) with beta-arrestin and cyanidin 3-rutinoside to cure night blindness. *Bioinformation 8*, 128–133.

(178) Gray-Keller, M. P., Detwiler, P. B., Benovic, J. L., and Gurevich, V. V. (1997) Arrestin with a single amino acid substitution quenches light-activated rhodopsin in a phosphorylation-independent fashion. *Biochemistry 36*, 7058–7063.

(179) Sommer, M. E., and Farrens, D. L. (2006) Arrestin can act as a regulator of rhodopsin photochemistry. *Vision Res. 46*, 4532–4546.

(180) Buee, L., Troquier, L., Burnouf, S., Belarbi, K., Van der Jeugd, A., Ahmed, T., Fernandez-Gomez, F., Caillierez, R., Grosjean, M.-E., Begard, S., Barbot, B., Demeyer, D., Obriot, H., Brion, I., Buee-Scherrer, V., Maurage, C.-A., Balschun, D., D'hooge, R., Hamdane, M., Blum, D., and Sergeant, N. (2010) From tau phosphorylation to tau aggregation: what about neuronal death? *Biochem. Soc. Trans. 38*, 967–972.

(181) Lee, G., and Rook, S. L. (1992) Expression of tau protein in non-neuronal cells: microtubule binding and stabilization. *J. Cell Sci. 102 (Pt 2)*, 227–237.

(182) Miller, E. C., Teravskis, P. J., Dummer, B. W., Zhao, X., Huganir, R. L., and Liao, D.

(2014) Tau phosphorylation and tau mislocalization mediate soluble A b oligomer-induced AMPA glutamate receptor signaling deficits *39*, 1214–1224.

(183) Gomez-Ramos, A., Diaz-Hernandez, M., Rubio, A., Diaz-Hernandez, J. I., Miras-Portugal, M. T., and Avila, J. (2009) Characteristics and consequences of muscarinic receptor activation by tau protein. *Eur. Neuropsychopharmacol. 19*, 708–717.

(184) West, S., and Bhugra, P. (2015) Emerging drug targets for Abeta and tau in Alzheimer's disease: a systematic review. *Br. J. Clin. Pharmacol. 80*, 221–234.

(185) Delobel, P., Mailliot, C., Hamdane, M., Sambo, A.-V., Begard, S., Violleau, A., Delacourte, A., and Buee, L. (2003) Stable-tau overexpression in human neuroblastoma cells: an open door for explaining neuronal death in tauopathies. *Ann. N. Y. Acad. Sci. 1010*, 623–634.

(186) Simon, D., Garcia-Garcia, E., Royo, F., Falcon-Perez, J. M., and Avila, J. (2012) Proteostasis of tau. Tau overexpression results in its secretion via membrane vesicles. *FEBS Lett. 586*, 47–54.

(187) Miller, E. C., Teravskis, P. J., Dummer, B. W., Zhao, X., Huganir, R. L., and Liao, D. (2014) Tau phosphorylation and tau mislocalization mediate soluble Abeta oligomer-induced AMPA glutamate receptor signaling deficits. *Eur. J. Neurosci. 39*, 1214–1224.

(188) Zempel, H., Thies, E., Mandelkow, E., and Mandelkow, E.-M. (2010) Abeta oligomers cause localized Ca(2+) elevation, missorting of endogenous Tau into dendrites, Tau phosphorylation, and destruction of microtubules and spines. *J. Neurosci. 30*, 11938–11950.

(189) Naini, S. M. A., and Soussi-Yanicostas, N. (2015) Tau Hyperphosphorylation and Oxidative Stress, a Critical Vicious Circle in Neurodegenerative Tauopathies? *Oxid. Med. Cell. Longev. 2015*, 151979.

(190) Musch, A. (2004) Microtubule organization and function in epithelial cells. *Traffic 5*, 1–9.

(191) Moore, A. T., Fitzke, F. W., Kemp, C. M., Arden, G. B., Keen, T. J., Inglehearn, C. F., Bhattacharya, S. S., and Bird, A. C. (1992) Abnormal dark adaptation kinetics in autosomal dominant sector retinitis pigmentosa due to rod opsin mutation. *Br. J. Ophthalmol. 76*, 465–469.

(192) Mudher, A., and Lovestone, S. (2002) Alzheimer's disease-do tauists and baptists finally shake hands? *Trends Neurosci. 25*, 22–26.

8. ACKNOWLEDGEMENTS

First and foremost I would like to express my special appreciation and thanks to my supervisor Professor Dr. Pere Garriga Solé. He helped me to start my PhD programme in Spain which already became the most important and priceless trip in my life. By the time to time communication and discussion, I was deeply admired and infected by his enormous knowledge and meticulous scientific attitude. With the guidance and encouragement in three years, I can keep my science interest and continue the study. I am also thankful for the Spanish research atmosphere he created, which made me feel free during the study.

I would give my sincerely thanks to my thesis co-director Dr. Eva Ramon. I appreciate all her contributions of time, guidance, discussions and encouragements for my project. Her dedication towards science shocked me and motivated me in my life from the spirit. I am thankful for the excellent example she has provided as a successful woman bioscientist and researcher.

I also thank to professor Dr. Roser Masgrau (UAB) and Dr. Jesus Avila (CSIC-UAM) and all the other professors who gave me the kindly help on materials, techniques and equipment on my work.

The members of the GBMI group have contributed immensely to my personal and professional time at UPC. This group has been a source of friendship as well as collaboration. I am especially grateful for my labmates: Dr Mª Jesus Sanchez, who was my first working partner and gave me unselfish help for my DDHA-PC liposomes work, Dr. Margarita Morillo, who kindly assisted me on my work Dr. Merce Tena, who is beautiful, humorous and with her natural ebullience. She showed me totally unique Catalonia character. Dr. Sundaramoorthy Srinivasan, my India friend, who always helped me solving all the computer problems, fixing most of the equipment and downloading all the paid articles. PhD student Maria Guadalupe Herrera, my best friend, spending with me most of the time in parties, dinners and discussions related to the experiments. I also thank her for her pushing (also Eva) on my thesis writing with strict and honest heart. PhD student Miguel Antonio Fernandez, who is always taking care of the lab and giving me a lot of help on the experiments and articles. MSc Diana Rivera Rodriguez, she helped me to see the problems and questions with an open mind and optimism. I would honorary acknowledge them. We worked together most of the time with fun and happiness.

I wish to thank Professor Tzanko Tzanov and his former and current lab members; Dr. Carlos

Díaz, Dr. Tony Francesko, Dr. Margarida Fernandes, Petya Petkova, Kristina Ivanova, Ivaylo Stefanov and Dr. Javier Hoyo, who are always around sharing the equipment, reagents and cell culture room with us. Petya and Kristina, my best friends, are always full of enthusiasm for the life and work.

I have appreciated my friends Hongyang Xu, Jianqing Zhu, Weiyi Zhang, Yehua He who always encouraged me, comforted my complain and motivate me to be a better person.

Besides, I would thank my parents and my brother Xiaoguang Dong for their love and encouragement. They always support me at any time in all my pursuits.

在此，我万分感激父母董立义、赵桂芳和弟弟董晓光一直以来对我的鼓励与支持。这份坚实的感情更是增添了我追求梦想的勇气与信心。山高水长，唯愿亲情永存。

I gratefully acknowledge the Chinese Scholarship Council (CSC), the funding sources that made my PhD work possible.

Even mountains and seas cannot distance people with common aspirations. PhD period is the most memorable part of my life. I will miss GAIA, miss everyone, and miss Spain. Thank you.

Xiaoyun Dong

Universitat Politècnica de Catalunya

March 2016

APPENDIX

Buffers List

3.3.1.1 Competent cells preparation

- 100 mM $CaCl_2$ solution, autoclaved and kept at 4ºC until use.
- 100 mM $CaCl_2$ containing 20% of glycerol solution, autoclaved and kept at 4ºC until use.

3.3.1.2 Ultra-competent cells preparation

- SOB solution: 0.5% yeast extract, 2% tryptone, 10 mM NaCl, 2.5 mM KCl, 10 mM $MgCl_2$, 10 mM $MgSO_4$ dissolved in milliQ water. It was autoclaved to sterilize and kept at 4ºC.
- TB solution: 10 mM PIPES, 15 mM $CaCl_2$ and 250 mM KCl. Then dissolved in milliQ water and adjust pH to 6.7 with KOH or HCl and then add 55 mM $MnCl_2$, dissolved in milliQ water. It was sterilized by filtration with 0.45 μm filter and kept at 4ºC.

3.3.1.3 DNA transformation

- 2YT medium: 1.6 g Tryptone, 1.0 g Yeast Extract, 0.5 g NaCl, adjust pH to 7.2 in 100 ml ddH_2O and autoclaved.
- LB medium: 1.0 g Tryptone, 0.5 g Yeast Extract, 0.05 g NaCl, pH 7.2 in 100 ml ddH_2O and autoclaved.

*3.3.2.1 DNA Maxi-p*rep p*urification*

- Resuspension buffer (R3): 50 mM Tris-HCl, 10 mM EDTA, pH 8.0.
- Lysis buffer (L7): 0.2 M NaOH, and 1% (w/v) SDS.
- Precipitation buffer (N3): 3.1 M potassium acetate, pH 5.5.
- Equilibration buffer (EQ1): 0.1 M sodium acetate with pH 5.0, 0.6 M NaCl, and 0.15% (v/v) TritonX-100.
- Wash buffer (W8): 0.1 M sodium acetate with pH 5.0 and 825 mM NaCl.
- Elution buffer (E4): 100 mM Tris-HCl, pH 8.5 and 1.25 M NaCl

3.3.2.2 DNA agarose gel electrophoresis

- TAE buffer (10x): 48.4 g Tris Base, 7.44 g EDTA dissolved in 800 ml ddH_2O, 11.42 ml CH_3COOH was added and homogenized. Add more ddH_2O to 1 L.
- EB buffer: 2 μl EB dissolved in 100 ml 1x TAE buffer.

3.4.1 Coupling 1D4 antibody to sepharose beads

- 1 mM HCl (pH 2~3): 41.6 μl of 12 M/37% HCl dissolved in 500 ml ddH_2O, adjust pH 2~3.
- Coupling buffer: 0.1 M $NaHCO_3$ pH 8.3 containing 0.5 M NaCl.
- Beads storage buffer: 2 mM Na_2PO_4 (pH 6.0) with 0.004% (w/v) NaN_3.

3.4.2 Purification of Rho WT and G90V, N55K mutants from mammalian cells

- Solvent buffer (DDHA-PC liposomes study (3.5.2)): 137 mM NaCl, 2.7 mM KCl, 1.5 mM KH_2PO_4, and 8 mM Na_2HPO_4, pH 7.4.
- Solvent buffer (DMPC/DHPC bicelles study (3.5.2)): solvent buffer was also named as Bicelles buffer A: 10 mM BTP, 140 mM NaCl, 2 mM $MgCl_2$, 2 mM $CaCl_2$, pH 6.0.
- Washing buffer: solvent buffer with 0.05% (w/v) DM.
- Elution buffer: washing buffer with 100 μM 1D4 9-mer peptide.

3.4.4 Extraction of G protein transducin (Gt) from bovine retina

- Tris buffer A: 20 mM Tris, pH 7.4, 1 mM $CaCl_2$, 2 mM DTT.
- Tris buffer C: 10 mM Tris, pH 7.4, 100 mM NaCl, 5 mM $MgCl_2$, 2 mM DTT.
- Tris buffer D: 10 mM Tris, pH 7.4, 0.1 mM EDTA, 2 mM DTT.
- Tris buffer E: 20 mM Tris, pH 7.5, 100 mM NaCl, 50% glycerol, 5 mM DTT and 5 mM $MgCl_2$.
- 47% sucrose: 117.5 g sucrose in 250 ml Tris buffer A.
- 30% sucrose: 75 g sucrose in 250 ml Tris buffer A.
- 25% sucrose: 62.5 g sucrose in 250 ml Tris buffer A.

0.1 mM PMSF was added in all the buffers before used.

3.5.1 DMPC/DHPC bicelles preparations

- Bicelles buffer A: 10 mM BTP, 140 mM NaCl, 2 mM $MgCl_2$, 2 mM $CaCl_2$, pH 6.0.
- Buffer A containing 0.05% (w/v) DM was used as a DM-buffer A control buffer.
- Buffer A containing 2% (w/v) DMPC/DHPC bicelles was prepared as the description above.

The bicelles buffer A was used in all the experiments associated with DMPC/DHPC bicelles.

3.5.2 DDHA-PC liposomes preparation and protein insertion

- During the DDHA-PC liposomes preparation process, the solvent buffer (see section 3.4.2) was used and all the experiments involving DDHA-PC liposomes.
- DM detergent buffer: solvent buffer containing 0.05% (w/v) DM.
- DDHA-PC liposomes buffer: solvent buffer containing 0.375 mM DDHA-PC liposomes with 0.5 μM WT rhodopsin or mutants, which would be 750:1, as per the above description.

3.6.4.1 SDS-PAGE and Coomassie blue staining

- 4x protein loading buffer: 0.0625 M Tris, 2% SDS, 10% Glycerol, 0.4 M DTT, 0.1% Blue Bromophenol dissolved in ddH_2O.
- 1x TGS buffer: 3 g Tris, 14.4 g Glycine, 1 g SDS pH 8.3, up to 1 L with ddH_2O.
- Coomassie brilliant blue buffer: 10% (v/v) MetOH, 10% (v/v) AcOH and 0.025% (w/v) Coomassie-G.
- Coomassie destain buffer: 400 ml Methanol, 100 ml Glacial Acetic Acid dissolved in 1 L ddH_2O.

3.6.4.2 Blue Native PAGE (BN-PAGE)

- Loading buffer: 5% glycerol and 0.01% Ponceau Red.
- Running buffer: the gel running buffer is 50 mM Tricine, 15 mM Bis-Tris and 0.02% Coomassie blue G with pH 7.0.

3.6.5 WB

- TBS buffer: 8.7 g NaCl, 1.21 g Tris, 0.4 ml HCl in 1L ddH_2O, pH 8.0.
- TTBS buffer: 1 ml Tween 20 dissolved in 1L TBS solution.

3.6.6 Arrestin R175E purification by Bio-scale mini profinity cartridges

- Arrestin buffer: 10 mM MOPS pH 7.2 containing 50 mM NaCl and 0.1 mM PMSF and protease inhibitor (filtered before use).
- Arrestin elution buffer: Arrestin buffer containing 0.1 M NaF.

3.6.10 Lowry protein assay

- Lowry solution A (10 ml): 0.1 M NaOH (40 mg) and 0.2 g Na_2CO_3 dissolved in 10 ml ddH_2O
- Lowry solution B (10 ml): 0.1 g potassium sodium tartrate tetrahydrate and 50 mg $CuSO_4$ dissolved in 10 ml ddH_2O. $CuSO_4$ was dissolved first to avoid any aggregation.

MAPT(Tau) gene sequence

Human MAPT / Tau transcript variant 4 natural ORF mammalian expression plasmid (HG10058-UT)

Red font is gene. ggtacc is **KpnI.** tctaga **is XbaI. Black letters on blue is stop codon**

gacggatcgggagatctcccgatcccctatggtgcactctcagtacaatctgctctgatgccgcatagttaagc
cagtatctgctccctgcttgtgtgttggaggtcgctgagtagtgcgcgagcaaaatttaagctacaacaaggca
aggcttgaccgacaattgcatgaagaatctgcttagggttaggcgttttgcgctgcttcgcgagtacatttata
ttggctcatgtccaatatgaccgccatgttgacattgattattgactagttattaatagtaatcaattacgggg
tcattagttcatagcccatatatggagttccgcgttacataacttacggtaaatggcccgcctggctgaccgcc
caacgacccccgcccattgacgtcaataatgacgtatgttcccatagtaacgccaatagggactttccattgac
gtcaatgggtggagtatttacggtaaactgcccacttggcagtacatcaagtgtatcatatgccaagtccgccc
cctattgacgtcaatgacggtaaatggcccgcctggcattatgcccagtacatgaccttacgggactttcctac
ttggcagtacatctacgtattagtcatcgctattaccatggtgatgcggttttggcagtacaccaatgggcgtg
gatagcggtttgactcacggggatttccaagtctccaccccattgacgtcaatgggagtttgttttggcaccaa
aatcaacgggactttccaaaatgtcgtaataaccccgccccgttgacgcaaatgggcggtaggcgtgtacggtg
ggaggtctatataagcagagctcgtttagtgaaccgtcagatcctcactctcttccgcatcgctgtctgcgagg
gccagctgttgggctcgcggttgaggacaaactcttcgcggtctttccagtactcttggatcggaaacccgtcg
gcctccgaacggtactccgccaccgagggacctgagcgagtccgcatcgaccggatcggaaaacctctcgagaa
aggcgtctaaccagtcacagtcgcaaggtaggctgagcaccgtggcgggcggcagcgggtggcggtcggggttg
tttctggcggaggtgctgctgatgatgtaattaaagtaggcggtcttgagacggcggatggtcgaggtgaggtg
tgggtttagtgaaccgtcagatcctcactctcttccgcatcgctgtctgcgagggccagctgtcaggcttgaga
tccagctgttggggtgagtactccctctcaaaagcgggcattacttctgcgctaagattgtcagtttccaaaaa
cgaggaggatttgatattcacctggcccgatctggccatacacttgagtgacaatgacatccactttgcctttc
tctccacaggtgtccactcccaggtccaagtttaaactttaatacgactcactataggggccgccaccaagctt
ggtacc
ATGGCTGAGCCCCGCCAGGAGTTCGAAGTGATGGAAGATCACGCTGGGACGTACGGGTTGGGGGACAGGAAAGA
TCAGGGGGGCTACACCATGCACCAAGACCAAGAGGGTGACACGGACGCTGGCCTGAAAGCTGAAGAAGCAGGCA
TTGGAGACACCCCCAGCCTGGAAGACGAAGCTGCTGGTCACGTGACCCAAGCTCGCATGGTCAGTAAAAGCAAA
GACGGGACTGGAAGCGATGACAAAAAAGCCAAGGGGGCTGATGGTAAAACGAAGATCGCCACACCGCGGGGAGC
AGCCCCTCCAGGCCAGAAGGGCCAGGCCAACGCCACCAGGATTCCAGCAAAAACCCCGCCCGCTCCAAAGACAC
CACCCAGCTCTGGTGAACCTCCAAAATCAGGGGATCGCAGCGGCTACAGCAGCCCCGGCTCCCCAGGCACTCCC
GGCAGCCGCTCCCGCACCCCGTCCCTTCCAACCCCACCCACCCGGGAGCCCAAGAAGGTGGCAGTGGTCCGTAC
TCCACCCAAGTCGCCGTCTTCCGCCAAGAGCCGCCTGCAGACAGCCCCCGTGCCCATGCCAGACCTGAAGAATG
TCAAGTCCAAGATCGGCTCCACTGAGAACCTGAAGCACCAGCCGGGAGGCGGGAAGGTGCAAATAGTCTACAAA
CCAGTTGACCTGAGCAAGGTGACCTCCAAGTGTGGCTCATTAGGCAACATCCATCATAAACCAGGAGGTGGCCA
GGTGGAAGTAAAATCTGAGAAGCTTGACTTCAAGGACAGAGTCCAGTCGAAGATTGGGTCCCTGGACAATATCA
CCCACGTCCCTGGCGGAGGAAATAAAAAGATTGAAACCCACAAGCTGACCTTCCGCGAGAACGCCAAAGCCAAG
ACAGACCACGGGGCGGAGATCGTGTACAAGTCGCCAGTGGTGTCTGGGGACACGTCTCCACGGCATCTCAGCAA
TGTCTCCTCCACCGGCAGCATCGACATGGTAGACTCGCCCCAGCTCGCCACGCTAGCTGACGAGGTGTCTGCCT
CCCTGGCCAAGCAGGGTTTGTAAactcgagtctagagcggccgccgaattcgggcccgtttaaacccgctgatc
agcctcgactgtgccttctagttgccagccatctgttgtttgcccctcccccgtgccttccttgaccctggaag
gtgccactcccactgtcctttcctaataaaatgaggaaattgcatcgcattgtctgagtaggtgtcattctatt
ctgggggtggggtggggcaggacagcaaggggaggattgggaagacaatagcaggcatgctggggatgcggt

gggctctatggcttctgaggcggaaagaaccagctggggctctaggggtatccccacgcgccctgtagcggcg
cattaagcgcggcgggtgtggtggttacgcgcagcgtgaccgctacacttgccagcgccctagcgcccgctcct
ttcgctttcttcccttcctttctcgccacgttcgcaggctttccccgtcaagctctaaatcgggggctccctttt
agggttccgatttagtgctttacggcacctcgaccccaaaaaacttgattagggtgatggttcacgtagtgggc
catcgccctgatagacggtttttcgccctttgacgttggagtccacgttctttaatagtggactcttgttccaa
actggaacaacactcaaccctatctcggtctattcttttgatttataagggattttgccgatttcggcctattg
gttaaaaaatgagctgatttaacaaaaatttaacgcgaattaattctgtggaatgtgtgtcagttagggtgtgg
aaagtccccaggctccccagcaggcagaagtatgcaaagcatgcatctcaattagtcagcaaccaggtgtggaa
agtccccaggctccccagcaggcagaagtatgcaaagcatgcatctcaattagtcagcaaccatagtcccgccc
ctaactccgcccatcccgcccctaactccgcccagttccgcccattctccgccccatggctgactaatttttt
tatttatgcagaggccgaggccgcctctgcctctgagctattccagaagtagtgaggaggctttttggaggcc
taggcttttgcaaaaagctctcgggagcttgtatatccattttcggatctgatcagcacgtgatgaaaaagcct
gaactcaccgcgacgtctgtcgagaagtttctgatcgaaaagttcgacagcgtctccgacctgatgcagctctc
ggagggcgaagaatctcgtgctttcagcttcgatgtaggagggcgtggatatgtcctgcgggtaaatagctgcg
ccgatggtttctacaaagatcgttatgtttatcggcactttgcatcggccgcgctcccgattccggaagtgctt
gacattggggaattcagcgagagcctgacctattgcatctcccgccgtgcacagggtgtcacgttgcaagacct
gcctgaaaccgaactgcccgctgttctgcagccggtcgcggaggccatggatgcgatcgctgcggccgatctta
gccagacgagcgggttcggcccattcggaccgcaaggaatcggtcaatacactacatggcgtgatttcatatgc
gcgattgctgatccccatgtgtatcactggcaaactgtgatggacgacaccgtcagtgcgtccgtcgcgcaggc
tctcgatgagctgatgctttgggccgaggactgccccgaagtccggcacctcgtgcacgcggatttcggctcca
acaatgtcctgacggacaatggccgcataacagcggtcattgactggagcgaggcgatgttcggggattcccaa
tacgaggtcgccaacatcttcttctggaggccgtggttggcttgtatggagcagcagacgcgctacttcgagcg
gaggcatccggagcttgcaggatcgccgcggctccgggcgtatatgctccgcattggtcttgaccaactctatc
agagcttggttgacggcaatttcgatgatgcagcttgggcgcagggtcgatgcgacgcaatcgtccgatccgga
gccgggactgtcgggcgtacacaaatcgcccgcagaagcgcggccgtctggaccgatggctgtgtagaagtact
cgccgatagtggaaaccgacgccccagcactcgtccgagggcaaaggaatagcacgtgctacgagatttcgatt
ccaccgccgccttctatgaaaggttgggcttcggaatcgttttccgggacgctggctggatgatcctccagcgc
ggggatctcatgctggagttcttcgcccaccccaacttgtttattgcagcttataatggttacaaataaagcaa
tagcatcacaaatttcacaaataaagcatttttttcactgcattctagttgtggtttgtccaaactcatcaatg
tatcttatcatgtctgtataccgtcgacctctagctagagcttggcgtaatcatggtcatagctgtttcctgtg
tgaaattgttatccgctcacaattccacacaacatacgagccggaagcataaagtgtaaagcctggggtgccta
atgagtgagctaactcacattaattgcgttgcgctcactgcccgctttccagtcgggaaacctgtcgtgccagc
tgcattaatgaatcggccaacgcgcggggagaggcggtttgcgtattgggcgctcttccgcttcctcgctcact
gactcgctgcgctcggtcgttcggctgcggcgagcggtatcagctcactcaaaggcggtaatacggttatccac
agaatcaggggataacgcaggaaagaacatgtgagcaaaaggccagcaaaaggccaggaaccgtaaaaaggccg
cgttgctggcgtttttccataggctccgccccctgacgagcatcacaaaaatcgacgctcaagtcagaggtgg
cgaaacccgacaggactataaagataccaggcgtttccccctggaagctccctcgtgcgctctcctgttccgac
cctgccgcttaccggatacctgtccgcctttctcccttcgggaagcgtggcgctttctcatagctcacgctgta
ggtatctcagttcggtgtaggtcgttcgctccaagctgggctgtgtgcacgaacccccgttcagcccgaccgc
tgcgccttatccggtaactatcgtcttgagtccaacccggtaagacacgacttatcgccactggcagcagccac
tggtaacaggattagcagagcgaggtatgtaggcggtgctacagagttcttgaagtggtggcctaactacggct
acactagaagaacagtatttggtatctgcgctctgctgaagccagttaccttcggaaaaagagttggtagctct
tgatccggcaaacaaaccaccgctggtagcggtggtttttttgtttgcaagcagcagattacgcgcagaaaaaa
aggatctcaagaagatcctttgatcttttctacggggtctgagcgcggaacccctatttgtttatttttctaaa
tacattcaaatatgtatccgctcatgaattaattcttagaaaaactcatcgagcatcaaatgaaactgcaattt

attcatatcaggattatcaataccatatttttgaaaaagccgtttctgtaatgaaggagaaaactcaccgaggc
agttccataggatggcaagatcctggtatcggtctgcgattccgactcgtccaacatcaatacaacctattaat
ttcccctcgtcaaaaataaggttatcaagtgagaaatcaccatgagtgacgactgaatccggtgagaatggcaa
aagtttatgcatttctttccagacttgttcaacaggccagccattacgctcgtcatcaaaatcactcgcatcaa
ccaaaccgttattcattcgtgattgcgcctgagcgagacgaaatacgcgatcgctgttaaaaggacaattacaa
acaggaatcgaatgcaaccggcgcaggaacactgccagcgcatcaacaatattttcacctgaatcaggatattc
ttctaatacctggaatgctgttttcccagggatcgcagtggtgagtaaccatgcatcatcaggagtacggataa
aatgcttgatggtcggaagaggcataaattccgtcagccagtttagtctgaccatctcatctgtaacatcattg
gcaacgctacctttgccatgtttcagaaacaactctggcgcatcgggcttcccatacaatcgatagattgtcgc
acctgattgcccgacattatcgcgagcccatttatacccatataaatcagcatccatgttggaatttaatcgcg
gcctagagcaagacgtttcccgttgaatatggctcataacacccttgtattactgtttatgtaagcagacagt
tttattgttcatgaccaaaatcccttaacgtgagttttcgttccactgagcgtcagaccccgtagaaatccgcg
cacatttccccgaaaagtgccacctgacgtc